Summer 1994

The Development of a Method to Extract High Purity Oxygen From the Martian Atmosphere

Dongchuan Wu
Old Dominion University

THE DEVELOPMENT OF A METHOD TO EXTRACT HIGH PURITY OXYGEN FROM THE MARTIAN ATMOSPHERE

By

Dongchuan Wu

B.S. August 1986, Shanghai University of Industry, China
M.S. May 1991, Old Dominion University

A Dissertation Submitted to the Faculty of
Old Dominion University in Partial Fulfillment of the
Requirements for the Degree of

DOCTOR OF PHILOSOPHY

MECHANICAL ENGINEERING

OLD DOMINION UNIVERSITY
August, 1994

Approved by:

_____
Dr. R. L. Ash (Director)

_____
Dr. R. A. Outlaw (Director)

_____
Dr. S. N. Tiwari

_____
Dr. A. S. Roberts Jr.

_____
Dr. S. K. Chaturvedi

ABSTRACT

THE DEVELOPMENT OF A METHOD TO EXTRACT HIGH PURITY OXYGEN FROM THE MARTIAN ATMOSPHERE

Dongchuan Wu
Old Dominion University, 1994
Directors: Dr. R.L. Ash and Dr. R.A. Outlaw

A glow-discharge in an ambient Mars atmosphere (total pressure of 5 torr, composed of 95% carbon dioxide) results in the dissociation of carbon dioxide molecules into carbon monoxide and oxygen. If the glow-discharge zone is maintained adjacent and close to a silver membrane, operated at temperatures above 400°C, atomic and molecular oxygen, produced by the glow-discharge, can be separated from the other species by atomic diffusion through the membrane to an ultrahigh vacuum region where the desorbed O_2 is then collected. Experiments have been conducted to study the behavior of the glow discharge in both molecular oxygen and carbon dioxide environments, and to study the interaction of atomic and molecular oxygen with silver. It was found that, with this geometry, more than 75% of the CO_2 was dissociated into CO and O with only 5 mA discharge current and that the permeation flux increased linearly with discharge current. Only 0.65% of the generated atomic oxygen was adsorbed at the membrane because it quickly recombined to form O_2 as it migrated toward the membrane. The atomic oxygen arriving at the membrane, bypassed the thermal dissociative adsorption and therefore had a much higher sticking coefficient.

This higher sticking coefficient resulted in a greatly increased surface concentration of oxygen which greatly increased the oxygen flux through the membrane.

The sticking coefficient of the atomic oxygen on silver was estimated by using a Langmuir type model and was found to be close to 1 at room temperature. Since most of the gas phase atomic oxygen quickly recombined to form O_2 as it migrated toward the silver membrane, both a small amount of atomic oxygen and a relative large amount of molecular oxygen components will adsorb on the hot Ag membrane. But because of the much higher sticking coefficient for atomic oxygen on silver, the atomic component dominated the adsorption.

It was also found that the oxygen flux through the Ag membranes is diffusion controlled and therefore proportional to the reciprocal of the membrane thickness. Supported pin hole free Ag membranes with thicknesses of 12 μm have been developed in this work. Furthermore, a pin hole free Ag membrane that was grown by a combination of Ar ion bombardment assisted physical vapor deposition and intermediate burnishing with a thickness less than 1 μm is being developed which will substantially improve the oxygen flux level. Thickness of 1 μm will permit flux levels of at least 10^{16} molecules/cm^{2}s. With this flux level, less than 1.5 m^2 membrane surface area would be needed to support an astronaut on a continual basis on the Mars surface. The results of this work show that this approach of producing oxygen from the CO_2 Martian atmosphere can eliminate mechanical filtration, compression and high temperature heating of the Mars atmosphere proposed previously by electrochemical methods.

ACKNOWLEDGEMENTS

The author wishes to thank his father and mother, who implanted in him the desire to know the unknown, and the confidence to tackle the sometimes difficult and frustrating tasks. The author wishes to thank Dr. R.A. Outlaw for his seemingly infinite amount of patience, his continued encouragement and his guidance during the learning process and subsequent accomplishment of the research presented here. The author wishes to thank his advisor, Dr. R.L. Ash for his guidance in this work and his valuable help in writing this dissertation. The author also extends his appreciation to the other committee members: Dr. S.K. Chaturvedi, Dr. A.S. Roberts Jr. and Dr. S.N. Tiwari for their critical review of the dissertation and valuable comments. The author also wishes to thank his wife Winnie for her patient and support during this program.

This work was supported by NASA Langley Research Center through grant NAG1-1140, monitored by Dr. R.A. Outlaw.

TABLE OF CONTENTS

Page

LIST OF FIGURES

LIST OF SYMBOLS

A	membrane surface area
AES	Auger electron spectroscopy
C	concentration, number of oxygen atoms per cm^3 of Ag, cm^{-3}
D	diffusivity, cm^2-s^{-1}
f	limiting conductance of valve insert, cm^3-s^{-1}
J	flux density, cm^{-2}
K	permeability, cm^{-1}-s^{-1}
LEED	Low-energy-electron diffraction
N	concentration, number of oxygen atoms per cm^2 of Ag, cm^{-2}
N_a	number of of oxygen atoms per cm^3 of Ag
N_v	number of interstitious vacancies per cm^3 of Ag
n	gas number density, cm^{-3}
P	pressure, dyne-cm^{-2} ($1.33x10^3$ times pressure in torr)
P_d	pressure at UHV interface, dyne-cm^{-2} (1.33×10^3 times pressure in torr)
P_0	upstream side pressure, dyne-cm^{-2} (1.33×10^3 times pressure in torr)
P_p	pump pressure, dyne-cm^{-2} (1.33×10^3 times pressure in torr)
q	fractional coverage
Q	gas throughput

QMS	Quadrupole mass spectrometer
R	universal gas constant, 8.314×10^7 erg-mol^{-1}-K^{-1}
s	sticking coefficient
S	solubility, cm^{-3}
S_0	entropy factor
t	time, s
T	temperature, K
UHV	ultrahigh vacuum
V	volume of measurement chamber, cm^3
x	variable distance through membrane, cm
X_v	atom fraction of the interstitial vacancies
Γ	mean jump frequency
m_v	chemical potential
m_v^0	standard chemical potential
ΔE_v	internal energy per mole vacancy
ΔE_v^0	standard internal energy per mole vacancy
ΔF_v	free energy due to vacancies.
ΔH	solution enthalpy
ΔS_m	mixing entropy
ΔS_v	vibrational entropy per mole vacancy
ΔS_v^0	standard vibrational entropy per mole vancancy

Subscripts

a	atoms
m	molecules
eq	equilibrium
gd	glow discharge

Chapter 1

INTRODUCTION

Round trip missions to Mars will require advances in the technology base used for space mission planning and design. Not only do one-way trip times approach 200 days, but the consumables required by humans and the propellant required for the return trip become limiting constraints on the types of missions which can be planned and executed. A plan called "Mars Direct" has been proposed and considered practical for the near term piloted Mars mission[1,2]. In this plan two launches of a heavy lift booster, optimized for Earth escape, are required to support the mission with a crew of four. The first booster launch delivers an unfueled and unmanned Earth Return Vehicle, together with an unmanned fuel factory, which will manufacture the oxygen and propellant primarily out of indigenous resources, to the martian surface. After propellant production is completed, a second launch delivers a habitation module containing a crew of four, a pressurized ground rover, and an aerobrake/landing engine assembly, to the prepared site, where they conduct extensive regional exploration for 1.5 years and then return directly to Earth in the Earth Return Vehicle. Assuming a 600 days surface stay and 200 days for the return trip, this plan will require 3.2 tons of oxygen for the continuous life support of a crew of four (1.0 kg/man-day as for NASA standards[3]). Further, this number does not include oxygen, as an oxidizer, needed to fuel the ground rover and the Earth Return

Vehicle. Obviously, production of oxygen on the surface of Mars is a very important element in the planning of future human expeditions to Mars.

Viking lander measurements and recent studies[4,5] determined that the Martian atmosphere is comprised of primarily CO_2 (95.3 percent), N_2 (2.7 percent), Ar (1.6 percent), with only small amounts of other components. The average surface pressure of the Martian atmosphere is between 5 and 6 torr, or less than one-hundredth of the surface pressure on Earth. The temperature is low, ranging between 190 and 240 K at mid latitudes. Ash, Dowler and Varsi[6] first proposed that the Martian atmosphere was the simplest source for rocket propellant, and Stancatti et. al.[7] suggested decomposing the CO_2 molecules, which make up most of its atmosphere, to produce oxygen on Mars.

A system using thermal energy to dissociate CO_2 molecules followed by the extraction of oxygen using stabilized zirconia cells was suggested in 1979[7] and has been tested subsequently by the researches at the University of Arizona[8]. When carbon dioxide gas is heated to high temperatures, it partially dissociates into CO and O. The ZrO_2 electrochemical cell with platinum electrodes, which has the advantage of no moving parts, was used to extract the oxygen. Unfortunately, the thermal dissociation rates for CO_2 are not very efficient. At a temperature of 1100 K, the partial pressure of oxygen (in 1 atmosphere of CO_2) is on the order 7.6×10^{-4} torr[9]. As a result, the system must be operated either at higher temperatures or at lower efficiency, which means higher energy consumption and introduces possible reliability concerns for the electrochemical cells.

Outlaw suggested using a glow discharge to dissociate CO_2 molecules into CO and O, followed by the permeation of O atoms through a hot silver membrane to accomplish separation[10]. This technique uses kinetic energy from plasma electrons to dissociate CO_2 molecules, permitting dissociation to occur at relatively low temperatures. Preliminary tests indicated that steady state dissociation rates of 10 to 50 percent could be expected, depending on the discharge current. Another advantage for this approach is that the glow discharge can operate at pressures which are close to Martian ambient conditions, so the system may not require preliminary filtration and compression or a pumping stage like the pure thermal dissociation approach. Glow-discharge oxygen production also has the potential to be integrated with the stabilized zirconia cell systems, using thin silver coatings as one of the electrodes for both glow-discharge permeation and electrochemical pumping via the zirconia cell. Since glow-discharge dissociation has the advantage of lower operating temperatures and can operate in the pressure range typical of the Martian atmosphere, it may be more of a desirable approach. Here zirconia cells can operate as an oxygen pump, utilizing their inherent advantage of no moving parts and allowing the collected oxygen to be pressurized to high levels for storage.

Ultimately, this technique may be developed to generate sufficient quantities of oxygen to support astronauts on the Mars surface and to provide the oxidizer needed in propellant for the return trip to Earth. The objections of this study are (1) to study and optimize the effectiveness of the glow discharge in breaking up O_2 and CO_2 molecules, (2) to establish the relations between the molecular dissociation rate and the glow-discharge current and the voltage, along with the glow-discharge chamber pressure and

the influence of changing cathode-anode separations on the overall oxygen flux transported through the membrane, (3) to study the adsorption and desorption of atomic oxygen on a silver surface at different temperatures, in order to determine whether there is a surface limitation for oxygen transport, (4) to characterize the diffusion controlled oxygen transport and (5) to develop a thin film silver membrane, which can be used to maximize oxygen production.

A summary of the literature survey on glow discharge properties, surface properties and the permeation properties are presented in Chap. 2. The permeation analysis is presented in Chap. 3. A description of the experimental apparatus and the experimental procedures are presented in Chap. 4. The results and the discussions are presented in Chap. 5. The conclusions of the study are presented in Chap. 6.

Chapter 2

LITERATURE SURVEY

2.1 Glow-discharge Properties

Plasmas have been used extensively in the deposition and etching of thin films devices because the energetic ions and electrons can break the chemical bonds of gas molecules efficiently, and the ion can be accelerated to kinetic energies up to 1000 eV. Plasmas may be formed in different electric fields, such as microwave, rf or dc fields. The glow-discharge is one stage of the dc electric discharge which has a very distinctive feature of a large positive space charge layer at the cathode, with a strong field at the surface with considerable potential drop. The normal glow-discharge is a self-sustaining discharge with a cold cathode emitting electrons due to secondary emission mostly due to positive ion bombardment. In a dc electric field, if there is one free electron, formed near the cathode (perhaps by a cosmic ray or some UV photon), the electric field will accelerate the electron towards the anode which, depending on the mean free path, will produce ionization. As the intensity of the electric field is increased to a critical level, the ionized atoms will gain enough energy to produce secondary electrons by bombarding the cathode surface which leads to a multiplication of the number of electrons and results

in the discharge becoming self-sustaining. Visible emission also can be observed at this stage. This is gaseous *breakdown* and a *glow-discharge.*

There are several states for a dc discharge[11-21]. The first state is called the Townsend discharge, just after breakdown. During Townsend discharge, the discharge current increases with small increases in voltage. The next state is called normal glow-discharge. Electrons are created by ionization and by the secondary electrons generated from ion impact at the cathode surface. Initially, the glow region covers only portions of the cathode surface, and is sustained at nearly constant voltages while the currents increased (as the cathode coverage increases). If the power is increased further, after the cathode surface is fully covered by the glow region, the cathode will begin to heat up and the voltage will start to increase rapidly with increases in current. This state is called *abnormal glow-discharge*. Eventually, thermionic emission will occur, and become the dominant electron generating process. At this point the discharge voltage decreases and the glow evolves into an Arc. Fig. 2.1 shows the different states of a dc glow-discharge. It also shows that the discharge voltage decreases with increasing discharge pressure. With higher discharge pressure, the normal glow-discharge region is wider; so, it is more tolerant to the current fluctuation and the glow-discharge becomes more stable.

Figure 2.2 shows the structure of a dc normal glow-discharge. It contains a cathode sheath, a cathode dark space, a negative glow zone, a Faraday dark space, and a positive column. The cathode sheath, negative glow and positive column regions are luminous and can be seen visually. Most of the potential drop occurs in the cathode sheath and the cathode dark space. This potential drop will accelerate ions from the

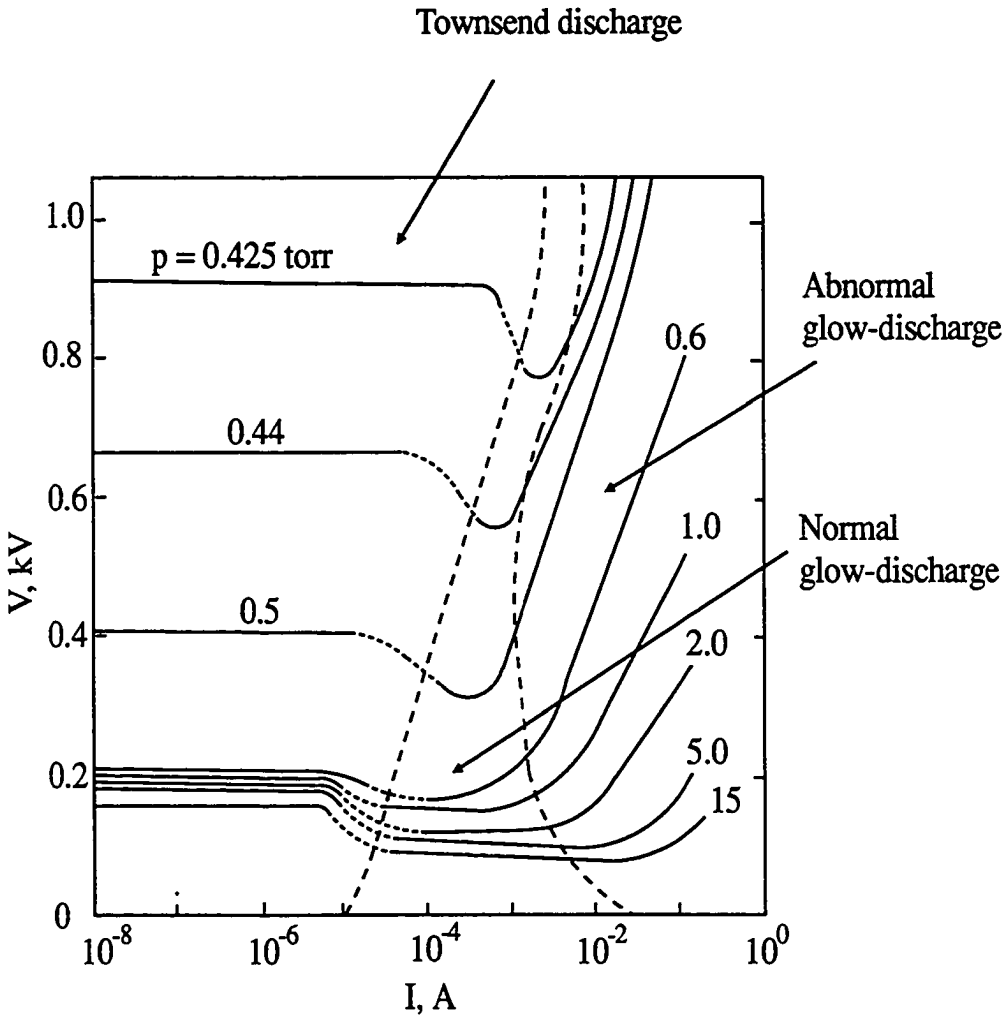

Fig. 2.1 Measured V - I characteristics of discharge in neon between copper disks 9.3 cm in diameter, gap width 1.6 cm [15].

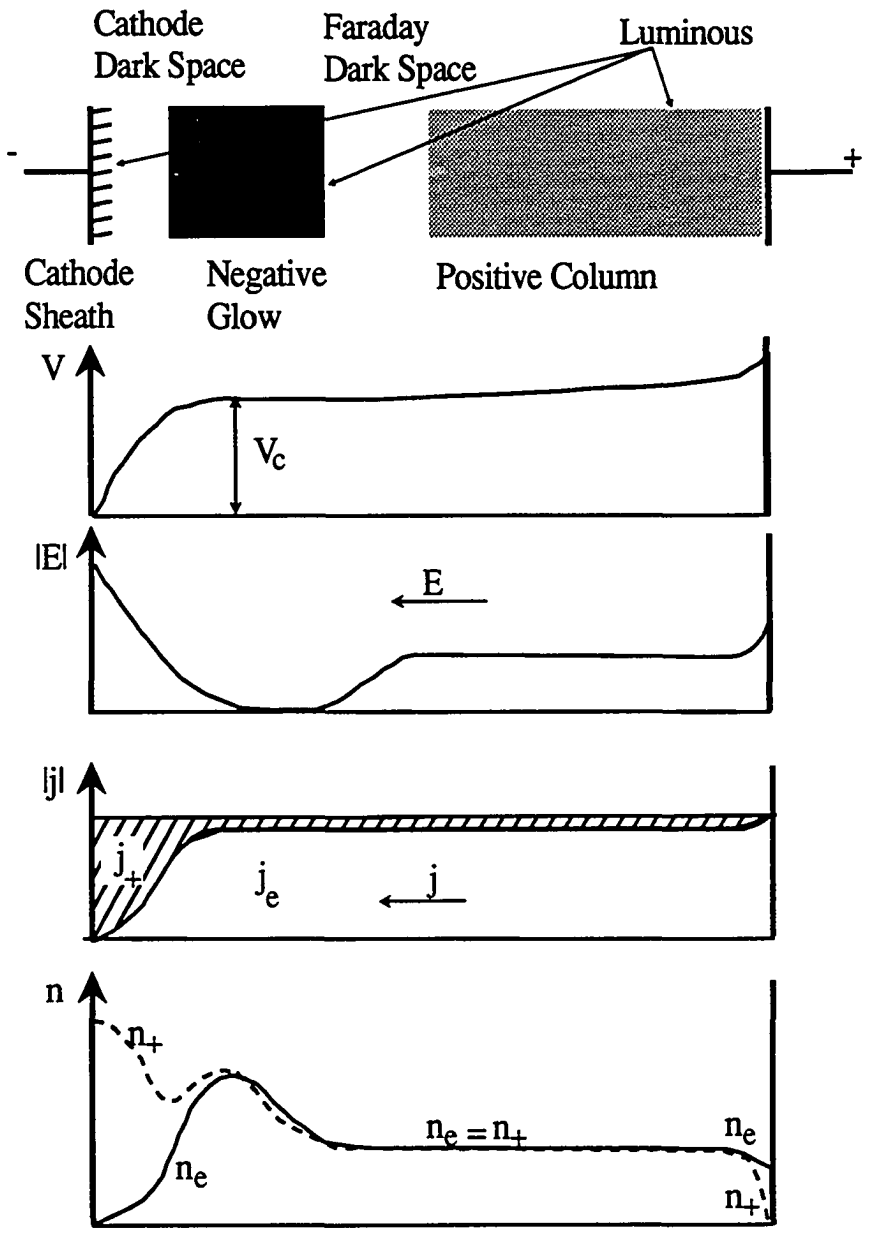

Fig. 2.2 Classical picture of the structure of a dc glow-discharge. After breakdown, the discharge arranges itself into characteristic regions to provide for particle and energy input [12].

negative glow region to the cathode where they will cause secondary electron emission with a probability of approximately 0.1 to 0.05. The secondary electrons will then be accelerated back through the cathode dark space by the potential and enter the negative glow region. Because of the large electric field that exists in the cathode dark space region, the electron density in this region is small. The electron density achieves maximum value at the negative glow region and gradually approaches a constant value in the positive column. There are approximately equal numbers of ions and electrons in the negative glow and positive column regions. Electron energy measurements within the positive glow show typical values of 2 - 10 eV. The source of energy input to the negative glow region includes the energetic secondary electrons emitted from the cathode and accelerated across the cathode dark space, and direct acceleration of the electrons in the glow by the electric field. The extent of the negative glow is determined by the range over which the energetic electrons lose their energy. This determines the location of the end of the negative glow region. However, there is a small electric field in the plasma regions of the discharge, and this electric field will increase the temperature of the electrons by acceleration and subsequent scattering. It will take a certain distance before the electrons reach their equilibrium energy and no light will be emitted at this distance. Beyond this distance, in the positive column, the electrons have equilibrated with the plasma in a small electric field. The local electric field accelerates the electrons and represents the main energy input source. The main losses in the positive column are diffusion to the walls and radiation from line emission.

Chemical reactions occurring in electrical discharges have attracted the attention of a large number of investigators for a long time[13,15-28]. The mechanism of such reactions, in many cases, can be explained in terms of dissociation into neutral fragments by electron impact. It has been found that dissociative excitation in low-current density discharges, such as the positive column of a glow-discharge, proceed as a result of single encounters between electrons and gas molecules in the ground state. Quantitative data on molecular dissociation in a discharge of this type are very limited. A direct measurement of the cross section for dissociation by electron impact is not possible in electrical discharges, since the electrons have a widely distributed range of energies. However, electronic collision processes can be measured in terms of a rate coefficient defined as the number of events produced by an electron in drifting a unit distance in the direction of the applied electric field. In turn, the dependence of the rate coefficient on average quantities, such as the discharge current and the applied field, can be determined. In the highly intricate structure of a dc glow-discharge, the homogeneous positive column is characterized by the fact that its electric field is uniform for all distances from the cathode, which has been the primary focus of past research on that region.

Corvin and Corrigan[22] used a pressure difference method to study the dissociation of CO_2 in the positive column of a glow discharge. The reaction rate was determined by separating and measuring the noncondensable products formed. The effects of the cathode and anode regions of the discharge were eliminated by varying the interelectrode distance to obtain the axial electric field in the positive column and also the molecular dissociation rate per unit length of column. The number of dissociating

collisions α_d/p by an electron drifting unit length along the field direction of the positive column was measured for values of E/p between 11 and 32 V/cm-torr showing corresponding values of α_d/p of 0.15 and 0.67 at these limits. The measured rate coefficients show that dissociation proceeds via uncharged species. The reaction mechanism $CO_2 + e^- <--> CO + O + e^-$ was found to be consistent with the observed phenomena. They suggested that the dissociative excitation is to a $^3\Pi$ state of CO_2, about 6.1 eV above the ground state. The collision cross section increased with voltage to a maximum of $3.5x10^{-17}$ cm^2 at 6.9 eV, and then decreased rapidly with increasing electron energies.

Volchenok, Komarov and Kupriyanov[23] used very sensitive and highly accurate mass spectrometers to study the chemical reactions which occur in the positive column of a gas discharge. The pressure in the discharge tube was 2 torr, and the flow velocity was 0.9 m/sec. They measured the concentration of atomic oxygen in glow discharges in O_2, CO and CO_2 mixed with He and found that the absolute concentration of atomic oxygen varied linearly with discharge current, as shown in Fig. 2.3. They did not observe a growth of the peak with m/e = 12 due to C atoms, and concluded that the reaction did not involve carbon atoms. They suggest the same reaction mechanism as that found by Corvin and Corrigan.

Sabadil and Pfau[24] used two different methods (the ozone method and the Wrede-Harteck method) to study the dissociation of oxygen in the positive column of a glow-discharge. The discharge pressure varied from 0.5 to 2.0 torr. The ozone method involves the reaction of atomic oxygen and molecular oxygen with S, on a surface cooled

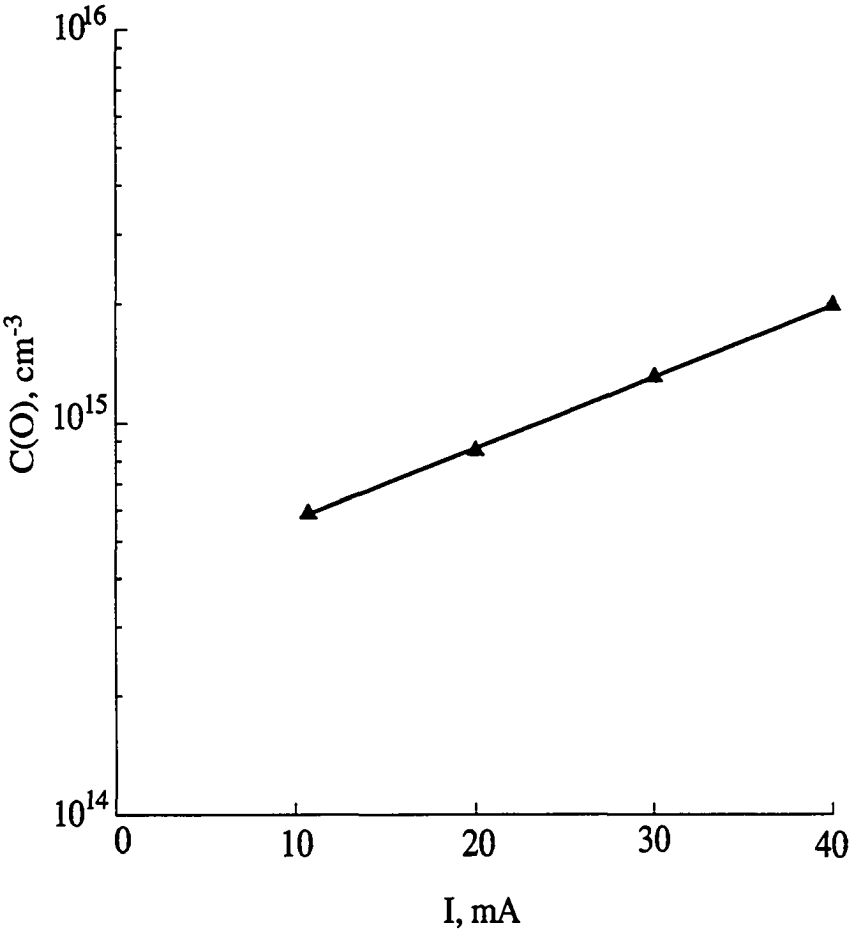

Fig. 2.3 Absolute concentration of atomic oxygen as a function of the discharge current for CO_2 - He (1:10).

by liquid nitrogen, as a form of O_3. When the surface was warmed to room temperature, an O_3 discharge was initiated which generated conversion, $2O_3 \rightarrow 3O_2$. The Wrede-Harteck method is based on the dependence of the flow conductivity upon the mass of the different oxygen particles for molecular flow conditions. Based on the good agreement between the dissociation rate found in the middle part of the positive column (W-H method) and at the end of the positive column (O_3 method) at not too high currents, they conclude an uniform axial distribution of the O atoms in the positive column exists. It was also found that the degree of dissociation increased with increasing discharge current and decreased with increasing pressure. Figure 2.4 shows the relative O concentration as a function of the current for different values of pressure.

In summary, past researchers have proved that glow-discharge can break the chemical bonds of gas molecules effectively, via electron impact. Since most of the potential drop occurs in the cathode sheath and the cathode dark space, the energetic secondary electrons emitted from the cathode will accelerated across the cathode dark space and enter the negative glow region. The extent of this region is determined by the range over which the energetic electrons lose their energy. Because both the electron energy and the electron density are maximum at negative glow region, it appears that the breakdown of the molecular bond must be most efficient in this region as well. Unfortunately, because of the highly complicated structure of a dc glow-discharge, the chemical reaction in the glow-discharge has only been investigated in the homogeneous positive column. Even in this region, very little quantitative information is available on the dissociation of CO_2 and O_2 molecules. With this limited information, however, the

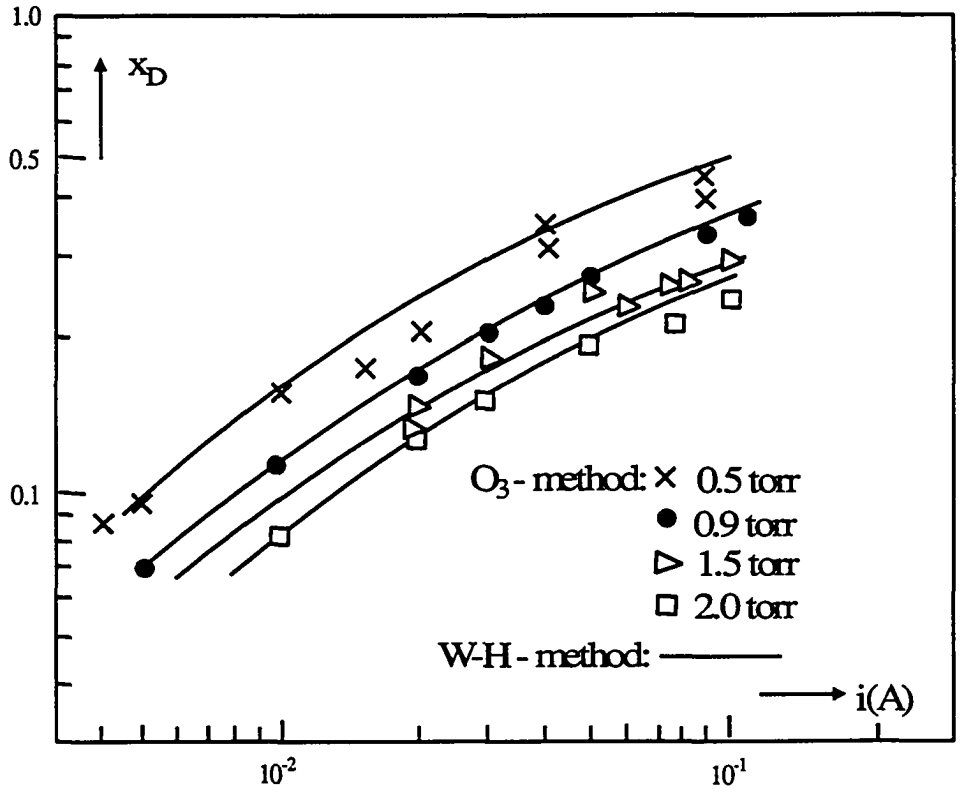

Fig. 2.4 Relative O concentration x_D as a function of the current for different values of pressure.

reaction mechanisms of $CO_2 + e^- <--> CO + O + e^-$ and $O_2 + e^- <--> O + O + e^-$ in a glow-discharge have been recognized and verified. It was found that the degree of dissociation in the positive column of a glow-discharge increased with increasing discharge current and decreased with increasing pressure. All of the above observations have been obtained below two torr, which is much smaller than the pressure range of this experiment, and was limited to the prolonged positive column region. With a compressed positive column as with this experiment, the efficient dissociation in the negative glow region will have a strong influence on the distribution of the atomic oxygen in the positive column. Also with higher discharge pressure (5 torr), it is expected that the reduced mean free path will cause the atomic oxygen to recombine to form O_2 quickly, resulting in a non-uniform axial distribution of O atoms in the positive column region.

2.2 Surface Properties

Another question considered here is how the atomic and molecular oxygen interact with the silver membranes since they will play the role of an oxygen filter to extract oxygen from mixtures of CO_2, CO, O_2 and O in the glow-discharge.

The interaction between oxygen and a silver surface has received much attention over the past 70 years, mainly because of the high activity of silver for the selective epoxidation of ethylene. Ethylene oxide is primarily an intermediate stage for various organic syntheses, such as the production of solvents, artificial fibers, preparations for textiles, and detergents. To produce ethylene oxide, ethylene is transformed by reaction with atomic oxygen adsorbed on a silver surface (T ≈ 250°C) according to:

$$CH_2{=}CH_2 + \frac{1}{2}O_2 \xrightarrow{Ag} CH_2\text{-}CH_2 \quad (O)$$

Almost all of the present understanding of this system was derived from studies of molecular oxygen adsorbed on the (100), (110), and (111) single-crystal surfaces of silver [30-50]. The inconsistencies among these studies show unequivocally that the chemical binding of oxygen on silver is not well understood at this time. These discrepancies seem to arise from the various oxygen exposure conditions employed. The results of these studies are summarized briefly for each of the three surfaces.

O/Ag(100). While only limited research has been reported for this surface, the sticking coefficient for oxygen on this surface is on the order of 10^{-5} to 10^{-6}. This is a very small value, which suggests that the molecular orbitals of the oxygen are, in general, repelled by the surface and that adsorption occurs most likely at defects. Based on work function measurements, the existence of two binding states of oxygen on this surface have been tentatively proposed[30]: One state, which exists alone at temperatures above 97°C, and a second state, which increases in relative concentration with decreasing temperature. Oxygen exposure causes a decrease in the spot intensity of the 1 x 1 low-energy-electron diffraction (LEED) pattern of the clean surface. The appearance of new diffraction spots upon oxygen adsorption is a controversial topic. Two observations have been presented in the literature[30,42]. One observation claims that new diffraction spots appear, the occurrence of which suggests that adsorption is either disordered or in a phase with a 1 x 1 structure. The second observation is that oxygen adsorption causes facets of the (410) plane to form which are inclined 14° relative to the (100) surface domains. Regardless of the surface distribution that actually occurs, the overall surface concentration of oxygen is very low. Auger electron spectroscopy (AES) shows only a barely detectable oxygen signal (The minimum detectable concentration is about 1%). Thermal desorption of adsorbed oxygen from this surface occurs near 240°C.

O/Ag(110). The (110) surface is the most reactive toward oxygen with an initial sticking coefficient of approximately 10^{-3}. Although this is still a small value, the increased reactivity is probably because of the ribbed surface structure, where only the

O_2 molecules which are aligned with the valleys at the moment of collision are dissociatively adsorbed, as shown in Fig. 2.5. The initial sticking coefficient decreases with increasing temperature, an occurrence which may provide evidence for a precursor state for chemisorption of oxygen. Based on LEED patterns obtained from a room-temperature oxygen exposed (110) surface with various exposure conditions, the maximum surface coverage is proposed to be half a monolayer $\approx 5 \times 10^{14}$ atoms cm^{-2}. In addition to the precursor state, three adsorbed states of oxygen have been proposed: (1) an adsorbed dioxygen state; (2) an adsorbed dissociated oxygen state; and (3) a subsurface dissociated oxygen state. The dioxygen state has been observed most commonly at temperatures below -153°C where van der Waals forces predominate and it produces a diffraction pattern which indicates a 2 x 1 to 2 x 7 structure, depending on the coverage. It has also been proposed that a dioxygen adsorbed state exists at 200°C, following oxygen exposures at or exceeding 0.1 torr. However, it is not clear presently if these dioxygen states are the same. The dissociated oxygen state is formed by exposure at temperatures equal to or greater than -103°C or by heating an already exposed surface above -103°C. This state is the most prominent adsorbed state of oxygen above -103°C, but the binding site is unknown. None of the bonding models proposed today take into account probable adsorbate-induced surface reconstruction nor are they consistent with the available data. The subsurface dissociated oxygen which is stable up to 327°C is formed by heating an oxygen-exposed surface above 147°C. Above 327°C, the surface and subsurface oxygen atoms combine and desorb as O_2. It has also been suggested that this subsurface oxygen migrates to the surface at temperatures near 267°C[31].

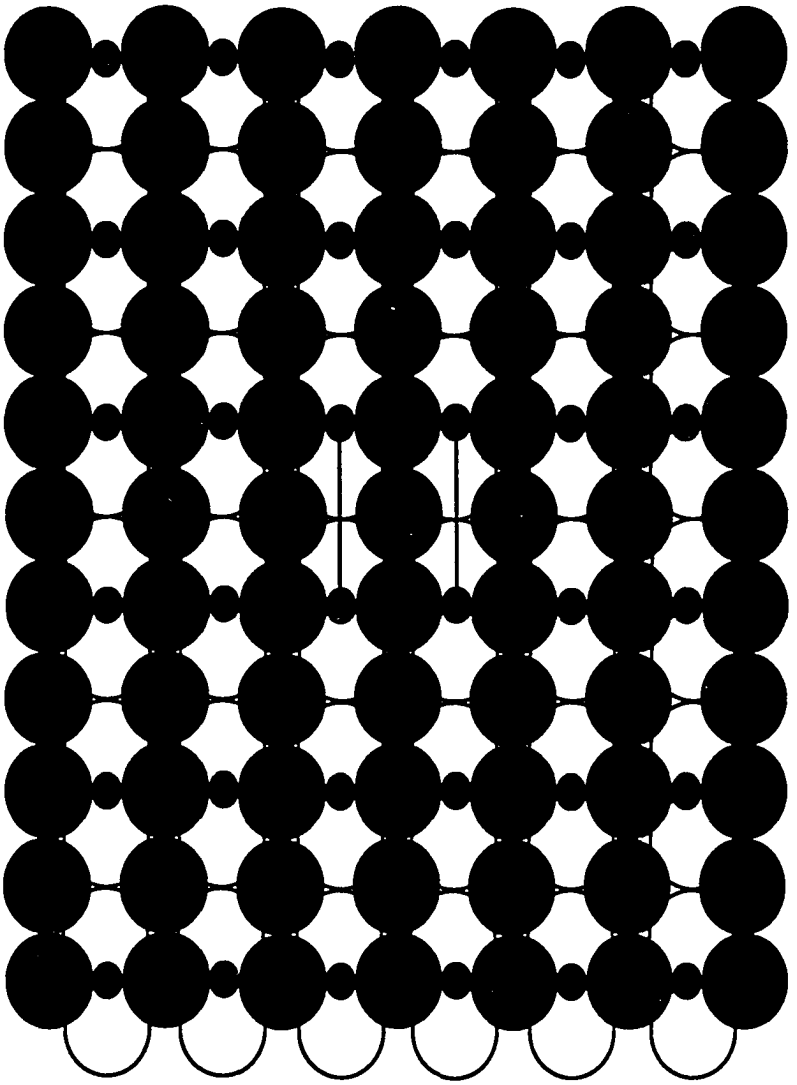

Fig. 2.5 Hard sphere model of the Ag(110) face with adsorbed oxygen atoms (small spheres) [30].

O/Ag(111). The (111) surface is similar in oxygen reactivity to the (100) surface in that it has a sticking coefficient on the order of 10^{-6}. At temperatures below -123°C, the prominent surface species is O_2, which desorbs near -58°C. This suggests, as in the (100) case, that van der Waals forces are dominant. Above -58°C, the adsorbed state of oxygen is controversial. It is not clear whether an adsorbed dioxygen species exists above -58°C. An exposure of 1 to 2 torr oxygen in the range of 127°C to 227°C results in a diffraction pattern with a p(4 X 4) structure. This structure is stable up to a temperature of approximately 307°C, where it associatively desorbs as O_2. As for the (110) surface, a subsurface state is proposed which desorbs above 327°C.

In summary, past research on the surface properties for the O/Ag system has documented a very small sticking coefficient with virtually no adsorption on the (100) and (111) planes and the estimated maximum surface coverage is only about half a monolayer on the (110) plane at room temperature[30,34]. This indicates little oxygen affinity for adsorption on single crystal silver and suggests a barrier to oxygen dissolution into the bulk. Polycrystalline silver was used in our research, and it contains all the binding states associated with the single crystalline surfaces described above. In addition, the higher grain boundaries, facets and other defect densities associated with polycrystalline silver could be important for oxygen adsorption and dissolution into the silver surface. Therefore, studies of single-crystal surfaces may only offer a general indication of the behavior of a polycrystalline surface. As for the (110) surface, a subsurface state is proposed which desorbs above 327°C. A temperature of 350°C, which is the low end of the temperature range in our experiments, is sufficient for desorption of the surface

oxygen to occur. Hence, no surface-controlled phenomena appear to be able to limit the thermal evolution of oxygen from the surface in our experiments.

All the above studies have only been concerned about the interactions of molecular oxygen with silver single crystalline surfaces. As shown in Fig. 2.5, for chemisorption to occur, the oxygen molecules need to hit the surface at specific locations and in the right orientation in order to be dissociated into atoms and absorbed subsequently. On the other hand, if the incoming gas is atomic oxygen, it will be much easier for it to find an available surface site for absorption since it already exists as a single atom and does not require extra energy for dissociation. Outlaw in his permeation experiments[51] found that simply adding a dc glow-discharge dramatically increased the transport rate of pure oxygen through a polycrystalline silver membrane. When the upstream O_2 gas was replaced by CO_2, only a small permeation signal was observed, but the application of the glow discharge increased the transport flux substantially, by about two orders of magnitude. The presumed reason was due to the atomic oxygen generated by the glow-discharge. Figure 2.6 shows the changes of the flux level before and after the glow-discharge was initiated. Similar phenomena have been observed in the permeation of hydrogen through Molybdenum via glow-discharge[52]. This is very important for our experiments since one of the primary products of the CO_2 dissociation via glow-discharge is atomic oxygen. Unfortunately, no detailed experimental work has been done at present to study the behavior of the interaction of atomic oxygen with silver primarily.

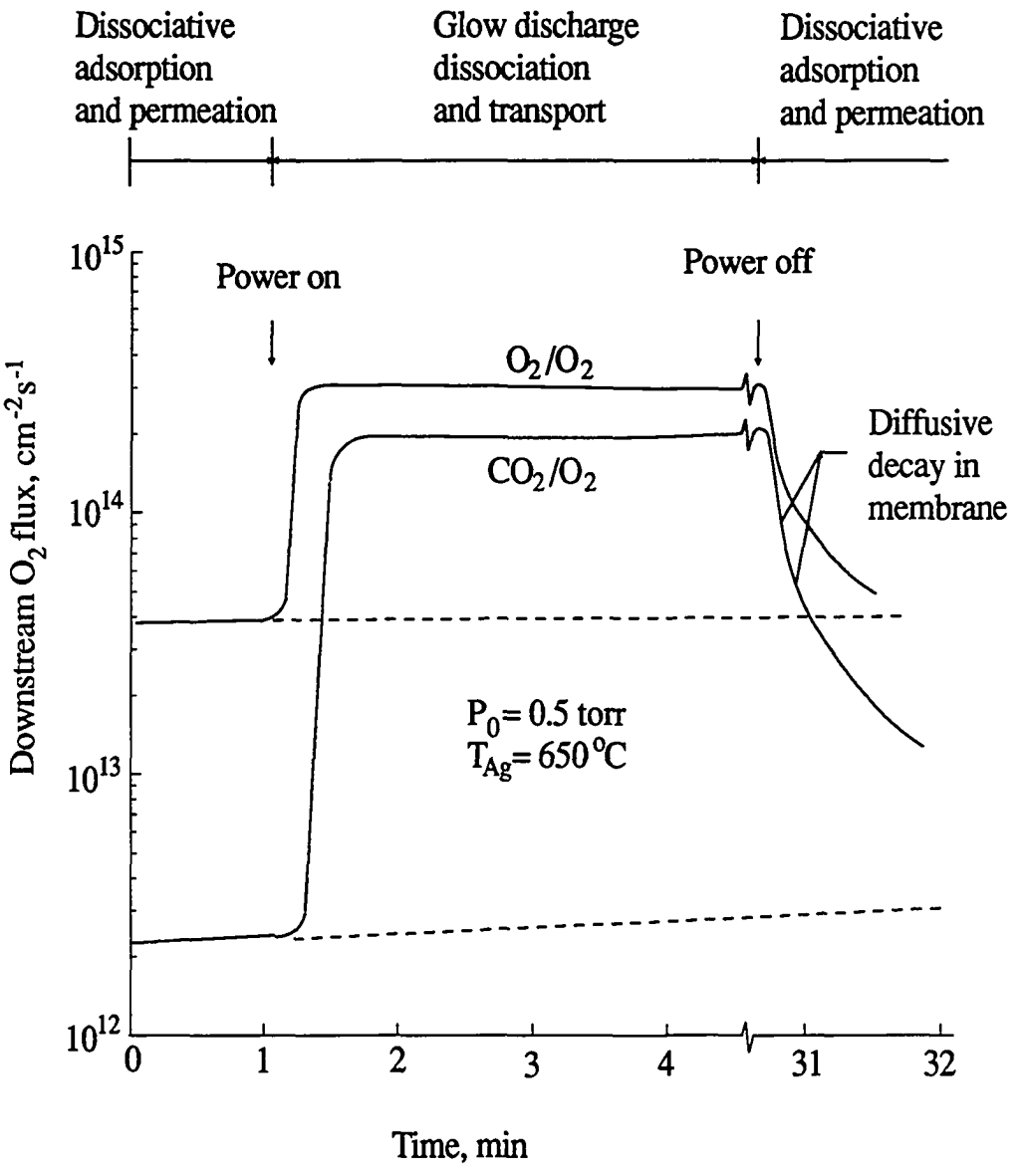

Fig. 2.6 Downstream oxygen flux variations due to oxygen permeation with and without supply side glow-discharge-assisted dissociation. The dashed lines represent the permeation from dissociative adsorption.

2.3 Transport Properties

Past research on surface properties have shown that molecular oxygen must first dissociate into atomic oxygen before it can be adsorbed and incorporated into the octahedral sites of the silver lattice. The reported data have shown that the sticking coefficient for molecular oxygen on silver is very small. There is virtually no information available on the sticking coefficient of atomic oxygen on the silver, justifying the present study. After an oxygen atom is incorporated into the octahedral sites of the silver lattice, it will diffuse through the silver lattice by way of oxygen concentration gradients. It will not matter whether the concentration of the oxygen atoms at the top few layers of the upstream surface has come from the molecular or atomic oxygen in the gas phase. Hence, the transport properties should be the same for ordinary oxygen permeation as for the oxygen permeation with glow-discharge. The studies of the transport properties via ordinary oxygen permeation should apply for the case of oxygen permeation with glow-discharge.

Although the number of investigations into the surface physics of molecular oxygen on silver are quite extensive, very little work has been done on the transport properties of oxygen through silver. Among the most fundamental diffusion mechanisms, the interstitial mechanism is the most encountered one in gas-metal systems because of the relative small solution size in comparison to the size of solvent matrix. In the interstitial mechanism, atoms naturally dissolve in a host lattice by occupying interstitial positions and can diffuse through the lattice structure without normally occupying rational

lattice sites. As a result the solute atoms, which are capable of forming interstitial solutions, must be relatively small compared to those of the solvent matrix. This mechanism is generally confined to the first ten or so elements of the periodic table. Most of the gases, such as He, H_2, N_2, and O_2 dissolve interstitially in a variety of metals, where they dissociate and are atomically dispersed in the solid phase. The generally small size of the interstitials permits rather free jumping between interstices with no need to wait for the arrival of a vacancy. Oxygen in Ag is one of such gas-metal system. Generally speaking, for such a system, Sievert's Law applies for the case of ideal solutions and perfect gases where the concentration of dissolved gas is proportional to the gas pressure:

$$C=SP^n \tag{2.1}$$

where C is the concentration of dissolved gas, S is the solubility, P is the gas pressure and n equals 1. For bimolecular gases, if dissociation precedes solution of the gas; e.g., O_2 (gas) $\rightarrow$ 2O (dissolved), n equals 1/2.

Thermodynamics predicts that pure perfect crystals are unstable and tend to absorb defects from their surroundings. The equilibrium concentration of the impurities in crystals can be expressed by the equation:

$$S=S_0\exp(-\frac{\Delta H}{RT}) \tag{2.2}$$

where S is the solubility coefficient, S_0 is an entropy factor, and ΔH is the solution enthalpy. This equation indicates that the number of solute atoms that can be dissolved by the system is zero at 0°K and increases exponentially with temperature.

Eichenauer and Meuller[53] studied polycrystalline silver in 1962 using the desorption technique which is based on observing the release of gas from a gas-charged

metal body. The gas escaping from the metal is transferred to a collector vessel and the accumulation over time is tracked using pressure measurements. The diffusion and solubility coefficients can be calculated from the resulting gas release curves. The gas released from a metal usually follows the laws of volume diffusion, however, there are many processes with which the escape of an atomically dissolved gas from a solid can be effected. There is a strong possibility that interface processes may govern or at least influence the gas release and hence cause misinterpretation of the results. To isolate this problem, Eichenauer and Muller[53] used specimens of different dimensions and shapes to determine if there is surface interference upon desorption. All the specimens was prepared with 99.995% pure silver, melted in a vacuum (10^{-3} torr) in a quartz crucible, and poured into chills. The specimens were rolled and turned into three different sizes and shapes: cylinders with 0.53 cm diameter and 29.85 cm long, small spheres of 0.98 cm diameter and large spheres of 2.99 cm diameter. To remove surface impurities, all the specimens were pickled for 1 hour in a 10% aqueous solution of hydrochloric and tartaric acids. The oxygen used in the experiment was produced at 300°C from potassium permanganate, condensed in a vessel chilled with liquid nitrogen and purified by repeated distillation, freezing out all likely impurities. All the 38 measurements were performed in the temperature range between 412°C and 863°C, at various pressures. The results are shown in Figs. 2.7 and 2.8. The solubility, S, and diffusivity, D, for oxygen in silver were found to obey the following relationships:

$$S=1.42x10^{21}\exp(-\frac{11860}{RT}) \quad cm^{-3} \tag{2.3}$$

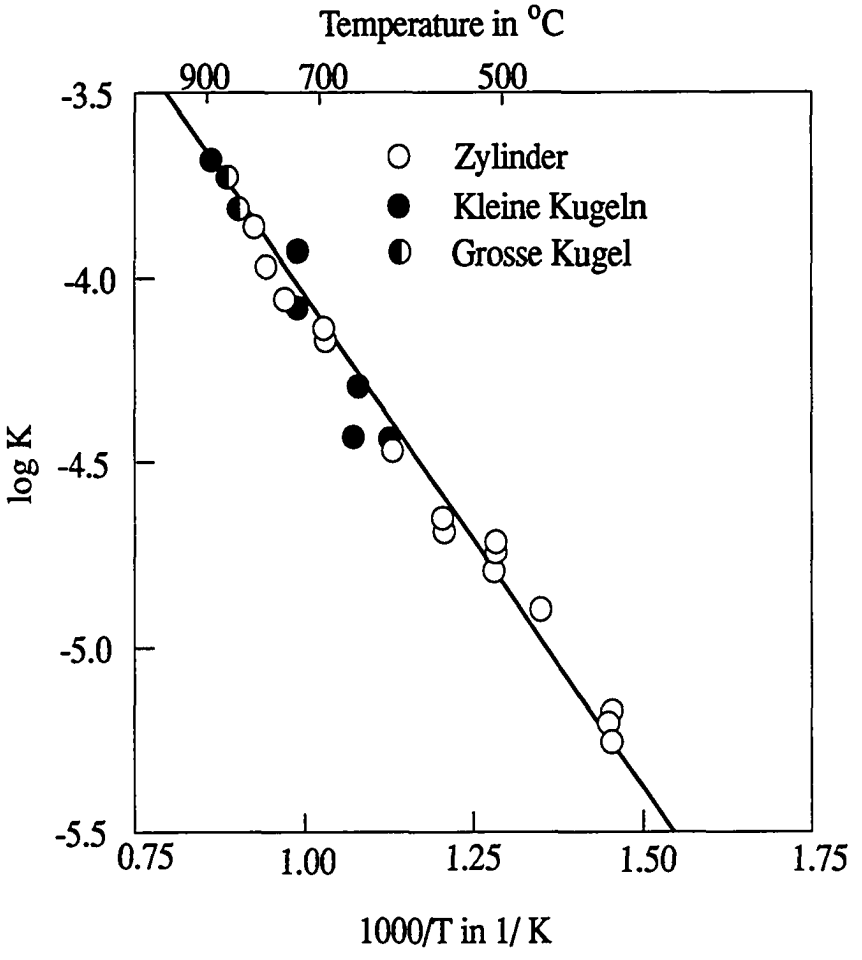

Fig.2.7 Permeability of oxygen in polycrystalline silver as a function of reciprocal temperature [53].

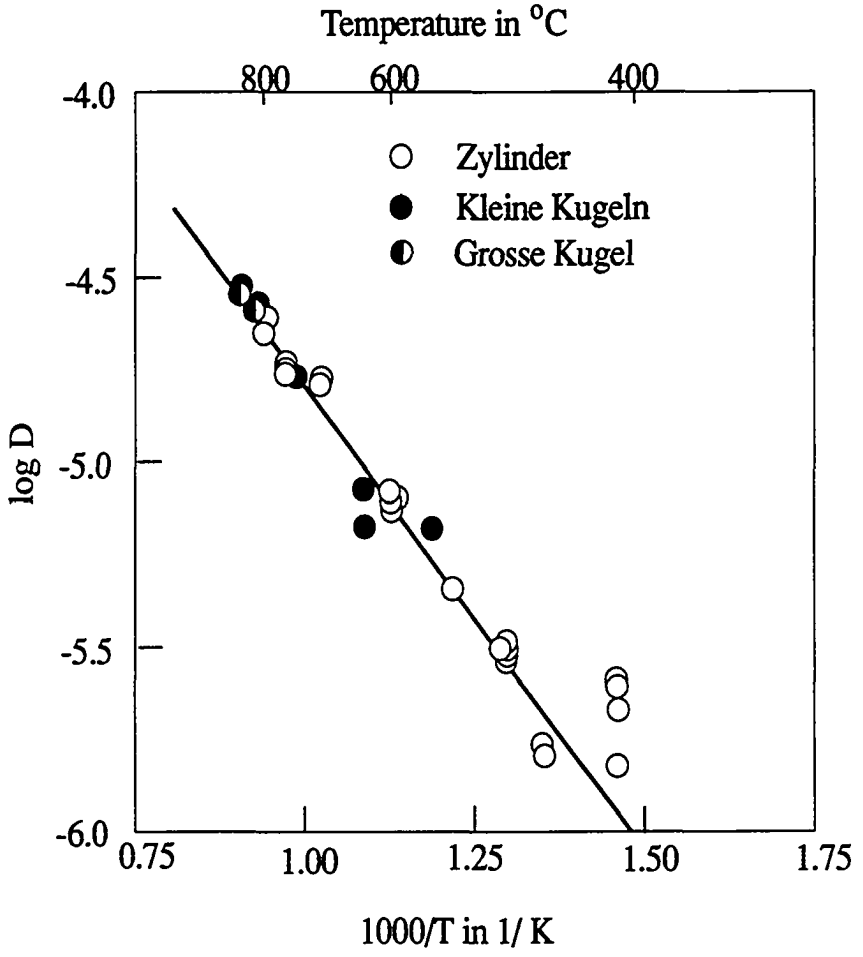

Fig. 2.8 Diffusivity of oxygen in polycrystalline silver as a function of reciprocal temperature [53].

and

$$D=3.66x10^{-3}\exp(-\frac{11000}{RT}) \quad cm^2s^{-1} \tag{2.4}$$

According to the measurements at constant temperature and different pressures, it was found that Sievert's Law ($C = SP^{1/2}$) applied to the solubility of oxygen in silver. The dissolution of oxygen and subsequent migration of oxygen atoms through silver followed the dissociation of the oxygen molecules into atoms at the surface. Within the error limits, the gas release curves of all specimens followed the law of volume diffusion. The low solubility and very slow development of diffusion below 400°C impeded measurements in this temperature range, most likely because of the increasing stability of the surface adsorption below 400°C. Since it was found that the activation energy for diffusion is relatively low (11 kcal/mole), it was concluded that the diffusion takes place between interstitial sites.

Coles[54] studied the permeability of silver to oxygen, using the same desorption technique, for the purpose of developing an oxygen gas leak for an accelerator ion source. He did not report what kind of silver was used. The temperature range was between 500°C and 850°C. He found that the process obeyed Sievert's Law, in agreement with Eichenauer and Muller[53]. However, the permeability he measured was almost one decade higher than those obtained by Eichenauer and Muller. Silver is known to be very sensitive to impurities, which restrict grain growth, since the segregation of these impurities to the grain boundaries tends to slow down or stop intergranular transfer of silver atoms from smaller to larger grains. Some experiments with refined silver (99.9% purity) did not yield reproducible results and subsequent microscopic examination

revealed pores in the edge zone of the refined silver specimens. Since Coles did not report the purity of his silver, an explanation for the higher permeability level, compared with Eichenauer and Muller's cannot be determined. It is possible that his diffusion is greater due to defects and a higher grain boundary density. If there was porosity, it could also result in an increased solubility. As studied by Coles, one of the convenient ways to eliminate many of the gas impurity problems is to introduce the desired gas through a permeation membrane which is specific to that gas alone, thus effecting a filtration of impure gas for the desired species. Nickel and palladium are used to purify and introduce hydrogen isotopes into a vacuum system. Vitreous silica is used as a helium membrane and silver is used to introduce oxygen. In order to examine gas purity and system response associated with using silver to introduce oxygen, Beavis[55] studied oxygen permeation through a silver tube at a temperature of about 550°C. A monopole gas analyzer was used to record the changes in mass-spectra continuously during the experiment. It was found that silver could be contaminated heavily with hydrogen, carbon, and sulfur. However, after long periods of oxygen flow, the sulfur dioxide, organic materials and carbon oxides decrease after the oxygen begins to flow at the expected steady state rate.

Ramanarayanan and Rapp[56] studied the diffusivity of oxygen through silver at high temperatures (750°C to 950°C) using the electrochemical technique. The experiment consisted of a solid electrolyte tube with an external porous platinum electrode and solid silver inside the tube. The silver was first melted and most of the oxygen was pumped out of it with an applied voltage of +1.5 V at 1100°C. The furnace was then cooled at

a rate of 15°C to 20°C per hour until solidification had proceeded from the bottom of the melt to the top. During solidification, the bottom of the metal was kept about 10°C cooler than the top of the metal. After solidification, the cell portion of the tube was adjusted until it was located in the constant temperature zone of the furnace. Pump-out curves of cell current vs time were recorded using applied voltages in the range from 0 to 200 mV. During the experiment, a purified argon atmosphere was maintained over the surface of the liquid or the solid metal. The experimentally determined values for the diffusivities and solubilities of oxygen in solid silver agreed closely with the values of Eichenauer and Muller[53].

Gryaznov, Gul'yanova and Kanizius[57] studied permeability and diffusivity of oxygen through polycrystalline silver at low temperatures using the permeation technique. A degassed silver tube (99.99% purity), 240 mm in length, with an outside diameter of 3 mm and a wall thickness of 0.2 mm was used as a membrane. After the tube was bent into a spiral shape, it was sealed within a molybdenum glass sphere which contained a mass-spectrometer. The system was first evacuated until the oxygen peak intensity, indicated by the mass spectrometer, was less than 0.03 volts. Then oxygen was admitted into the tube and increases in the oxygen peak were recorded until equilibrium was established. Employing the measured temperature, pressure difference and time, the diffusivity and permeability were calculated. The temperature range was between 250°C and 400°C. The permeability and the diffusivity were found to obey the following relationships:

$$K=5.92x10^{18}\exp(-\frac{20356}{RT}) \quad cm^{-1}s^{-1} \tag{2.5}$$

and

$$D=4.67X10^{-4}\exp(-\frac{8093}{RT}) \quad cm^2s^{-1} \tag{2.6}$$

The values of the activation energies are lower significantly than those obtained in previous research[53-56].

Outlaw, Sankaran, Hoflund and Davidson[58] studied permeability and diffusivity of oxygen through large grain polycrystalline silver membranes under ultrahigh vacuum conditions. Data were obtained over the temperature range between 400°C and 800°C. The specimens were prepared with 99.9999% pure silver, melted in a vacuum(10^{-8} torr) and spark machined into a disk geometry with a diameter of 10.7 mm, which means that less contaminated silver has been used compared with that of previous researchers. The permeability and diffusivity were determined directly from experiment and the solubility determined by calculation (Eichenauer and Muller determined solubility and diffusivity coefficients from experiment and the permeability was calculated). It was found that above 630°C, the permeability and diffusivity agreed closely with Eichenauer and Muller's, but below 630°C, they found a change in the slope of the diffusivity curve and the diffusion activation energy they determined is considerably higher than that of Eichenauer and Muller. Outlaw et. al. concluded that this could probably be explained by the higher efficiency of trapping at the lower temperatures. This trapping effect has also been observed for hydrogen in iron and hydrogen in alloyed copper[59].

Outlaw, Wu, Davidson and Hoflund[60] studied permeation of oxygen through Ag(110), Ag(poly), Ag(nano) and Ag2.0Zr, over the temperature range of 400-800°C. A surface limitation was confirmed by glow-discharge studies where the upstream O_2 supply was partially converted to atoms, which, for the same temperature and pressure, produced

more than an order of magnitude increase in transport flux. Furthermore, the addition of 2.0 wt % Zr to the Ag increased dissociative adsorption rates which in turn increased the transport flux by a factor of two. It was also observed that below a temperature of 630°C, the diffusivity exhibited an increase in activation energy of over 4 kcal/mol, which has been attributed to trapping of the atomic oxygen and/or kinetic barriers at the surface and subsurface of the vacuum interface. Above 630°C, the activation barrier decreases to its accepted value, consistent with zero concentration at the vacuum interface. Figures 2.9 and 2.10 show comparisons of permeability and diffusivity between polycrystalline silver, single crystalline silver and a silver alloy.

In summary, octahedral site diffusion has been shown to be the controlling mechanism for the O/Ag system. The permeability data as a function of temperature all follow a linear Arrhenius plot, as expected theoretically, with the activation energies comparable to each other. The diffusion activation energy at low temperatures, however, differs considerably in the literature. The reason was found to be at least partially due to the different purity of the silver samples used and was also because of a higher efficiency of trapping at lower temperatures[58,59]. The use of UHV techniques also permitted more accurate measurements at low temperatures. The square-root form of Sievert's Law has been found to apply in determining the solubility of oxygen in silver when only molecular oxygen is in the gas phase. When the glow-discharge was introduced to partially break the molecular bonds of molecular oxygen, to produce atomic

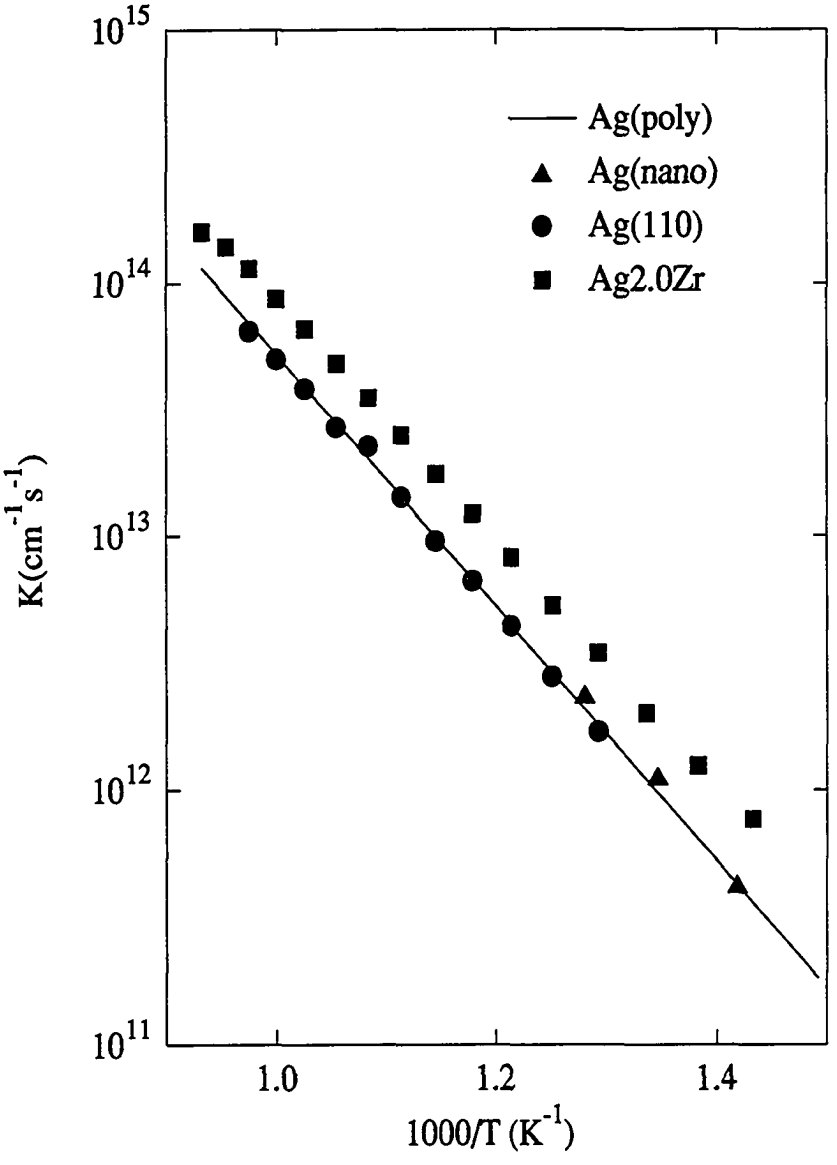

Fig. 2.9 The permeability of oxygen through Ag(110), Ag(poly) and Ag(nano) membranes.

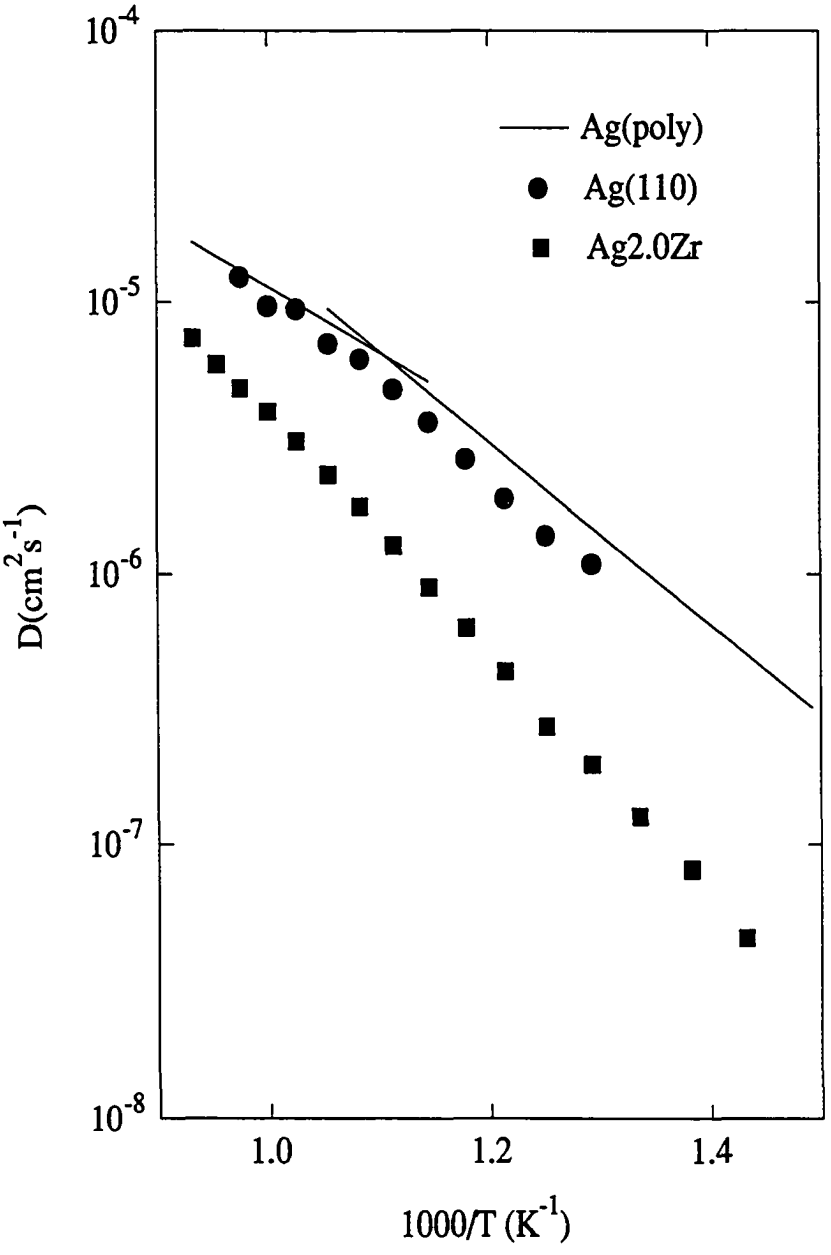

Fig. 2.10 Diffusivity values as a function of reciprocal temperatures for Ag(110), Ag2.0Zr and Ag(poly).

oxygen, a significant increase in the oxygen flux through the silver membrane was observed, which indicated that the silver was super-saturated with oxygen when atomic oxygen is present in the gas phase. The higher sticking coefficient for atoms results in a higher upstream surface concentration and therefore a higher oxygen flux through the membrane. Adding Zr to silver improves the dissociative adsorption rate significantly because of the higher affinity of Zr to oxygen. This results in a higher surface concentration of oxygen and therefore, a higher concentration gradient. In glow-discharge work, the concentration of oxygen atoms in the surface layers is also enhanced and no longer obeys the square-root relation of Sievert's Law. The overall transport rate will be affected significantly by the results of how much the surface can be super-charged with atomic oxygen. This is one of the major problems addressed in this research.

In this chapter, a summary of the literature survey on glow discharge properties, Ag surface properties and the properties of oxygen permeation through silver has been presented. The information on the theoretical analysis and the calculation of the oxygen flux through the Ag membrane and the diffusivity of atomic oxygen in Ag are presented in next chapter.

Chapter 3

THEORETICAL ANALYSIS

3.1 Diffusion of Oxygen Atoms in Ag Solid Solution

Atoms that normally reside in interstitial positions diffuse through silver by making a series of elementary jumps to nearest neighbor interstitial positions as shown in Fig. 3.1. The simplest forms of the diffusion equation are regarded as purely phenomenological descriptions, and relate the rate of flow of matter to its concentration gradient, which is known as Fick's first law:

$$J=-D_i\nabla C_i \tag{3.1}$$

and

$$\frac{\partial C}{\partial t}=D_i\nabla^2 C_i \tag{3.2}$$

The latter expression is known as Fick's second law. Here, J is the flux, defined as the number of particles passing through a plane of unit area per unit time, C is the concentration, and D_i are the diffusion coefficients (or diffusivities) along the three principal crystallographic axes.

In the one-dimensional case, consider two adjacent lattice planes located at x and $x + \Delta x$, as shown in Fig. 3.2. Suppose the concentration of the oxygen atoms per unit

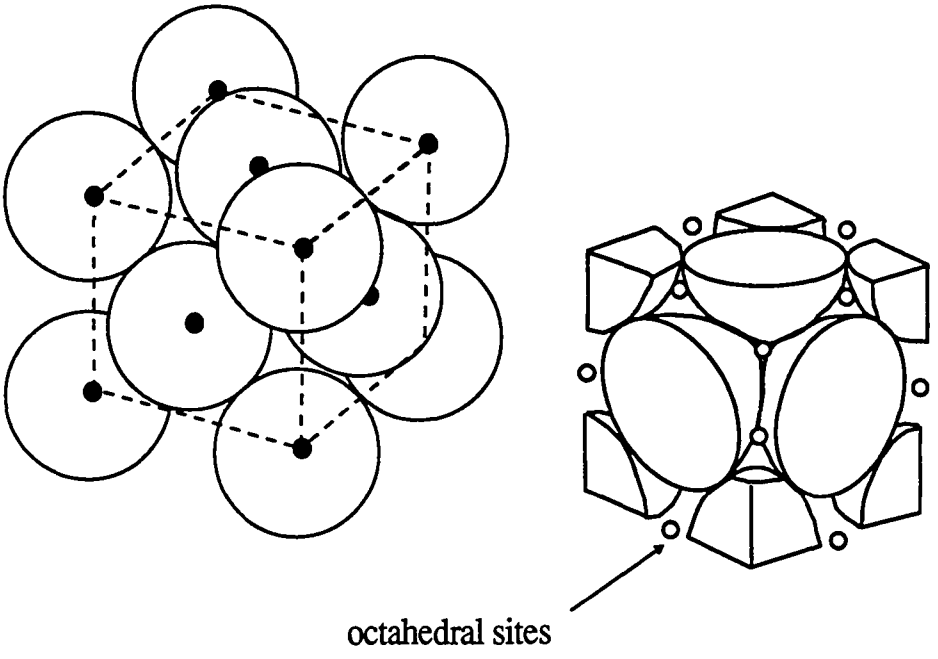

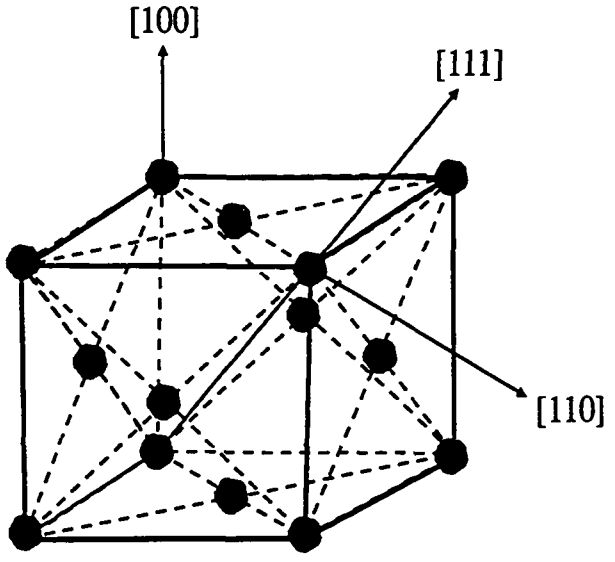

Fig. 3.1 Schematic view of face-centered cubic cell with O atoms on octahedral sites.

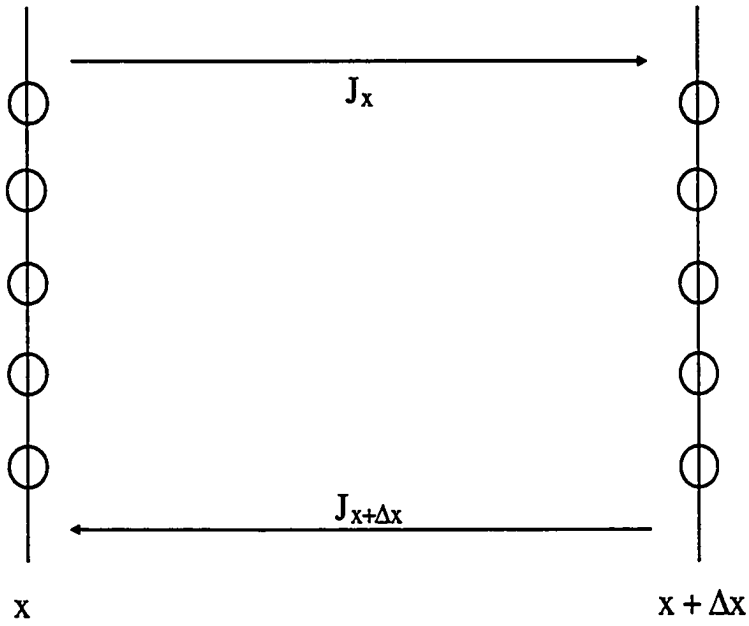

Fig. 3.2 Adjacent lattice planes illustrating one-dimensional diffusion in which atoms exchange positions by jumping Δx.

area at x is N_x and $N_{x+\Delta x}$ at $x+\Delta x$. Let all the diffusing atoms be of the same element and assume that the diffusivity coefficient, D, is independent of concentration. Furthermore, the atoms are restricted to diffusive jumps between nearest neighbor positions, which is generally the case for all real solids. Then, since there is equal probability for the atoms to jump in either direction, the flux of atoms moving from left to right at x is given by

$$J_x=\frac{1}{2}\Gamma N_x \tag{3.3a}$$

Similarly, at $x + \Delta x$, we can write

$$J_{x+\Delta x}=\frac{1}{2}\Gamma N_{x+\Delta x} \tag{3.3b}$$

where Γ, the mean jump frequency, is the average number of times that an atom changes lattice sites per second. Therefore, the net flux expressed in terms of concentration per unit area is given by

$$J=J_{x+\Delta x}-J_x=\frac{1}{2}\Gamma(N_{x+\Delta x}-N_x) \tag{3.4}$$

and in terms of concentration per unit volume and the concentration gradient:

$$J=\frac{1}{2}\Gamma(\Delta x)\frac{N_{x+\Delta x}-N_x}{\Delta x}=\frac{1}{2}\Gamma(\Delta x)\frac{\Delta N_x}{\Delta x} \tag{3.5}$$

Because Δx, the lattice spacing, is very small compared to the total diffusion path, we can replace $\Delta N/\Delta x$ by the concentration ΔC and taking the limit

$$J=\frac{1}{2}\Gamma(\Delta x)^2\frac{\partial C}{\partial x} \tag{3.6}$$

Here, Δx can be replaced by "a", the distance of separation of nearest neighbors. The extension of this derivation to three dimensions is done by taking the appropriate values

of Γ and a, along each of the principal crystallographic axes. Since Γ and the distance between nearest interstitial neighbors along all principle axes must be the same

$$J=-\frac{1}{6}\Gamma a^2\frac{\partial C}{\partial x} \tag{3.7}$$

For a silver crystal (FCC, face centered cubic), there are six principal crystallographic axes and the distance of the lattice spacings along the six principal axes are the same. So, Eq. (3.7) can be written as

$$J=-\frac{1}{12}\Gamma a^2\frac{\partial C}{\partial x} \tag{3.8}$$

If Eq. (3.8) is compared with Eq. (3.1), D equals:

$$D=\frac{1}{12}a^2\Gamma \tag{3.9}$$

Since interstitial diffusion requires that a vacant site be adjacent to the diffusing atom, the mean jump frequency will be a function of the probability that the diffusion atom possesses a nearest neighbor vacancy. Equation (3.9) can then be written as:

$$D=\frac{1}{12}a^2\Gamma' X_v \tag{3.10}$$

where X_v is the atom fraction of the interstitial vacancies and Γ' is a constant. This formalism does not include any correction for orientation effects.

In terms of classical thermodynamics, we can consider interstitial sites to behave as though they were a very dilute solute which forms an ideal solid solution with the host lattice. The change in entropy is then simply the ideal entropy of mixing:

$$\Delta S_m=-R[N_v\ln\frac{N_v}{N}+N_a\ln\frac{N_a}{N}] \tag{3.11}$$

where ΔS_m is the mixing entropy; N_a is the number of moles of oxygen atoms; N_v is the number of moles of interstitial vacancies; N is the total number of moles of the interstitial sites and R is the gas constant.

For the standard Helmholtz free energy of formation of the vacancies, we have

$$\Delta F_v = N_v(\Delta E_v - T\Delta S_v) + T\Delta S_m \tag{3.12}$$

where ΔF_v is the free energy due to vacancies; E_v is the internal energy per mole vacancy; S_v is the vibrational entropy per mole vacancy. This free energy must be a minimum if the crystal is in equilibrium; that is, the number of vacancies in the crystal will seek the value that minimizes the free energy at any given temperature, or

$$\frac{\partial F_v}{\partial N_v} = \Delta\mu_v = \Delta E_v - T\Delta S_v + RT \ln\frac{N_v}{N} = 0 \tag{3.13}$$

where μ_v is the chemical potential.

At equilibrium, $\mu_v = \mu_v^\circ$, and we can identify ΔE_v and ΔS_v as the standard internal energy and entropy of formation respectively, ΔE_v° and ΔS_v°. Thus, we finally obtain

$$\Delta E_v^0 - T\Delta S_v^0 + RT \ln\frac{N_v}{N} = 0 \tag{3.14}$$

Now since $X_v = \frac{N_v}{N}$, we have:

$$X_v = \exp\left(-\frac{\Delta E_v^0 - T\Delta S_v^0}{RT}\right) \tag{3.15}$$

Because vibration energy $T\Delta S_v^\circ$ is small compared to internal energy ΔE_v, Eq. (3.15) is frequently approximated as

$$X_v \approx \exp(-\frac{\Delta E_v^0}{RT}) \tag{3.16}$$

Substituting Eq. (3.16) into Eq. (3.10), yields:

$$D=\frac{1}{12}a^2\Gamma'\exp(-\frac{\Delta E_v^0}{RT}) \tag{3.17}$$

Although Eq. (3.17) is useful for some models, it seldom provides a convenient basis from which to calculate the diffusivity of atoms in a solid, since there is seldom an easy way to measure a flux directly, except by the diffusion of a gas into or out of a solid. Generally, the experimenter allows the diffusion to proceed for a fixed period of time, then halts the process abruptly. This permits calculation of D by solving the equation for Fick's second law:

$$\frac{\partial C}{\partial t}=D_i\nabla^2 C_i \tag{3.2}$$

Consider three adjacent lattice planes, labeled as shown in Fig. 3.3, where concentration is a function of position and time, the time rate of change of the concentration per unit area at position x is given by

$$\frac{\partial N_x}{\partial t}=\frac{N(t+\Delta t,x)-N(t,x)}{\Delta t} \tag{3.18}$$

Now the total number of atoms arriving at a plane x is given by

$$N_x^{+}=\frac{\Gamma}{2}[N_{x-\Delta x}\Delta t+N_{x+\Delta x}\Delta t] \tag{3.19a}$$

and the number leaving is

$$N_x^{-}=\Gamma N_x\Delta t \tag{3.19b}$$

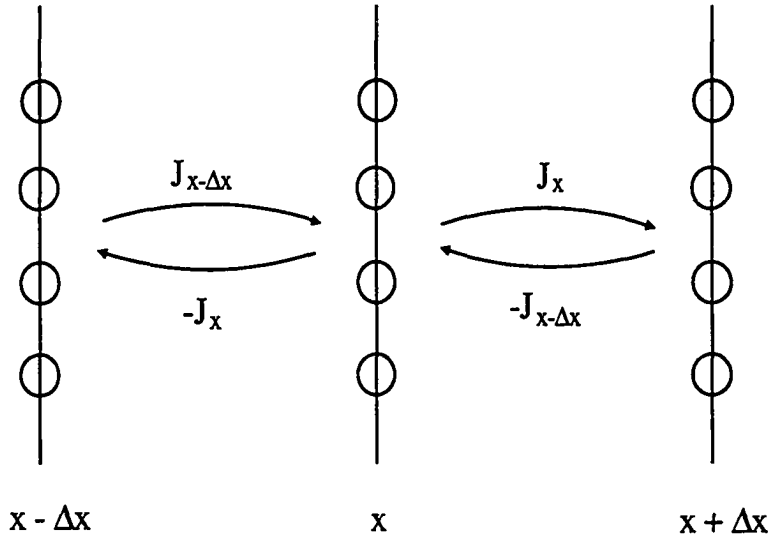

Fig. 3.3 Three adjacent lattice planes illustrating one-dimensional diffusion in which atoms exchange positions by jumping Δx.

Subtracting Eq. (3.19b) from Eq. (3.19a) and multiplying by $\Delta x/\Delta x$ gives

$$\frac{N_x^+ - N_x^-}{\Delta t} = \frac{N_x}{\Delta t} = \frac{\Gamma}{2}(\Delta x)^2 \frac{N_{x-\Delta x} - 2N_x + N_{x+\Delta x}}{(\Delta x)^2} \tag{3.20}$$

Because Δx, the lattice spacing, is very small, we can take the limit on the fraction part of the equation as $\Delta x \rightarrow 0$

$$\frac{\partial C}{\partial t} = \frac{1}{2}\Gamma(\Delta x)^2 \frac{\partial^2 C}{\partial x^2} = D\frac{\partial^2 C}{\partial x^2} \tag{3.21}$$

which is the one dimensional version of Eq. (3.2). Equation (3.21) is, in effect, the result of taking the second finite difference in the concentration gradient and equating it to the time dependent flow of atoms at a fixed point.

3.2 Calculation of Permeation Flux and Diffusivity

The permeation through a planar membrane was described generally by Crank[61]. From Fick's second law, we have the relation

$$\frac{\partial C}{\partial t}(x,t)=D\frac{\partial^2 C(x,t)}{\partial x^2} \tag{3.22}$$

where x is the distance through the membrane and t is the time.

Equation (3.22) can be solved, subject to the following initial and boundary conditions:

$$C(x,t=0)=g(x) \tag{3.23a}$$

$$C(x=0,t)=SP_0^{1/2}=C_1 \tag{3.23b}$$

$$C(x=d,t)=SP_d^{1/2}=C_2 \tag{3.23c}$$

where g(x) is an arbitrary function, d is the membrane thickness, S is the solubility, P_0 is the upstream pressure, and P_d is the pressure on the downstream side of the membrane, which is usually taken to be zero at the beginning of the experiment. In Eqs. (3.23b) and (3.23c), Sievert's square root law was applied. The 1/2 power was assumed, which indicates that the oxygen migrates through the solid as atomic atoms.

Upon considering the conditions given by Eq. (3.23), the solution to Eq. (3.22) is obtained as[61]

$$C(x,t)=C_1+(C_2-C_1)\frac{x}{d}+\frac{2}{\pi}\sum\left[\frac{C_2\cos n\pi x-C_1}{n}\sin\frac{n\pi x}{d}\exp\left(-\frac{Dn^2\pi^2 t}{d^2}\right)\right]$$

$$+\frac{2}{d}\sum\sin\frac{n\pi x}{d}\exp\left(-\frac{Dn^2\pi^2 t}{d^2}\right)\int g(x)\sin\frac{n\pi x}{d}dx \tag{3.24}$$

Now, if at t<0, a vacuum is maintained on the both sides of the membrane, then g(x)=0. If the upstream side of the membrane is then pressurized, $C_1 = SP_0^{1/2}$, $C_2 = 0$, and Eq. (3.24) becomes

$$C(x,t)=C_1[1-\frac{x}{d}-\frac{2}{\pi}\sum\frac{1}{n}\sin\frac{n\pi x}{d}\exp(-\frac{Dn^2\pi^2t}{d^2})] \tag{3.25}$$

According to Fick's first law, the gas flux, J, then is given by:

$$J(x=d,t)=-D(\frac{\partial C}{\partial x})_{x=d}=\frac{DSP_0^{1/2}}{d}[1+\frac{x}{d}-2\sum(-1)^n\exp(-\frac{Dn^2\pi^2t}{d^2})] \tag{3.26}$$

which for large time is

$$J(x=d,t\to\infty)=\frac{DSP_0^{1/2}}{d}=\frac{KP_0^{1/2}}{d}=J_{eq} \tag{3.27}$$

where the permeability is given by K=DS.

For the vacuum system being used, we have the relationship

$$f=\frac{Q}{n-n'} \tag{3.28}$$

where f is the conductance between the downstream side of the membrane and the ion pump; Q is the throughput or gas flux; n is the downstream number density and n' is the ion pump number density. Since n is much larger than n', Eq. (3.28) can be written as

$$f\approx\frac{Q}{n} \tag{3.29}$$

Using the ideal gas relation:

$$P_{eq}=nkT \tag{3.30}$$

and since $Q = J_{eq}A$, then

$$J_{eq}=\frac{P_{eq}f}{AkT} \tag{3.31}$$

were A is the surface area of the membrane. We can combine Eqs. (3.31) and (3.28) to obtain the permeability equation

$$K=\frac{P_{eq}fd}{P_0^{1/2}AkT} \tag{3.32}$$

In order to determine the diffusivity after the establishment of a steady-state permeation rate, the upstream or high-pressure side can be reduced to zero. Then, $C_1 = C_2 = 0$, and a linear concentration gradient through the membrane is:

$$C(x,t=0)=g(x)=SP_0^{1/2}(1-\frac{x}{d}) \tag{3.33}$$

Thus Eq. (3.24) becomes

$$C(x,t)=\frac{2}{d}\sum \sin\frac{n\pi x}{d}\ \exp(-\frac{Dn^2\pi^2t}{d^2})\int SP_0^{1/2}(1-\frac{x}{d})\ \sin\frac{n\pi x}{d}dx \tag{3.34}$$

Reset the time to zero which yields

$$C(x,t)=\frac{2SP_0^{1/2}}{\pi}\sum \frac{1}{n}\ \sin\frac{n\pi x}{d}\ \exp(-\frac{Dn^2\pi^2t}{d^2}) \tag{3.35}$$

and consequently, the flux is

$$J(x=d,t)=\frac{KP_0^{1/2}}{d}[-2\sum (-1)^n\ \exp(-\frac{Dn^2\pi^2t}{d^2})] \tag{3.36}$$

Since the membrane thickness is smaller than 0.03 cm, a single term approximation for this series can be used when $D_t >> 10^{-4}$. Under these conditions, the ratio of the first and second terms is $J_{n=2}/J_{n=1} \approx 0.01$ and J(x=d,t) can be written as

$$J(x=d,t)\approx\frac{2KP_0^{1/2}}{d}\ \exp(-\frac{D\pi^2t}{d^2}) \tag{3.37}$$

Dividing Eq. (3.38) by Eq. (3.28) gives the normalized flux as

$$\frac{J}{J_{eq}}=2\ \exp(-\frac{D\pi^2t}{d^2}) \tag{3.38}$$

The time varying total flux, J(t), and pressure within the system P'(t) are related by

$$V\frac{dP(t)}{dt}=AkTJ(t)-f[P(t)-P'(t)] \tag{3.39}$$

where V is the volume of the measurement chamber, P'(t) is the time varying pressure within the pumped volume and the A is the surface area of the conductance limiting orifice between the measurement chamber and the pump volume. Since P(t) >> P'(t), then

$$J(t)=\frac{V}{AkT}\frac{dP(t)}{dt}+\frac{f}{AkT}P(t) \tag{3.40}$$

A worst case condition occurs at high temperatures when dP(t)/dt is largest, but even at 800°C the ratio of the first term on the right-hand side to the second term of Eq. (3.36) is less than 0.02, so that the flux can be represented accurately as

$$J(t)\approx\frac{f}{AkT}P(t) \tag{3.41}$$

Dividing Eq. (3.41) by Eq. (3.31), yields the result

$$\frac{J(t)}{J_{eq}}\approx\frac{P(t)}{P_{eq}} \tag{3.42}$$

Combining the ratio of (3.42) with (3.38) gives

$$\frac{P(t)}{P_{eq}}=2\exp(-\frac{D\pi^2t}{d^2}) \tag{3.43}$$

where D is the diffusivity, and the time for $P(t)/P_{eq}$ = 0.1 can be determined experimentally.

In next chapter, I will describe the UHV permeation system used for this experiment and the experimental procedures for O_2 glow-discharge enhanced permeation, CO_2 glow-discharge enhanced permeation and the QMS study of glow-discharge dissociation of CO_2.

Chapter 4

EXPERIMENTAL

4.1 Vacuum System

An ultra-high vacuum system (UHV) was employed in this experiment because it enhanced detection of the oxygen flux at low temperatures over the background gases. In addition, without UHV, residual impurities could contaminate the silver membrane significantly and this could affect the adsorption and desorption of oxygen on the silver surfaces, compromising the experimental results. The vacuum system used here was an all metal sealed system made of 304L and 347 stainless steels, capable of being baked at temperatures up to 450°C. The chamber and the associated apparatus are shown in Fig. 4.1. The background pressure of the system was in the 10^{-11} torr range. At this background pressure, it can take more than 15 hours before a monolayer of contaminant (e.g. carbon from CO, CO_2 or CH_4) can be formed and compromise the experimental data (Experiment times were always less than 8 hours).

Figure 4.2 shows the schematic of the system. The main components which comprise the system are: a 500 liter/second diode ion pump (Ultek, D.I Pump), a titanium sublimation pump (Varian, TSP Cartridge on 2 3/4" ConFlat flange), a 20 liter/second triode ion pump (Varian, Triode VacIon Pump), an oil free molecular drag pump backed

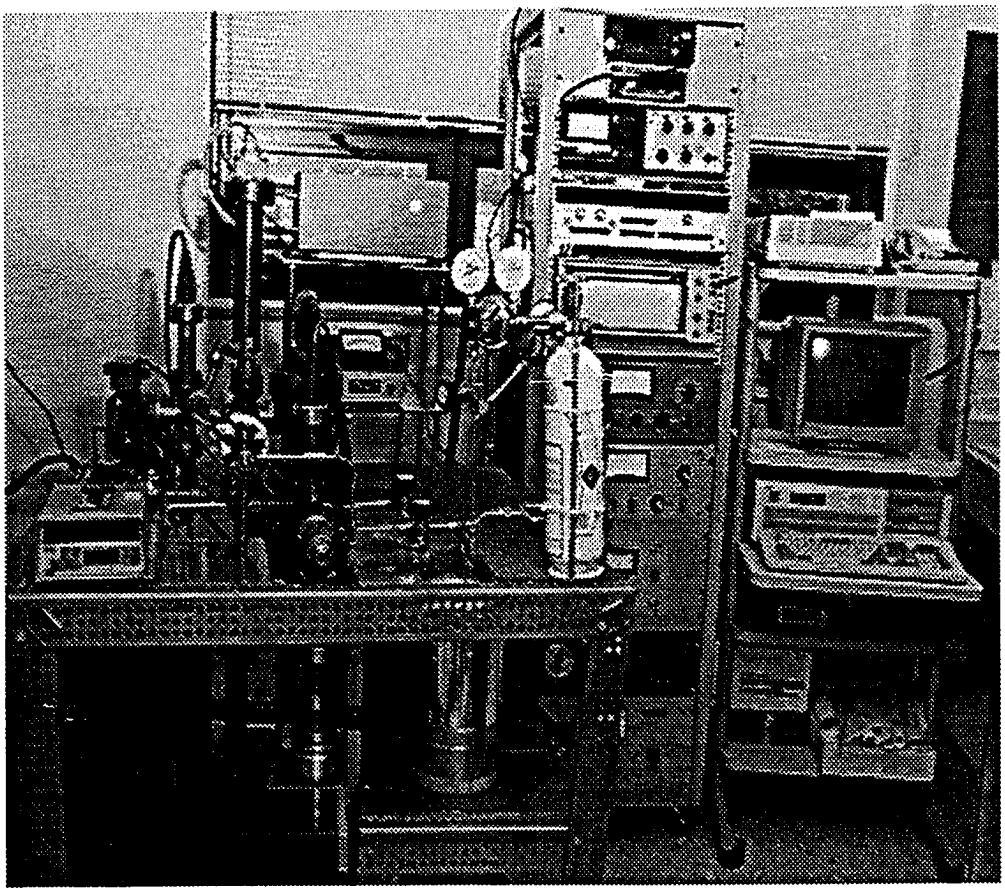

Fig. 4.1 Ultra-high vacuum permeation system and instrumentation.

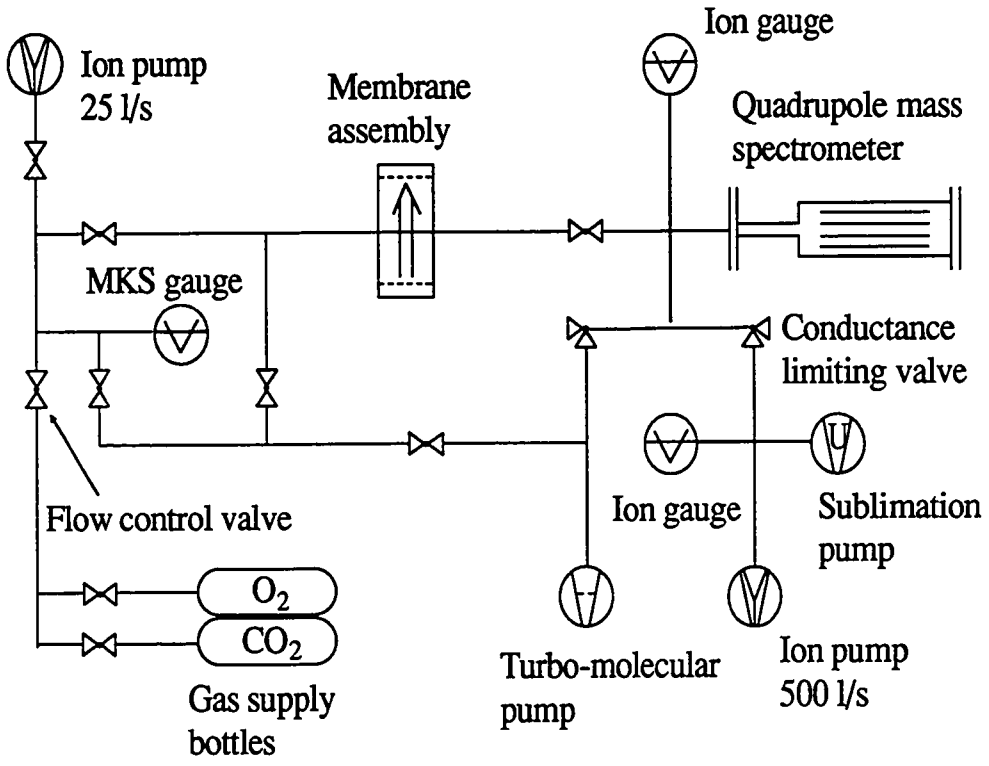

Fig. 4.2 Schematic of the ultra-high vacuum permeation system.

by a diaphragm pump (Alcatel, Drytel 30), two ionization gauges (Varian, UHV-24 Nude Bayard-Alpert Type Ionization Gauge Tube) and a quadrupole mass spectrometer (UTI, Model 100C), two capacitance manometer gauges (MKS Baratron, 10^{-3} to 10 torr and 10 to 1000 torr respectively) and a flow control valve (Granville-Phillips, Model 201 Servo Driven Valve). The stainless steel system envelope was previously vacuum fired at 600°C for 16 hours to minimize the hydrogen outgassing rate. The 500 liter/second ion pump and the sublimation pump were used on the downstream side of the membrane and the 20 liter/second ion pump was used on the upstream side of the membrane to permit appropriate cleanup of the system. The molecular drag pump was used to evacuate the system from atmospheric pressure to 10^{-6} torr and was used also as the upstream pressure control pump during the experiments.

There are three major chambers in the glow-discharge oxygen permeation system: (1) the glow-discharge chamber; (2) the downstream collector chamber and (3) the pump chamber which was operating under substantially lower pressures compared to the downstream collector chamber. The glow-discharge and collector chambers are separated by a silver membrane. A dc glow-discharge was maintained in the glow-discharge chamber to dissociate CO_2 and O_2, thus producing CO and O. The glow-discharge chamber pressure was controlled using a MKS Pressure/Flow Controller (Type 245) which controls a stepper motor powered valve (MKS Type 245). The intensity of the glow-discharge was controlled by a Kepco regulated dc power supply (BHK 2000-0.1M) which supplied current regulated power at voltages up to 2 kV. The temperature of the silver membrane was maintained and controlled by a Research Incorporated MicriStar

Programmable Temperature Controller (Model 828D) which controlled a Time Proportioned Zero Crossover Single-Phase Power Controller (Model 663B) that provided the power supply to the heater. The amount of oxygen transported through the membrane was monitored by an ion gauge and a quadrupole mass spectrometer (QMS) which resided inside the downstream chamber. The pressure within the downstream collector chamber was never allowed to exceed 10^{-5} torr. A small calibrated conductance, f, was used to separate the downstream chamber volume from the pump chamber volume, in order to provide a known conductance between the two volumes and therefore permit direct calculation of the flow rate out of the downstream chamber. The 500 liter/second ion pump and the titanium sublimation pump were attached to the pump chamber volume in order to provide sufficient pumping capacity to maintain the pressure difference between the pump chamber and the downstream collector chamber. The pressure measured by the ion gauge inside the pump chamber, together with the pressure measured by the ion gauge inside the downstream chamber could be used directly in the determination of the oxygen flow rate, and thus the permeating flux through the membrane. Figure 4.3 shows the valve/orifice configuration utilized as the calibrated conductance f. Valve A has two positions: open and closed. During bakeout, the valve was open (with a maximum flow rate of 8 liter/second) to facilitate maximum gas removal by the main ion pump. After bakeout and during permeation runs, the valve was in the closed position, thus providing a maximum 0.7 liter/second calibrated conductance path for the permeated oxygen.

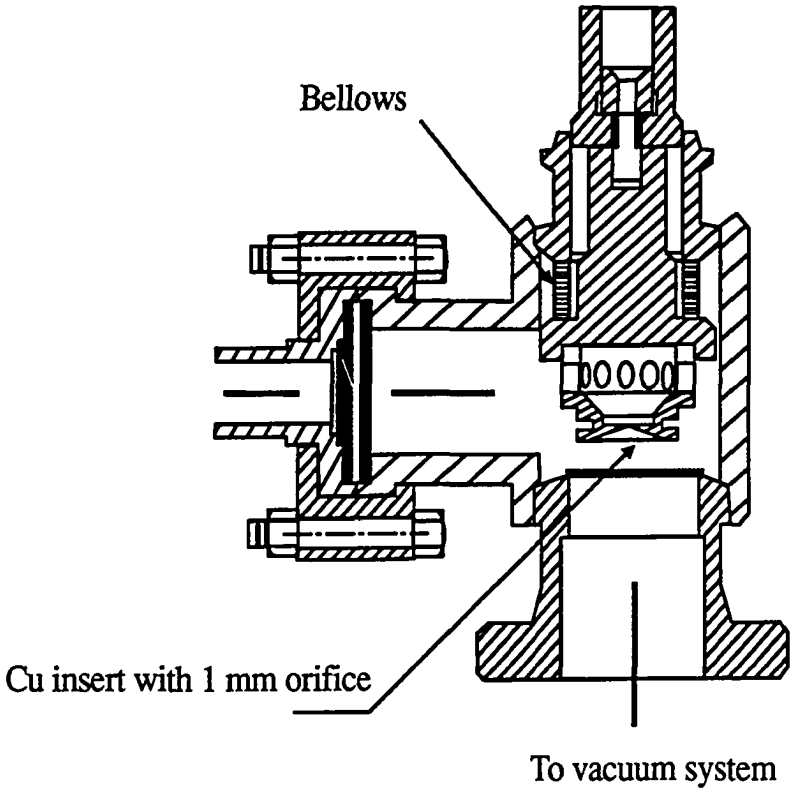

Fig. 4.3 Conductance limiting valve.

4.2 Glow-Discharge Chamber and Heater Assembly

Figure 4.4 shows schematically the upstream (supply) and downstream (detection) regions of the cell separated by the membrane. Since the oxygen atoms naturally tend to recombine or react with other species, a concerted effort has been made to keep the glow region close to the membrane by using the membrane as one of the electrodes (anode). The probe has been chosen to be the cathode to eliminate damages to the membrane surface caused by oxygen ion bombardment and to insure that the permeation occurs from ordinary oxygen atom and molecule adsorption. The glow-discharge probe was made of 0.5 mm thick silver sheet rolled into a tube of 2.54 mm outside diameter. The distance between the probe and the membrane was adjustable using a manipulator which was made from a bellow. The glow-discharge chamber wall was shielded by a quartz tube to prevent any discharge between the probe and the stainless steel chamber.

The heater assembly consisted of a heating wire, insulation, a cooling system, and a thermocouple temperature measurement as shown in Fig. 4.5. The heater spool was made of 0.02 inch diameter NiCr heating wire with a measured resistance of 10 Ω. The temperature of the membrane was measured by a thermocouple (0.13 mm diameter chromel-alumel) attached to the membrane from the downstream side of the membrane. The cooling system consisted of two external copper blocks mounted on each side of the insulated heater. The copper blocks contained internal cooling passages which were connected to teflon tubes carrying refrigerated water from a KMC Laser Cooler.

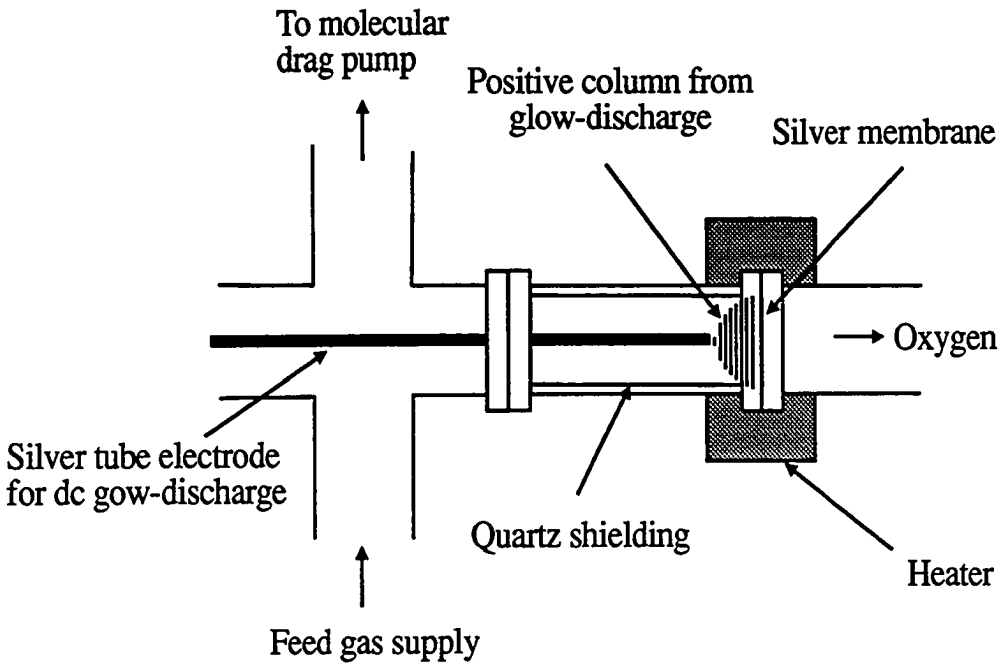

Fig. 4.4 Glow-discharge chamber showing silver membrane, glow-discharge electrode, glow-discharge region (upstream) and detection region (downstream).

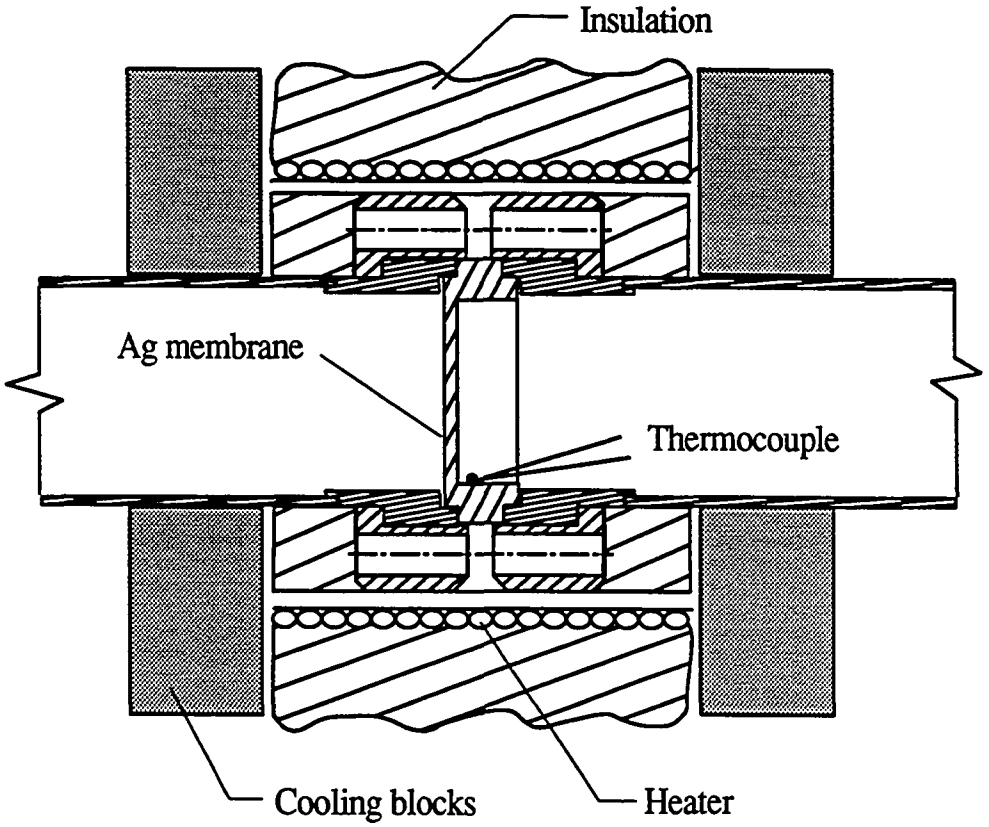

Fig. 4.5 Miniflange geometry with permeation membrane. Also shown is the heater wire, thermocouple and cooling blocks.

4.3 Silver Membranes and Supply Gases

The silver membrane for O_2 glow-discharge permeation experiment was made of 99.999 percent purity silver which was melted in a vacuum environment (10^{-8} torr) and was spark-machined into the disk geometry. The basic geometry of the silver membranes is shown in Fig. 4.6. The disk membrane was sealed between two conflat type stainless-steel mini-flanges (3.38 cm diameter) to separate the ultrahigh vacuum detection volume from the oxygen supply and glow-discharge volume. The membranes were prepared using a multi-step process, described in the following table:

Step	Process	Description
1.	Mechanical Polishing	Using 30 μm grit silicon for final finishing.
2.	Degrease	Laboratory detergent used in ultrasonic cleaning bath for 10 minutes.
3.	Rinse	Three runs using deionized water in ultrasonic cleaning bath, 10 minutes each time.
4.	Chemically cleaning	10 - 15 seconds dip into 4 parts HNO_3 to 1 part deionized water.
5.	Rinse	Deionized water bath, then rinse in running deionized water for 2 minutes.
6.	Dry	Blower, using oil-free and filtered N_2.

Attempts at electropolishing the manufactured silver membranes were only successful in about one out of five attempts and the process left as much or more surface contamination than chemical cleaning using the HNO_3 solution. A comparison of Auger

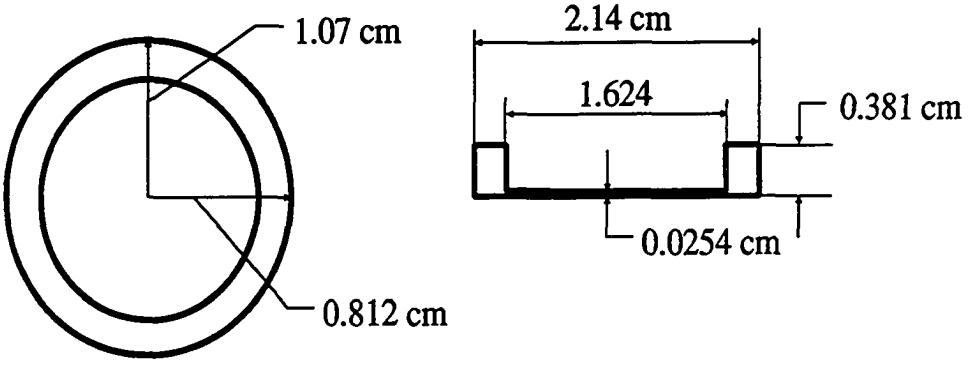

Fig. 4.6 Geometry of silver permeation membranes.

electron spectroscopy (AES) analyses of a chemically cleaned silver membrane surface conducted, with a sputter-cleaned silver membrane is shown in Fig. 4.7. The spectrum of the chemically cleaned membrane closely resembles the spectrum of the sputter-cleaned silver surface. While small contaminant levels of S, Cl, C, and O can be observed for the chemically cleaned surface, the S, Cl, and C peaks were easily removed (oxidized) during the first few permeation runs when oxygen was passed through the membrane.

The O_2 and CO_2 gases used in the experiments were research grade and were provided by Air Products and Chemical Inc. The minimum purity is 99.995%. For this experiment, it was further purified by passing the gas through a cold trap of dry ice and isopropyl alcohol. The purity of the gas was checked using a mass spectrometer and was verified to be high purity.

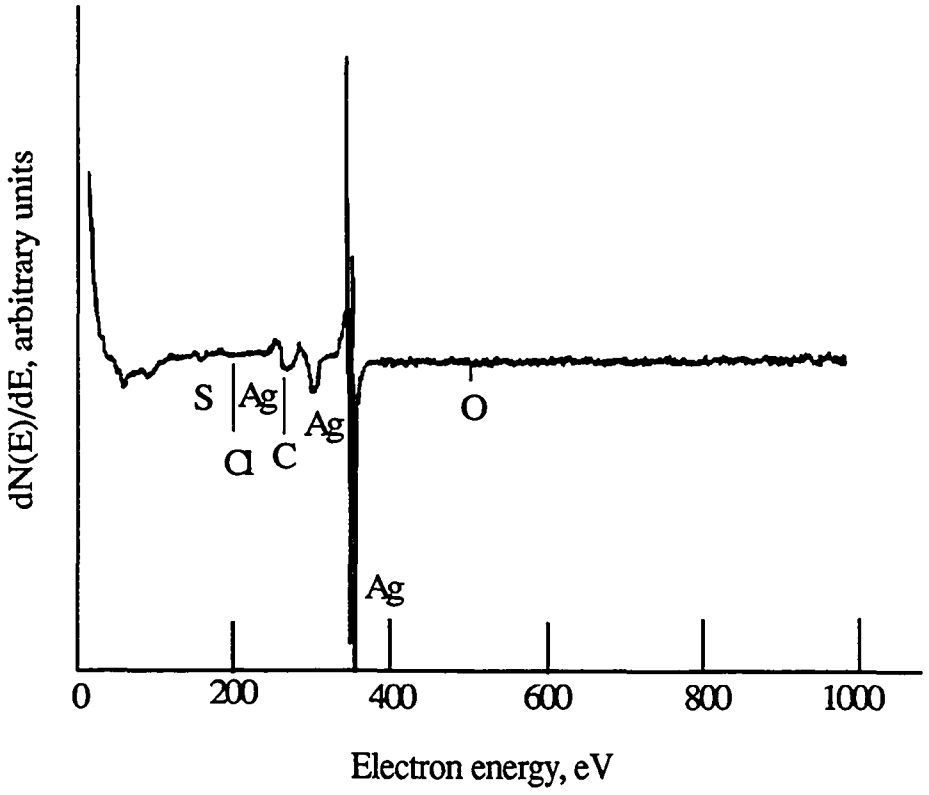

Fig. 4.7 AES survey of Ag membranes after polishing and chemical cleaning.

4.4 System Preparation

The system was first pumped down to 10^{-5} torr using the molecular drag pump. After that, the 500 liter/second ion pump and a 20 liter/second ion pump were started. The ion pump reduced the pressure to about 10^{-7} torr. System bakeout was then initiated via strip heaters, using a temperature ramp of about 25°C per hour, up to about 250°C. This bakeout temperature was maintained for at least two days and then cooled down to room temperature, at the same rate. The purpose of maintaining the elevated temperature during the heating period is to deplete the hydrogen concentrations and to oxidize the external surface (Cr_2O_3) to minimize the overall outgassing rate. This system had been previously baked to 450°C, so the lower temperature bake was sufficient to remove the surface H_2O and most of the other adsorbed species. During bakeout, valve A was open (8 liter/second) to facilitate maximum pumping speeds by the main ion pump. The ion gauge and quadrupole mass spectrometer, which contained a hot filament, were also degassed during the pump-down procedure. After cooling to room temperature, the titanium sublimation pump was operated several times (45 amps for 1 min) to further reduce the background pressure. The system was then ready for the experiments when an ultimate pressure on the 10^{-11} torr range was achieved.

4.5 Procedure for O_2 Glow-Discharge Enhanced Permeation

After the system had been baked and pumped down to its residual pressure at 10^{-11} torr range, the ion gauges in the downstream chambers were vacuum degassed with 100 mA emission current and the quadrupole mass spectrometer was vacuum degassed with 2.5 mA emission current. The degas operation is necessary because the outgassing of H and O from the bulk and the surface of the hot filaments in the ion gauge and quadrupole mass spectrometer head while in operation could significantly reduce the operation vacuum pressure obtainable and compromise the experimental results. Further, contaminant gases such as CO, CO_2 and CH_4 are minimized. The membrane was then heated up to 800°C at a rate of 50°C per hour controlled by MicriStar Temperature Controller. This procedure thoroughly vacuum degassed the membrane. The logarithmic picoammeter, which took the signal from the ion gauge and output to the chart recorder, was then calibrated using a standard picoampere source and a digital multimeter. The 20 l/s ion pump was then disconnected from the glow-discharge chamber and the turbo molecular drag pump was initiated to provide continuous pumping on the glow-discharge chamber during the experiment. The MKS capacitance manometer gauge was calibrated (zero adjusted). The emission current of the ion gauge and the quadrupole mass spectrometer were then reduced to 0.4 mA and 0.5 mA respectively (normal operation is 4.0 mA and 2.5 mA respectively) in order to minimize instrument pumping and outgassing.

The background gas spectra at room temperature appeared to be normal for stainless steel apparatus that have been vacuum fired and then baked out for several days. There was no significant O_2 signal and no change was observed in the QMS signal even after introducing 10 torr of pure oxygen into the upstream glow-discharge chamber as shown in Fig. 4.8a. However, as shown in Fig. 4.8b, the O_2 peak substantially increased and became the dominant signal after the silver membrane was heated. The data shown in Fig. 4.8b correspond to equilibrium conditions for the membrane temperature of 750°C and upstream O_2 pressure of 150 torr.

The glow-discharge permeation data were taken at 25°C increment over a temperatures range of 300°C to 650°C. First of all, a specific membrane temperature was stabilized, then O_2 was admitted into the glow-discharge chamber up to a particular pressure. After the equilibrium permeation was established, a dc glow-discharge was initiated with certain discharge current. A significant increase of oxygen flux through the silver membrane can be observed at this time. The change of flux level was recorded on the strip chart recorder. The glow-discharge was maintained until a new equilibrium was achieved. Then, the glow-discharge was deactivated and the decay of the ion current from the ion gauge was recorded till the flux level return to the original level without glow-discharge. This cycle was repeated many times with many different membrane temperatures, discharge currents, and discharge probe-membrane distances.

The O_2 diffusion data were taken at 25°C decrements over the temperature range of 800°C to 400°C by monitoring the signals of both the ion gauge and QMS. First of

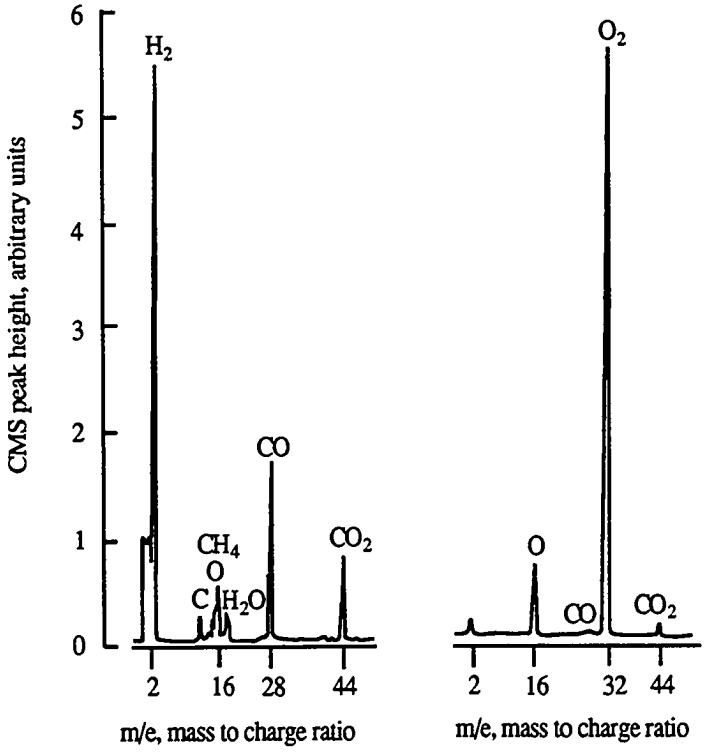

(a) Ag membrane at room temperature: P_{O_2}= 100 torr O_2(upstream pressure).

(b) Ag membrane at 750 C: P_{O_2}= 100 torr O_2(upstream pressure).

Fig. 4.8. QMS spectra of system.

all, the temperature was established, then oxygen was admitted to the upstream side of the membrane. After the quadrupole mass spectrometer indicated that the equilibrium flow had been established, the membrane temperature, upstream pressure and ion current from the ion gauge were recorded. The upstream pressure was then removed and the decay of the ion current was recorded on the strip chart recorder. The ion current from the ion gauge was converted to downstream oxygen collector chamber pressure by Eq.(A.1) in Appendix A, and together with the upstream pressure and the decay of the downstream pressure, the permeability and diffusivity were calculated using the Eqs. (3.34) and (3.45) for that specific temperature conditions. Figure 4.9 shows representative data for oxygen breakthrough to equilibrium (T_{Ag} = 600°C, P_0 = 100 torr O_2) and then pressure decay (T_{Ag} = 600°C, Po -> 0 torr O_2).

The pressure decay method was used to calculate the diffusivities for O/Ag, since it was experimentally simpler to establish equilibrium for a given P_0 and then open a pump valve to reduce the pressure to P_0 = 0. It avoided the "shock" of the hot silver membrane with a differential pressure up to 100 torr and avoided surface limitations of a bulk property. The curvature that occurs after the linear decay in the signal is due to the incorporation of oxygen into the stainless steel walls of the vacuum system at equilibrium and the subsequent increase in outgassing. When the high-pressure side is evacuated, a linear decay occurs as predicted by Eq.(3.43); but ultimately, as the pressure descends toward the background level, the data begin to curve because the charged walls now see an opposite concentration gradient that causes oxygen to desorb into the gas phase. This increase in oxygen gas flux results in an increased background pressure, but

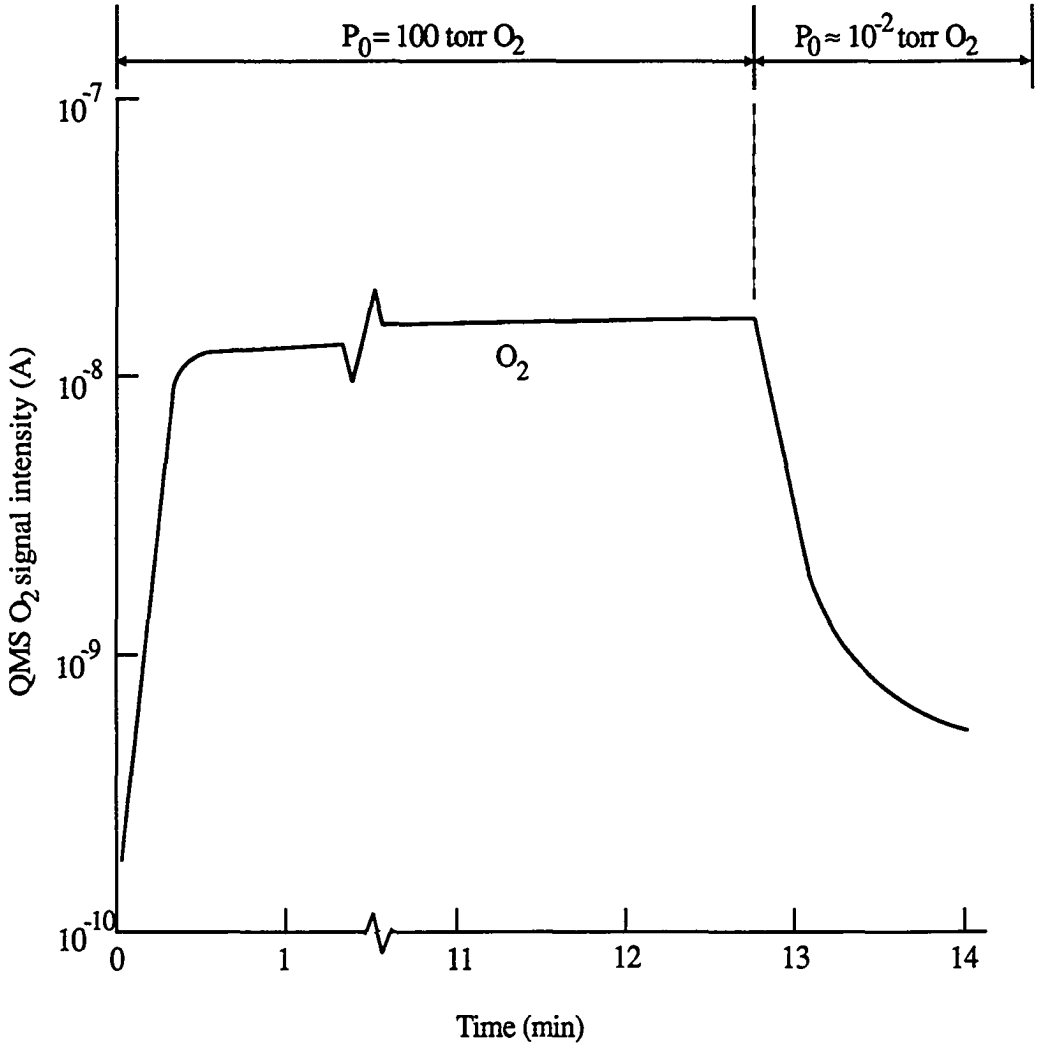

Fig. 4.9 Breakthrough and decay of oxygen through Ag0.05Zr membrane (T = 600°C).

is substantially less than the gas flux evolving from the membrane immediately after the upstream side of the membrane is evacuated, so it does not alter the linear decay necessary to determine the diffusivity. This effect has also been substantiated by separate experiment.

4.6 Procedure for CO_2 Glow-Discharge Enhanced Permeation

After the system was properly prepared and the residual pressure reached the 10^{-11} torr range, the membrane was heated up to 700°C at a rate of 50°C per hour. Then, CO_2 gas was admitted into the glow-discharge chamber up to a 5 torr pressure and a 400 V, 5 mA dc glow-discharge was initiated. It took more than eight hours before oxygen completely saturated the membrane and the permeation became stabilized.

The glow-discharge permeation data were taken at 25°C decrements over a temperature range of 700°C to 300°C. First of all, a specific membrane temperature was stabilized, then CO_2 was admitted into the glow-discharge chamber up to a prescribed pressure and a dc glow-discharge was initiated with specified discharge current. A significant increase in oxygen flux through the silver membrane was observed at this time. The change of oxygen flux level at the downstream side of the membrane was recorded using a strip chart recorder. The glow-discharge was maintained until a new equilibrium flux was achieved. Then, the glow-discharge was deactivated and the flux level was allowed to decay back to its original level (as that without glow-discharge). This cycle was repeated many times with many different membrane temperatures, discharge currents, glow-discharge chamber pressures, and discharge probe-membrane separation distances.

4.7 QMS Study of Glow-Discharge Dissociation of CO_2

In order to find out how much CO_2 was dissociated and how much O reached the membrane before it recombined to form O_2 or CO_2, a separate experiment was conducted using a copper disk with a small orifice as a membrane. The experimental apparatus, as shown in Fig. 4.10, was similar to the O_2 and CO_2 experiments except the ionization head of the QMS was brought closer to the orifice to enable a measurement of atomic oxygen before it recombined with other species. A turbo molecular pump (Balzers, TPH 180 H), backed with a Tribodyn pump (Danielson, TD-30/16) was used, instead of the ion pump, to provide a high pumping rate at low vacuum. The diameter of the orifice is about 0.05 mm as shown in Fig. 4.11. With this setup it was possible to create a pressure differences of about five to six orders of magnitude between the discharge region and the ionization chamber of the QMS. The ionization chamber pressure was in the middle of 10^{-5} torr range when the discharge chamber CO_2 pressure was 5 torr.

The QMS was first calibrated for 5 torr CO_2 gas with a reduced emission current of 3 mA. Then the glow-discharge was initiated and the CO_2 was dissociated into CO and O which will partially recombined to form O_2. The mixture of gas leaves the glow-discharge chamber through the orifice and was detected by the QMS. The data were taken with two different discharge currents (5 and 10 mA) and two different probe-membrane distances (2.5 and 5.0 mm).

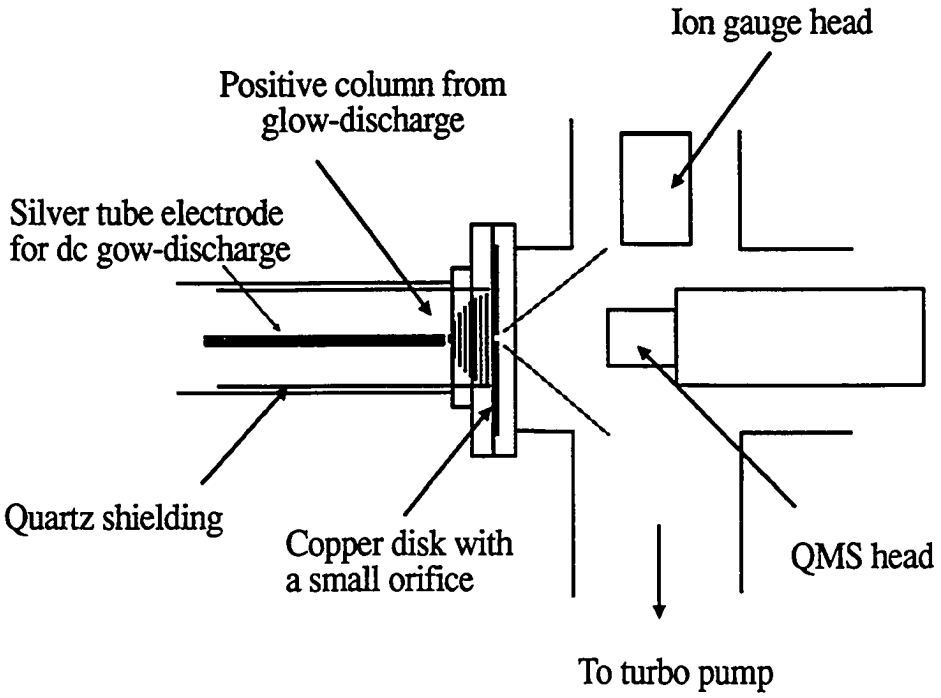

Fig. 4.10 Schematic of the glow-discharge chamber (upstream), the copper disk with a small orifice, and the detection chamber (downstream).

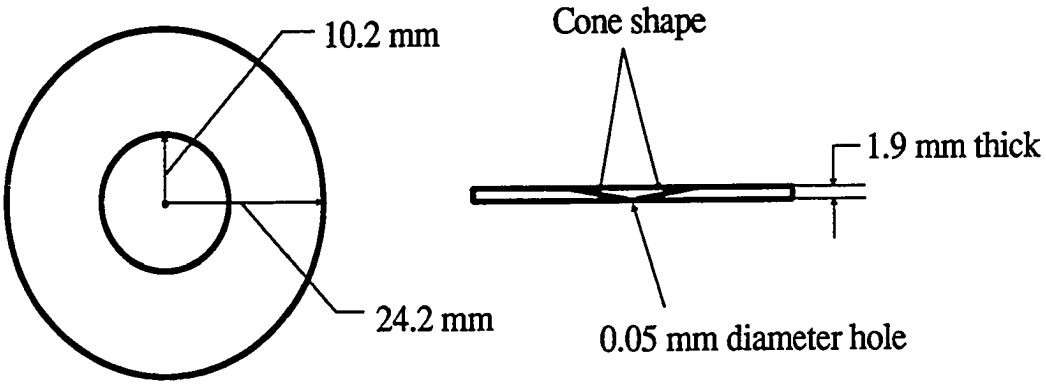

Fig. 4.11 Geometry of copper disk with a small orifice.

Chapter 5

RESULTS AND DISCUSSION

5.1 O_2 Glow-Discharge Enhanced Permeation of Oxygen through Ag

The transport of oxygen through Ag normally proceeds by a sequence of steps which include dissociative adsorption of molecular oxygen on the upstream surface, the dissolution of the atomic oxygen into the bulk, and the subsequent migration of the atoms between octahedral sites of the lattice (or through defects) until they arrive at the vacuum interface downstream where recombination to O_2 occurs with subsequent desorption to the gas phase[53-58]. Past research has shown that dissociative adsorption may limit the magnitude of the permeation because of the small O_2 sticking coefficient and because Ag has a very weak chemical affinity for the oxygen[30-49]. The sticking coefficient of molecular oxygen on silver has been studied in the past but data exists on its behavior as a function of temperature only up to 217°C[34]. In the present work, it appears that the surface concentration is not only controlled by the solubility and pressure but also by the sticking coefficient. For molecular oxygen, the sticking coefficient is small for all orientations ($< 10^{-4}$ for $T > 217°C$), but for atomic oxygen, the sticking coefficient appears to be much larger. It was reported previously[50] that a dc glow-discharge can

generate a much higher oxygen flux through a silver membrane than normal thermal dissociative permeation, but those effects have not been examined on a parametric basis. In order to understand more about the mechanism of the increased flux, oxygen transport as a function of a number of parametric variables, using a pure silver membrane, was studied over the temperature range of 300°C to 650°C.

Figure 5.1 shows that the permeation rate varies linearly with glow-discharge current. The main formation process of atomic oxygen in the glow-discharge is the excitation of the Herzberg ($A^3\Sigma^+$) and the Schuman-Runge ($B^3\Sigma^-$) system by electron impact, leading to the dissociation reactions:

$$e+O_2(X^3\Sigma_g^-)\rightarrow e+O_2(A^3\Sigma_u^+)\rightarrow e+O(^3P)+O(^3P)$$

$$e+O_2(X^3\Sigma_g^-)\rightarrow e+O_2(B^3\Sigma_u^-)\rightarrow e+O(^3P)+O(^1D)$$

The dissociation rate increases with the current due to the increasing electron concentration. When the current (primarily electrons) was increased, the dissociation of O_2 increased proportionately, thus resulting in a proportional increase in the O atom partial pressure and the oxygen flux through the membrane. The reversibility of this process, i.e., the decrease in the downstream flux with a reduction in discharge current, was also established. This is consistent with the work of Sabadil and Pfau[24] who also observed a linear increase in oxygen atoms with discharge current. They measured the atom densities by two methods (the ozone method and the Wrede-Harteck method) and the results were in good agreement with each other. At 500°C, with the geometry shown in Fig. 5.1, the flux increases 2.5×10^{13} $cm^{-2}s^{-1}$ for each mA of discharge current. Since the Ag membrane was the anode, no ion bombardment effects, such as surface

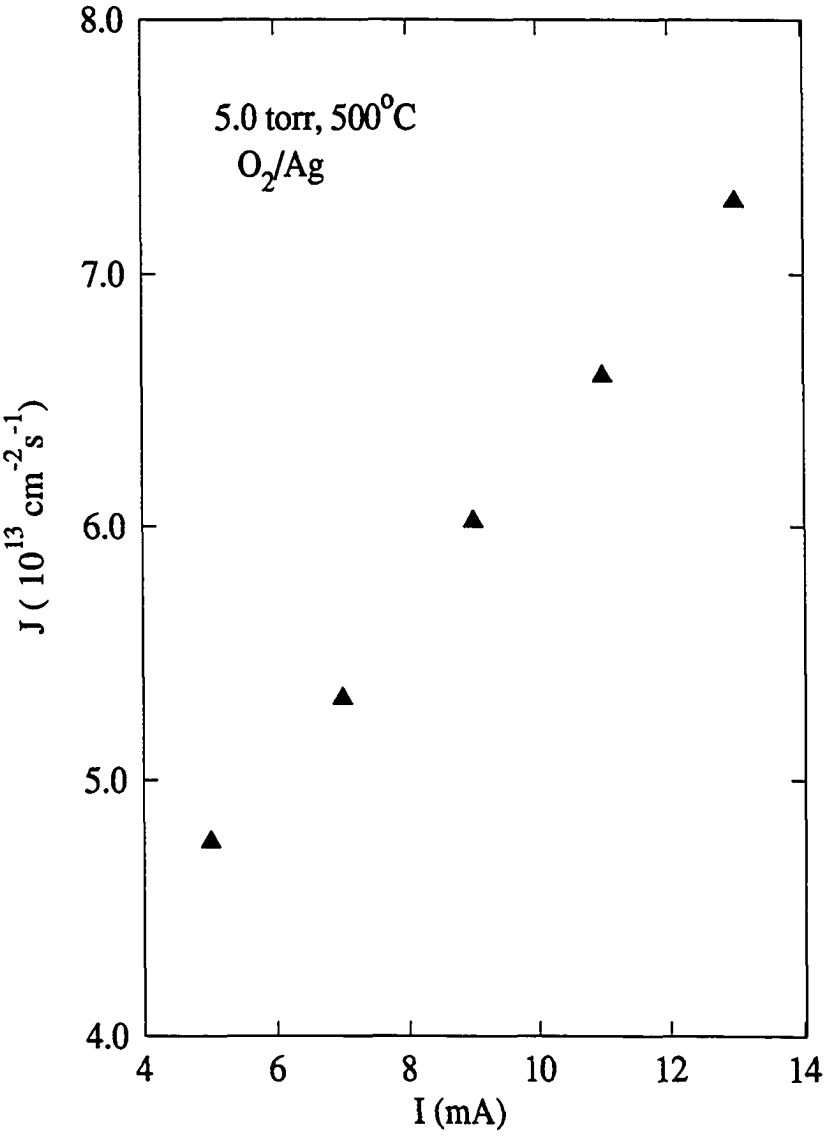

Fig. 5.1 Downstream flux as a function of glow-discharge current at 5.0 torr upstream pressure and 500°C membrane temperature.

modification and/or surface sputtering occurred. Although electron bombardment of the anode may have generated some loss of oxygen at the surface, the desorption cross section for this process is quite small ($\sigma<10^{-18}cm^2$)[62]. Furthermore, this process would work to decrease the downstream flux with increasing discharge current. It therefore appears that the increase in flux is due to an increase in the surface concentration of oxygen at the high-pressure interface. The distribution of dissociated atoms is, however, a strong function of the cathode probe distance from the membrane (see Fig. 5.2). For this geometry and discharge current, a 1-2 mm separation appears to maximize the atomic oxygen density in the vicinity of the membrane and therefore maximize the surface incidence flux rate.

Clearly, the glow discharge should have no affect on the diffusivity since that is a bulk property, independent of the gas phase. Figure 5.3 shows the diffusivity (D) measured at 3.0 torr O_2 with and without glow discharge and at 100 torr O_2 without glow discharge. The break in the diffusivity at 630°C has been observed previously and attributed to the higher efficiency of traps at low temperatures[60]. Predictably, there is no apparent variation in the diffusivity for any of these conditions, although enhanced diffusion of hydrogen through molybdenum in glow-discharge[52] has been reported. An atom will lose all of its gas phase energy when it is adsorbed and dissolved into the bulk. At this point, it becomes thermalized with the bulk and the diffusion is "random walk", controlled by the bulk temperature, the activation barrier between octahedral and defect sites, and the concentration gradient (availability of sites). Since the diffusion in the bulk is much slower than the adsorption and desorption steps, it is generally the rate

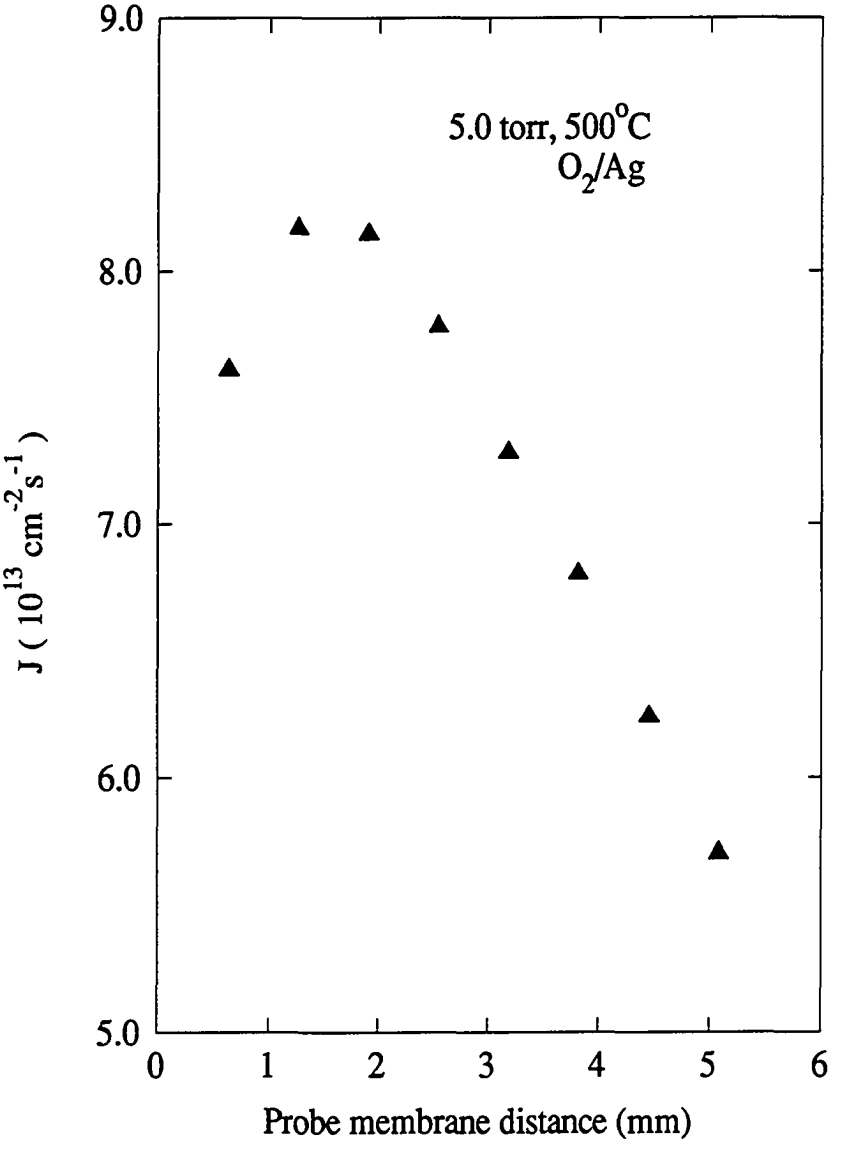

Fig. 5.2 Variation in the flux as a function of cathode to anode (membrane) distance.

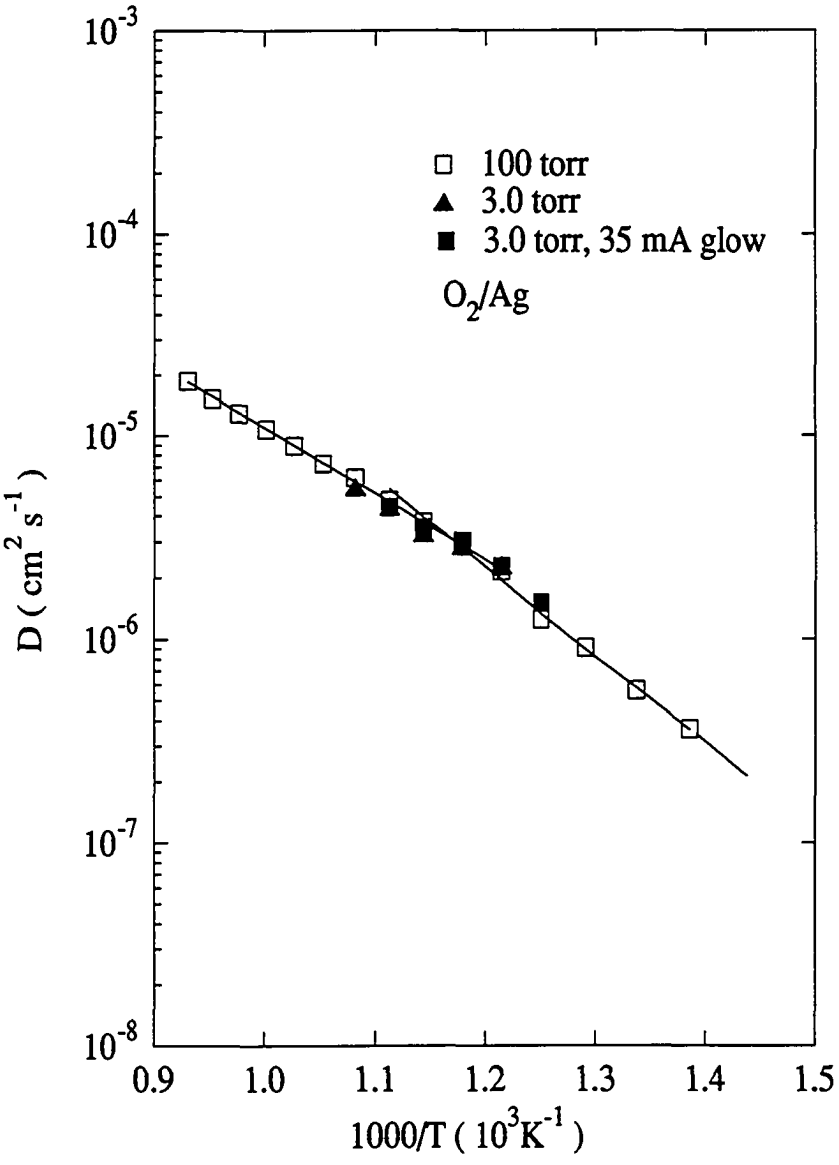

Fig. 5.3 Diffusivity as a function of reciprocal temperature with and without supply side glow-discharge-assisted dissociation.

controlling process. Assuming that diffusion obeys Fick's law and that atomic oxygen has a much higher sticking coefficient on Ag, it becomes clear that the significant increase in the downstream flux with glow-discharge is due primarily to the increasing oxygen concentration on the upstream surface (the concentration on the downstream surface is assumed to be zero), which, in turn, increases the concentration gradient through the membrane thickness. This situation is illustrated schematically in Fig. 5.4.

Figure 5.5 shows an Arrhenius plot of the oxygen permeation flux (J_{gd}) at a 5 torr upstream pressure with 5 mA glow-discharge conditions. Also shown is the permeation flux (J_m) with the same upstream pressure but without glow-discharge. Over the temperature range tested, the permeation flux exhibits two classical Arrhenius regions (exponential function of temperature) and one transitional region. The phenomenon of the flux increasing with the initiation of the glow discharge is most pronounced at lower temperatures (below 500°C). Since the permeation process includes the adsorption and dissolution steps, this is consistent with a higher sticking coefficient, and therefore, higher upstream concentration created by the atomic oxygen. The activation energy for the temperature below 425°C, ΔH_J=19.5 kcal/mol (since the glow-discharge precludes equilibrium, ΔH_J is reported instead of ΔH_K), is close to that for ordinary thermal dissociative permeation, ΔH_K=22.2 kcal/mol indicating that the overall process is diffusion controlled. Above 500°C, the magnitude of J_{gd} gradually approaches that of J_m which indicates that surface adsorption, desorption and dissociation processes become comparable with the adsorption processes for atomic oxygen. The behavior of the oxygen

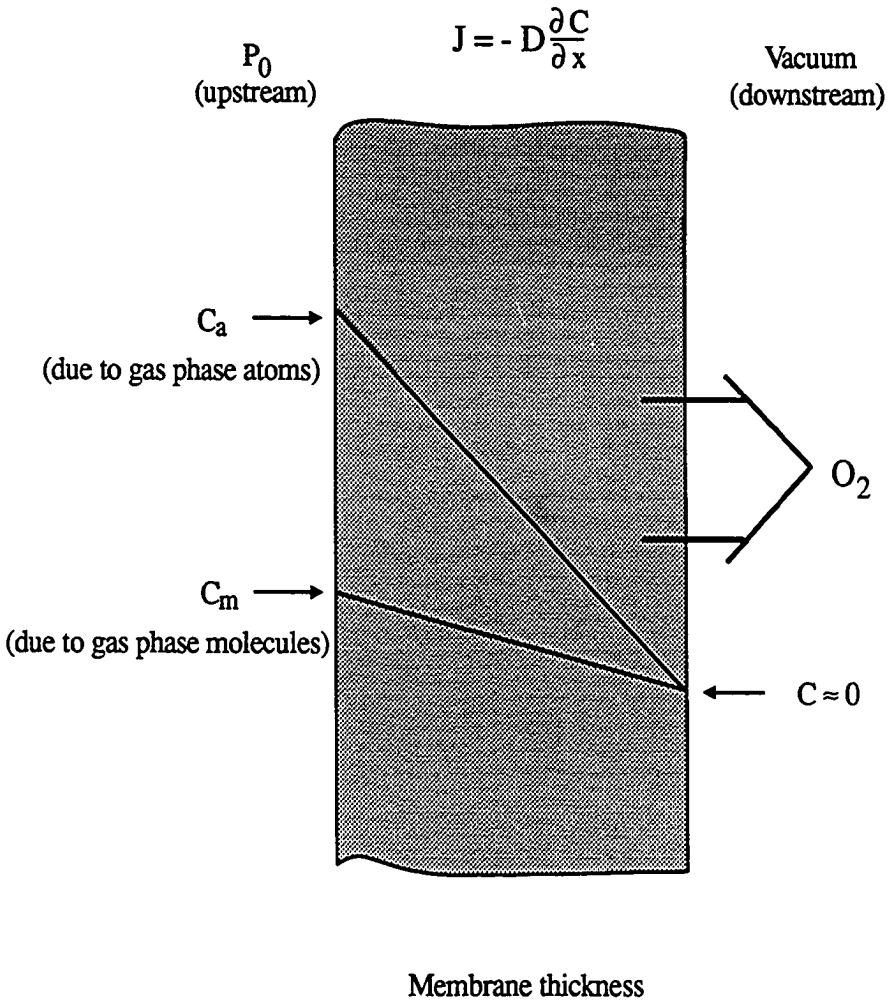

Fig. 5.4 The concentration profile of the oxygen in the membrane is presumed to be much greater with glow-discharge-assisted dissociation because $C_a > C_m$.

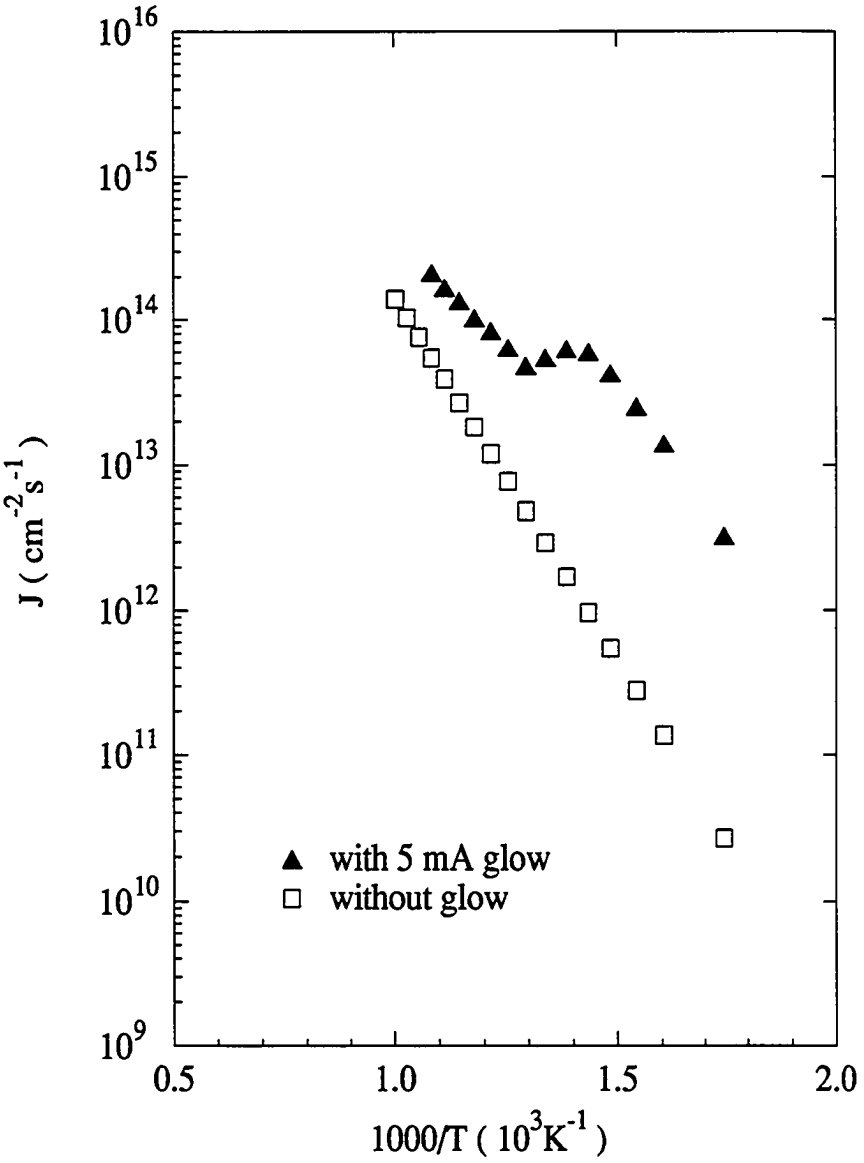

Fig. 5.5 Downstream flux as a function of reciprocal temperature.

flux with glow-discharge in the transitional region is very similar to the behavior that was observed in the permeation of atomic hydrogen through molybdenum[52] and quite likely represents atoms recombination and desorption back into the gas phase at higher temperatures. In any case, it represents an effective reduction in the adsorption and therefore the concentration gradient.

The concentration at the upstream surface, C_s, can be uniquely determined from Fick's first law and is shown in Fig. 5.6 with and without glow-discharge. The concentration from molecular dissociative adsorption varies linearly in an Arrhenius plot as expected, but this is not true for the glow discharge case. At lower temperatures, T<425°C, C_s follows J_{gd} where the magnitude is substantially greater than for molecular dissociative adsorption. At 400°C for example, C_s with glow-discharge is 4.56×10^{18} which is 78 times larger than the value of C_s without glow-discharge (5.84×10^{16}). This behavior reflects higher atomic sticking coefficients at low temperatures. Furthermore, J_{gd} and therefore C_s, appear to increase linearly with the glow discharge current, clearly indicating that the solubility limit has not been reached. On the other hand, the two cases approach each other at higher temperature (T>500°C) suggesting lower and lower atomic sticking coefficients with increasing temperature. The much higher surface concentration with glow-discharge clearly does not agree with Sievert's Law where the solubility of oxygen atoms in Ag should be the same regardless of whether it comes from atomic or molecular oxygen. From Sievert's Law, the surface concentration should increase exponentially with temperature and this does not appear to be the case with glow-discharge. All of the above effects further confirm the contention that there is a strong

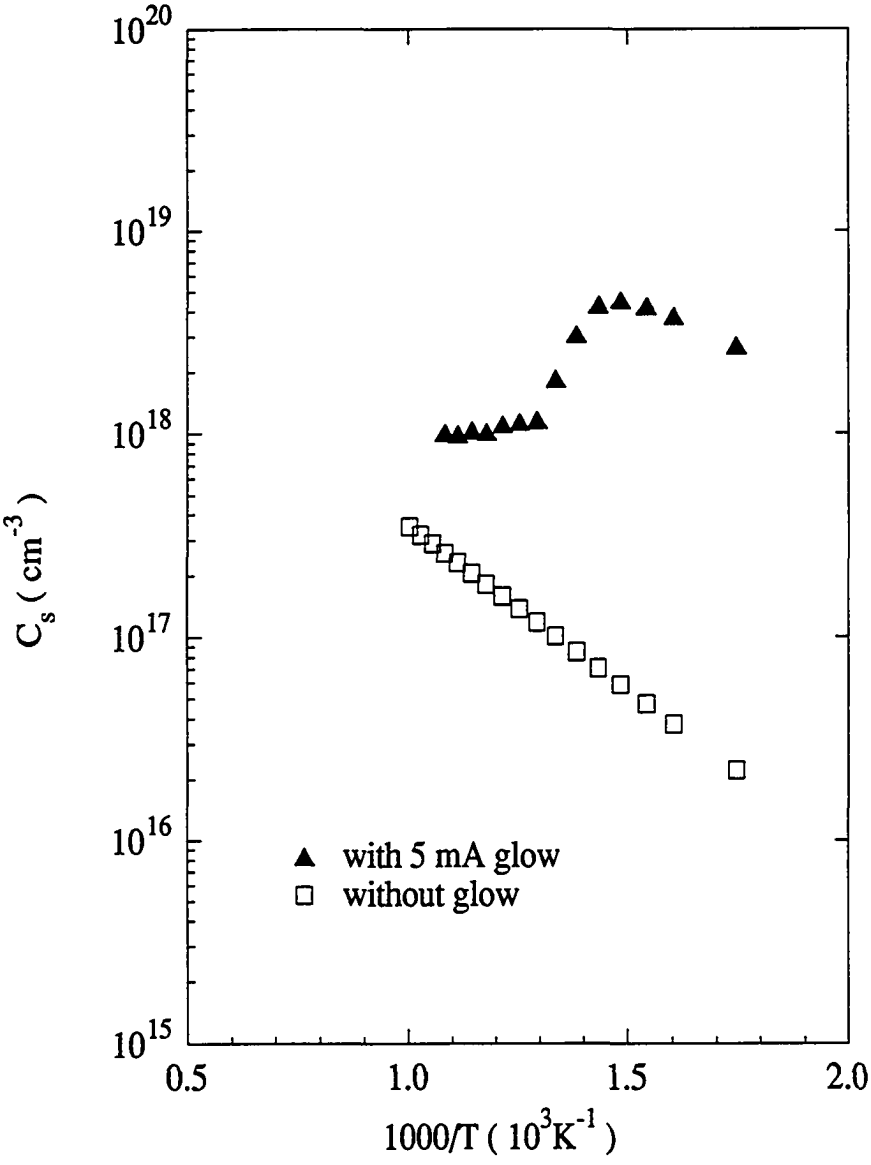

Fig. 5.6 The upstream concentration variation as a function of reciprocal temperature with and without glow-discharge.

surface effect not included in Sievert's Law. This clearly indicates that for the case of glow-discharge below 425°C, the adsorption rate is dominated by other surface effects, probably related to the sticking coefficient. With increasing temperatures, the rapidly decreasing sticking coefficient, in combination with the desorption from the bulk, results in a decreasing surface concentration which will finally approach the case without glow-discharge.

5.2 CO_2 Glow-Discharge Enhanced Permeation of Oxygen Through Ag

The previous research on oxygen permeation through silver has shown that when a glow-discharge was maintained in the vicinity of a silver membrane, the atomic oxygen thus generated (from the molecular oxygen stream), bypasses the dissociative adsorption step and increases the surface concentration of oxygen atoms significantly. This results in an increased concentration gradient across the membrane and a corresponding increase in the overall oxygen flux through the membrane, especially at lower temperatures. Obviously the same mechanism can be utilized in a CO_2 environment where atomic oxygen can be generated by dissociation of CO_2 via a glow-discharge. A preliminary QMS study (achieved by leaking some of the gases in the glow-discharge chamber to the detector chamber) indicated that a significant amount of CO_2 can be dissociated into CO and O, which recombined to form O_2, with a dc glow-discharge as shown in Fig. 5.7. Since the glow-discharge was best operated at low temperature and low pressures (below 10 torr), this approach can eliminate the gas compression step required by thermal dissociation methods and thus reduce the system energy consumption. Hence, this approach can ultimately reduce the equipment needed for oxygen collection systems on Mars. In order to evaluate this technique for possible future utilization in Mars oxygen plants, similar parametric studies, as conducted with pure oxygen have also been conducted for CO_2.

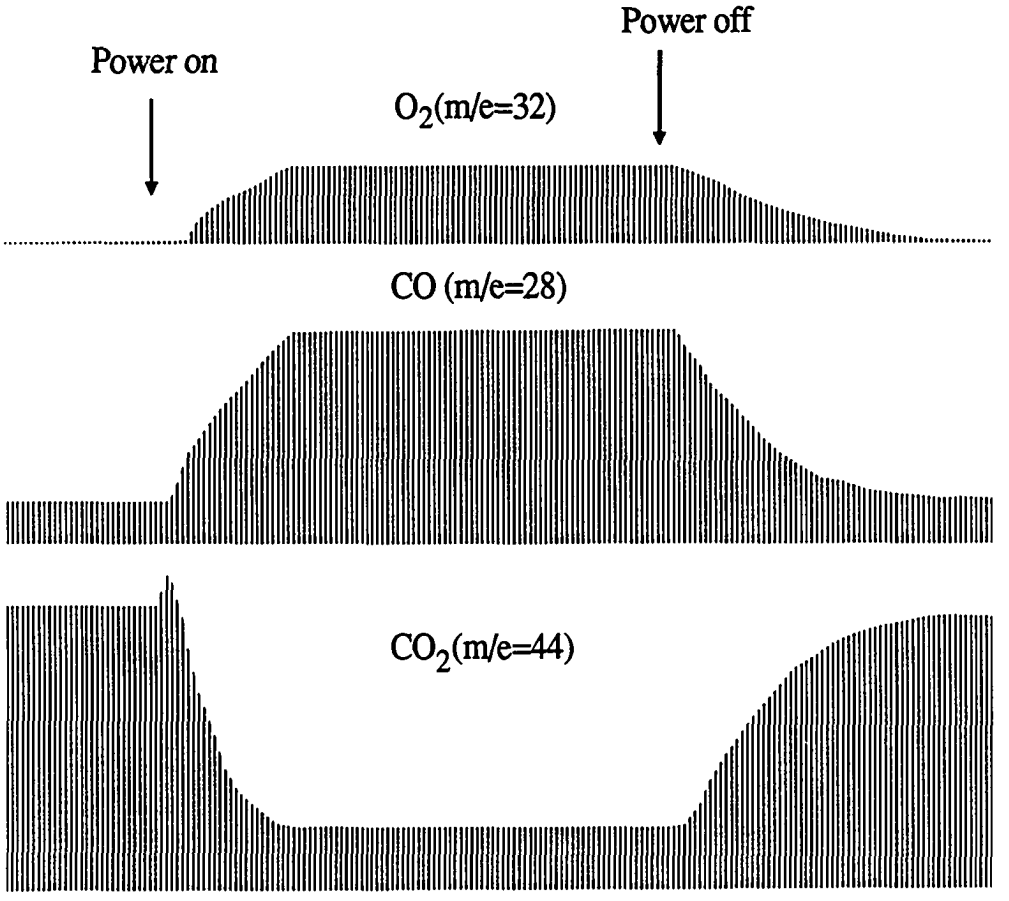

Fig. 5.7 QMS analysis of CO_2 dissociation before and after a dc glow-discharge is applied (This data was taken with a conductance limited connection with the upstream glow-discharge region).

Figure 5.8 shows the oxygen flux through the membrane as a function of probe-membrane separation distance. The oxygen flux through the membrane increases with decreasing probe-membrane separation distance. Since the oxygen flux through the membrane was contributed mostly by the atomic oxygen, as was found in the O_2 glow-discharge experiments, this indicates that the density of the atomic oxygen was not uniform inside the glow-discharge volume. Because the dissociation of CO_2 was most efficient in the negative glow region, close to the cathode probe, this provides clear evidence that the dissociated O atoms quickly recombined to form O_2 as they diffuse through the positive column and reach the membrane surface, under the pressure range tested here. When the probe was moved closer to the membrane, the distance between the negative glow and the membrane surface decreased, and the number of the oxygen atoms that travel through the positive column and reach the membrane without recombining to form O_2 increases. As a result, the oxygen flux through the membrane increases.

Figure 5.9 shows the oxygen flux through the membrane as a function of probe-membrane separation distance under the 2 torr condition as compared to the 5 torr condition. The oxygen flux through the membrane reaches a maximum at 2 mm, then starts to decrease with decreasing probe-membrane separation distance. At low pressures, the negative glow volume will expand due to an increased mean free path, as shown schematically in Fig. 5.10 for a comparison of 2 torr and 5 torr discharge conditions. If we move the probe too close to the membrane (after the negative glow region reached the

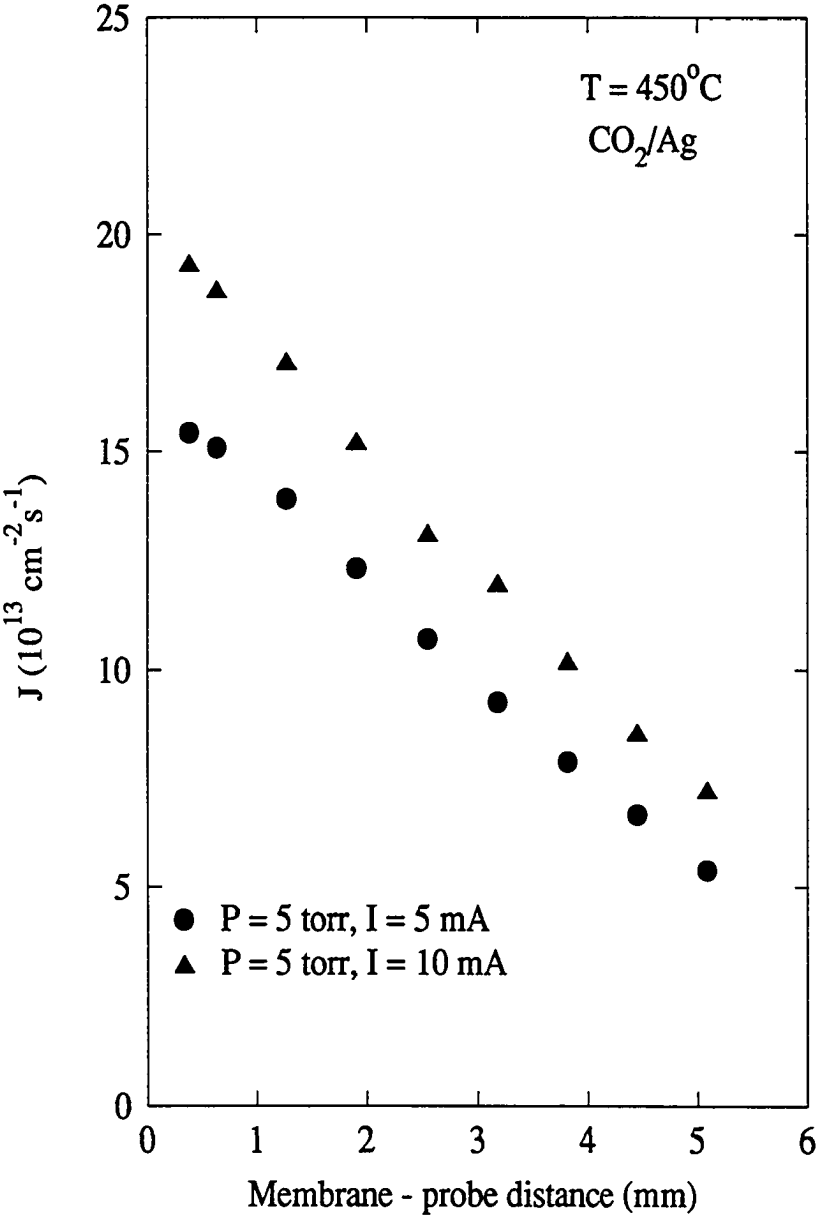

Fig. 5.8 Variation of permeation rate with membrane probe distance.

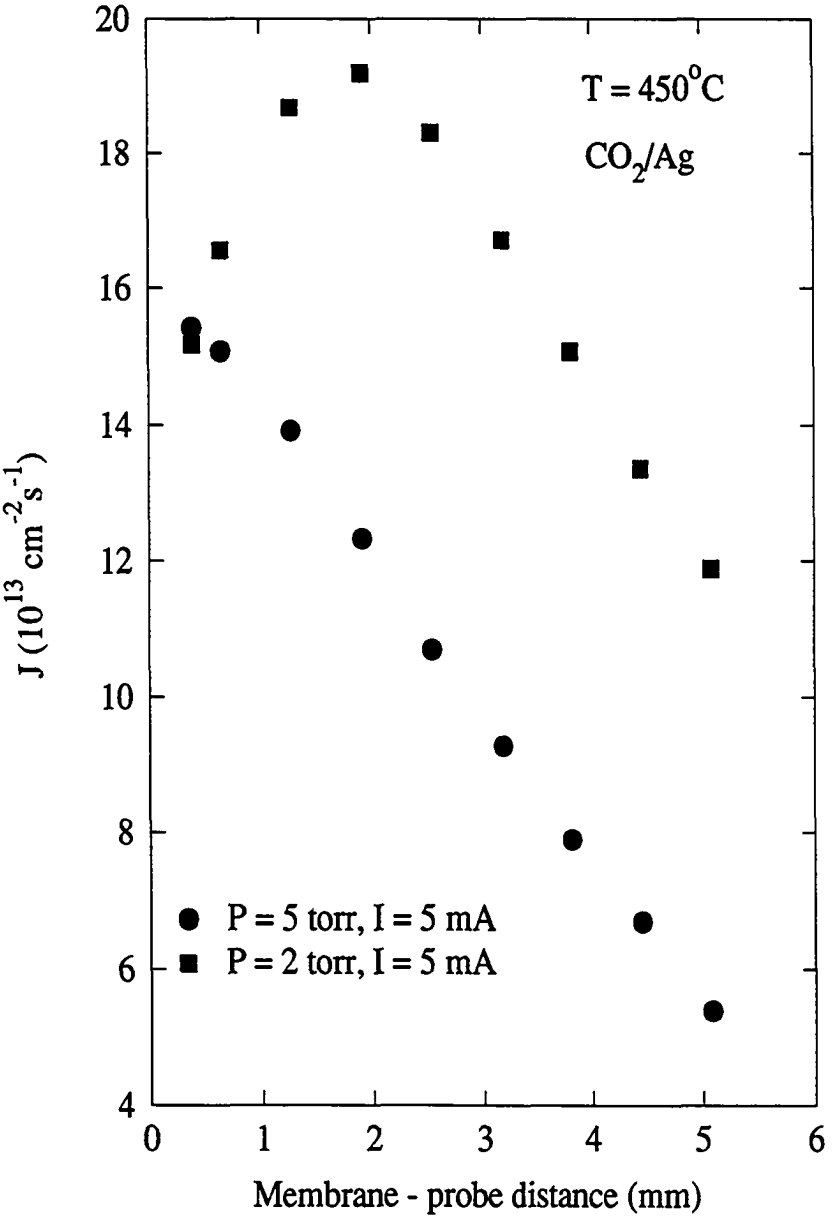

Fig. 5.9 Variation of permeation rate with membrane probe distance (comparison of 5 torr and 2 torr conditions).

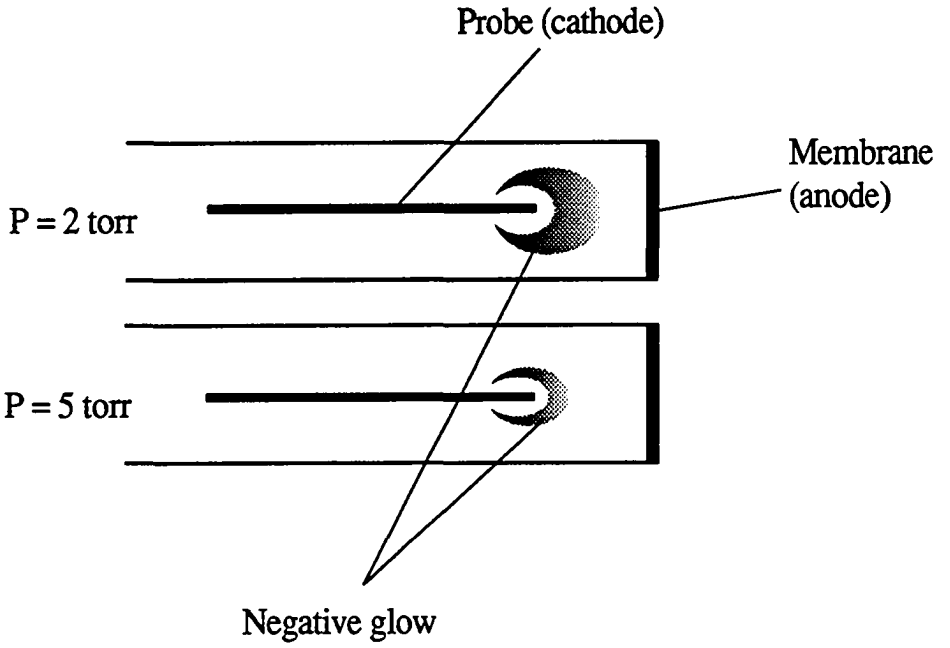

Fig. 5.10 Characteristic difference of 5 torr and 2 torr glow-discharge.

membrane), the efficiency of dissociation will drop off rapidly and the oxygen flux through the membrane decreases as shown in Fig. 5.9. This coupling of the effects of discharge pressure and the membrane probe distance makes the optimization more difficult.

Figure 5.11 shows that the oxygen flux through the membrane varies almost linearly at low glow-discharge currents (below 10 mA) and gradually reaching a constant value at higher discharge currents for both 600°C and 450°C membrane temperature conditions. This is consistent with the results of our O_2 glow-discharge experiment. At the lower discharge currents, it is also in agreement with the work of Sabadil and Pfau[24] who observed a linear increase in oxygen atoms with discharge current. As the discharge current increases, with a fixed total pressure, the partial pressure of the atomic oxygen increases due to the increasing electron densities inside the discharge volume. According to Sievert's Law, the oxygen concentration on the upstream surface should vary linearly with the atomic oxygen partial pressure in the gas phase. Since the total oxygen flux through the membrane is due primarily to the atomic oxygen generated via glow-discharge, as we found previously, the linear increase in the oxygen flux through the membrane with low discharge current correlates well with the variation in partial pressure of the atomic oxygen with discharge current. However, at higher currents, the increases of the oxygen flux through the membrane departs from the linearity and gradually approaches some constant value. As we explained previously, the negative glow region will first cover the top portion of the discharge probe at low discharge currents and then migrate along the probe as the discharge current increases. Since the

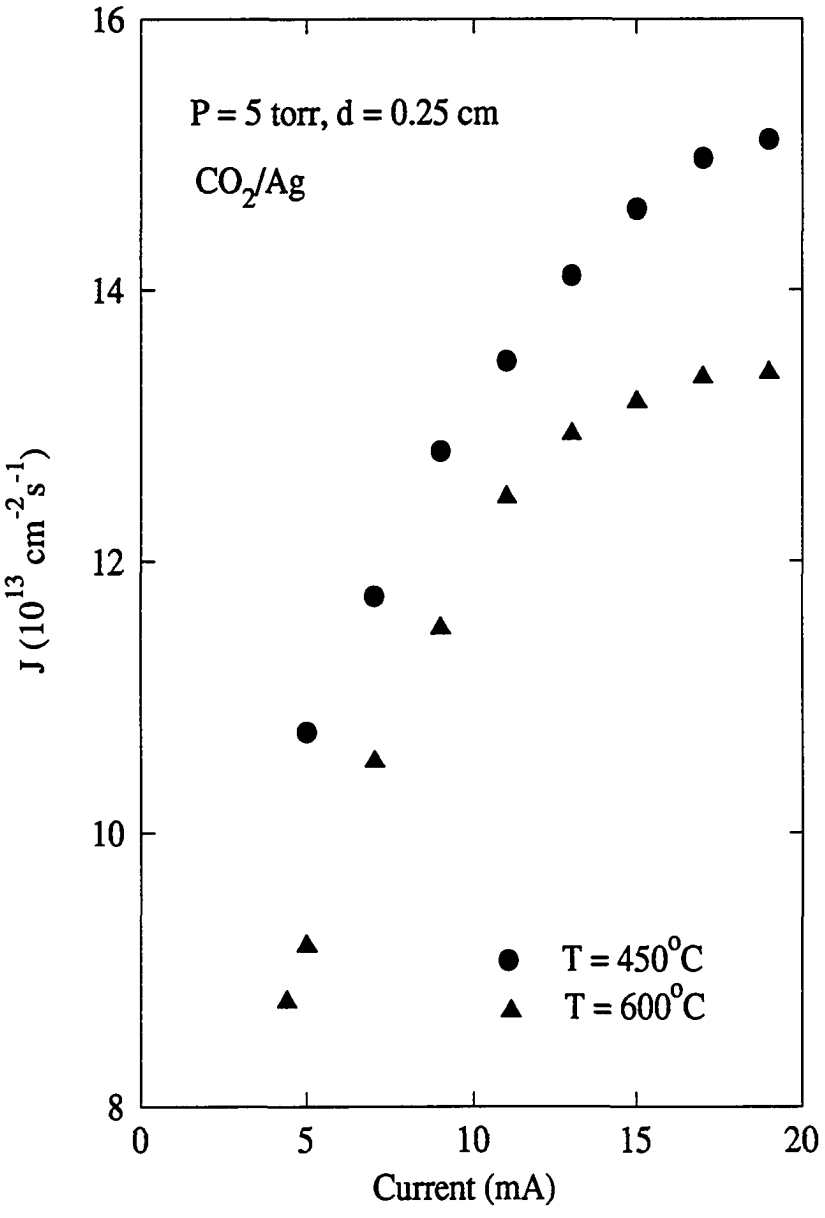

Fig. 5.11 Variation of permeation rate with dc glow-discharge currents for CO_2.

recombination of atomic oxygen is high at 5 torr pressure as we found previously, the additional atomic oxygen generated from the parts of the discharge probe other than the tip portion (at higher discharge current) will quickly recombined to form O_2 as it diffuses toward the surface of the membrane and as a result, the oxygen flux departs from the linear increase at low discharge current and gradually approach some limit as the current increases.

Figure 5.12 shows that the oxygen flux through the membrane decreases with upstream CO_2 pressure for fixed membrane-probe separation distances and discharge currents. As the density of the CO_2 molecules decreases, the probability of dissociation decreases and the oxygen flux through the membrane decreases as shown in Fig. 5.12 at pressure above 4 torr. But, due to the characteristics of the glow-discharge, the negative glow region, where the CO_2 was dissociated most efficiently, will expand as the pressure decreases and the distance between the negative glow and the membrane will decrease as well. At pressures below 4 torr, the geometrical factor (the decreasing separation distance between the membrane and the negative glow) dominate over the pressure effects causing the oxygen flux through the membrane to increase with further decreases in pressure. As the pressure was decreased further, to below 2 torr, the negative glow was no longer confined to the tip of the probe because of the increases in mean free path. The glow-discharge evolved into the whole volume and the efficiency of the dissociation decreased dramatically. As a result, the oxygen flux through the membrane dropped.

Figure 5.13 shows an Arrhenius plot of the oxygen permeation flux at 5 torr CO_2 upstream pressure and with 2.54 mm probe-membrane separation distance, with a 5 mA

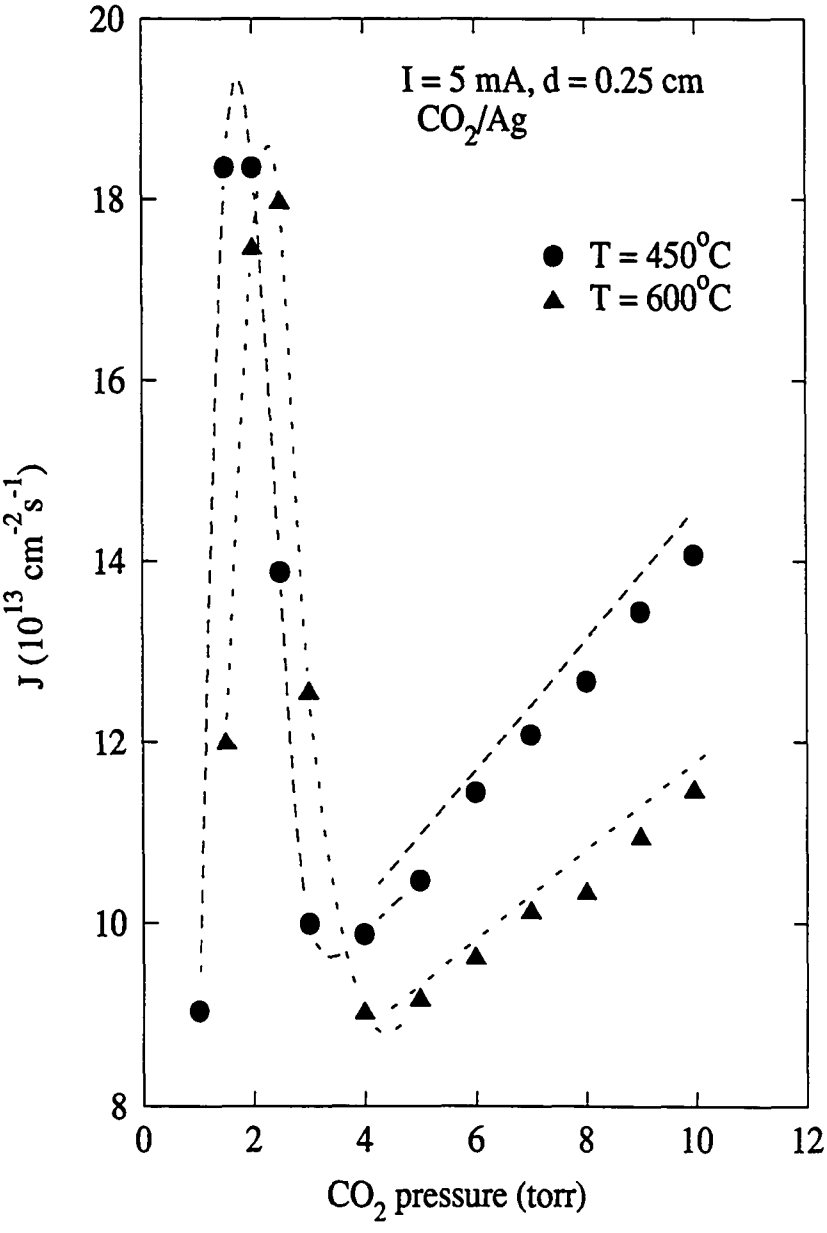

Fig. 5.12 Variation of permeation rate with upstream CO_2 pressure.

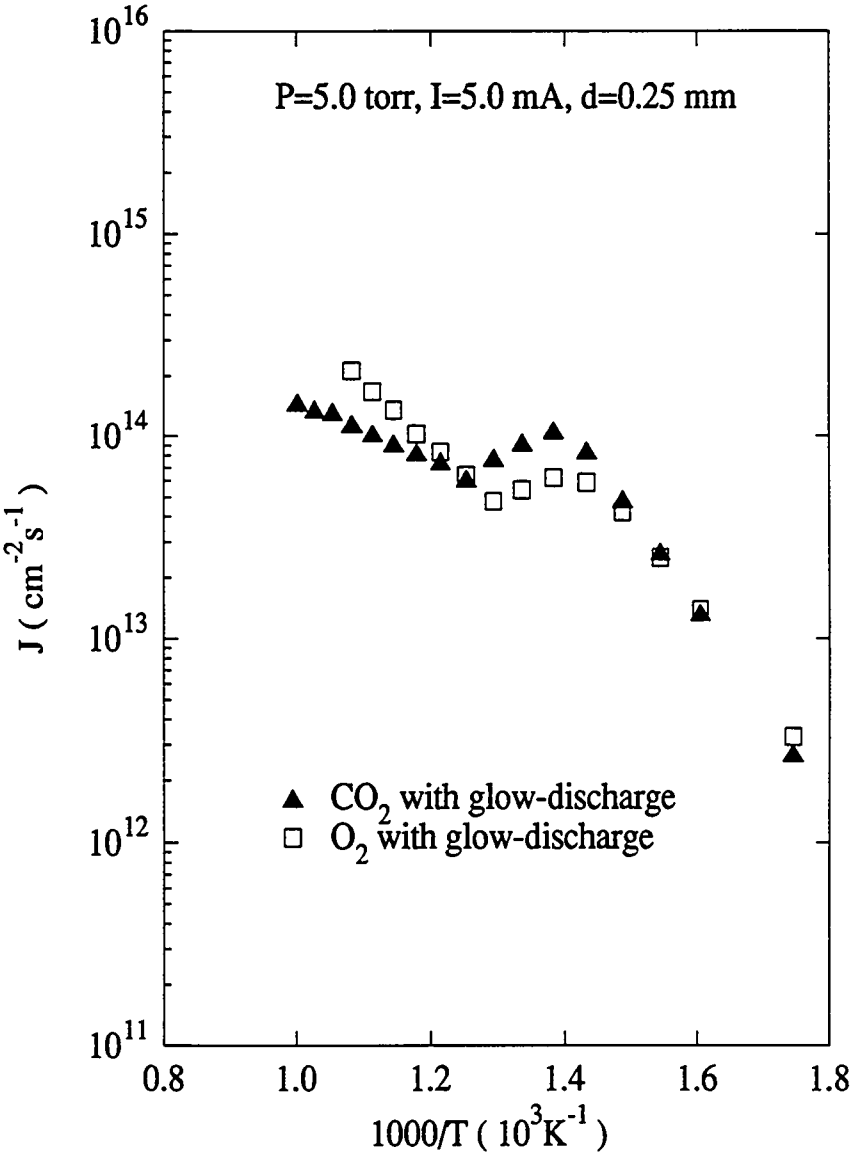

Fig. 5.13 Variation of Permeation rate with reciprocal temperature for CO_2 and O_2 via a constant current dc glow-discharge.

glow-discharge current. Also shown is the oxygen permeation flux at 5 torr O_2 upstream pressure under the same discharge conditions. The comparison with CO_2 upstream pressure without glow-discharge is impossible because the thermal dissociation of CO_2 is very small and the oxygen flux through the membrane is not detectable. As for O_2 with glow-discharge, the permeation flux for CO_2 with glow-discharge also exhibits two Arrhenius linear regions and one transitional region over the temperature range tested. Below 425°C, the activation energy for the process, ΔH_J = 21.4 kcal/mol, is about the same as for O_2 with glow-discharge, ΔH_K = 19.5 kcal/mol. This further confirmed that the overall process is diffusion controlled at low membrane temperatures. The magnitude of the oxygen flux level was about the same which indicates that the dissociation rate for CO_2 and O_2 in a glow-discharge was also about the same. The is in agreement with the close chemical bonding energies for O-O (498.37 kJ/mol)[67] compared to CO-O (532.2 kJ/mol)[67] without considering the recombination factors.

Above 425°C, the permeation curve also departs from linearity, as observed for O_2 glow-discharge, and gradually approaches another linear zone at higher temperatures. The overall process for this region is very complicated and is not well understood at this time. It is, as was described in O_2 glow-discharge case, due probably to atoms recombination and desorption back into the gas phase at higher temperatures.

At temperatures above 525°C, the activation energy for CO_2 with glow-discharge, ΔH_J = 7.0 kcal/mol, was much lower than that for O_2 glow-discharge permeation, H_J = 14.0 kcal/mol, and the magnitude of the flux level is also lower than that of O_2 with glow-discharge. Previous O_2 glow-discharge studies have shown that the adsorption rate

for atomic oxygen is substantially greater than that for molecular oxygen, where O_2 molecules are dissociatively adsorbed onto the surface. Hence, for the glow-discharge work, we can approximate the total oxygen flux with glow-discharge as being due primarily to the partial pressure of the atomic oxygen generated at low temperatures. Since the sticking coefficient for atomic oxygen on silver most likely decreases dramatically at higher temperatures as does molecular oxygen, the significance of the atomic oxygen contribution to the overall adsorption will decrease as well. This results in the higher oxygen flux level for O_2 with glow-discharge, compared to that of CO_2 with glow-discharge. So, the domination of the O_2 at high temperatures could be due to the molecular dissociative adsorption component that does not exist with CO_2.

The oxygen concentration of the upstream surface, C_s for CO_2 with glow-discharge, can also be determined from Fick's law (as for O_2 with glow-discharge) and the result is shown in Fig. 5.14. At temperatures below 425°C, the C_s follows J_{gd}, and the behavior of C_s as a function of temperature is about the same for both O_2 and CO_2 with glow-discharge. This clearly indicates that the yield of atomic oxygen in a glow-discharge for both O_2 and CO_2 is about the same and the adsorption rate is controlled by the partial pressure of the atomic oxygen in the gas phase. On the other hand, the rapid decrease in surface concentration for CO_2 with glow-discharge, in comparison with the slight decrease for O_2 with glow-discharge, at temperatures above 500°C further confirmed that the strong surface effects on the absorption of atomic oxygen at low temperatures quickly disappears with increasing temperatures and results in a rapid decrease in surface concentration for CO_2 with glow-discharge. In both cases, the oxygen concentration will

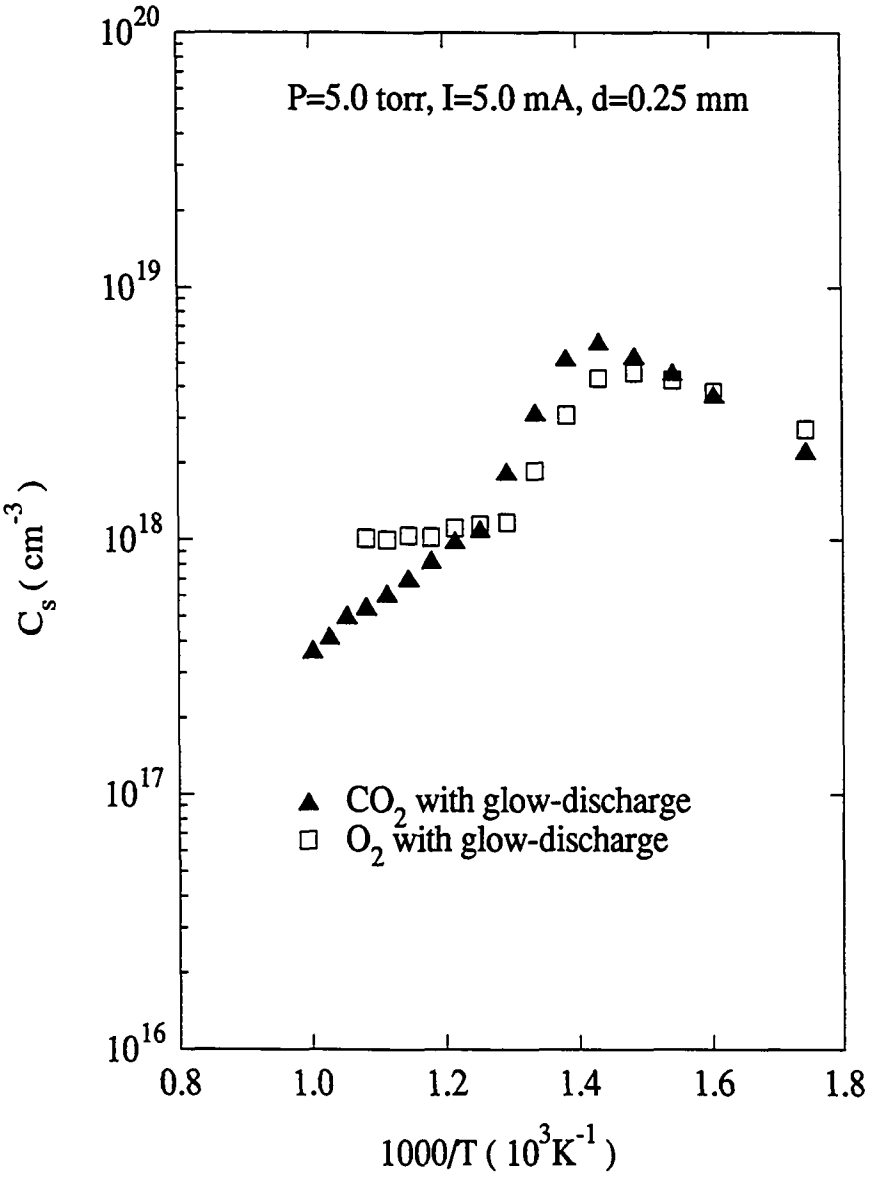

Fig. 5.14 The concentration variation as a function of reciprocal temperature with CO_2 and O_2 glow-discharge.

eventually approach the concentration level of thermal dissociative adsorption where the molecular oxygen dissociatively adsorbed onto the silver surface.

5.3 QMS Study of Glow-Discharge Dissociation of CO_2

Previous studies have shown that glow-discharge can break the chemical bond of O-O and CO-O but did not tell the dissociation rate and how much the atomic oxygen generated reached the membrane as atoms without recombination. The previous observation of oxygen flux as a linear function of membrane probe distance for both O_2 and CO_2 glow-discharge indicated that the recombination rate was high under 5 torr condition. In order to gain more understanding of the interaction of atomic oxygen with silver, it is necessary to know what is the proportion of atomic and molecular oxygen reaching the membrane, and to separate the surface oxygen concentration due to the atomic oxygen and to the molecular oxygen in the gas phase. The same system as for O_2 and CO_2 glow-discharge was used for this experiment except that a copper disk with a small orifice was substituted for the silver membrane to allow the atoms arriving at membrane to reach the downstream low pressure chamber immediately. The QMS ionization head was brought closer to the orifice to reduce the possible recombination of the atomic oxygen as it reached QMS.

Figure 5.15 shows the QMS spectrums before and after the glow-discharge was initiated. After the glow-discharge was initiated, the m/e(44) for CO_2 decreases and m/e(32) and m/e(28) for O_2 and CO increase significantly. Subtract m/e(16) components contributed by CO_2, CO and O_2, the left over is considered to be contributed by the atomic oxygen (m/e=16) reaching the membrane without recombination. The over all gas components for CO_2 glow-discharge under 5 and 10 mA, 2.5 and 5 mm conditions was

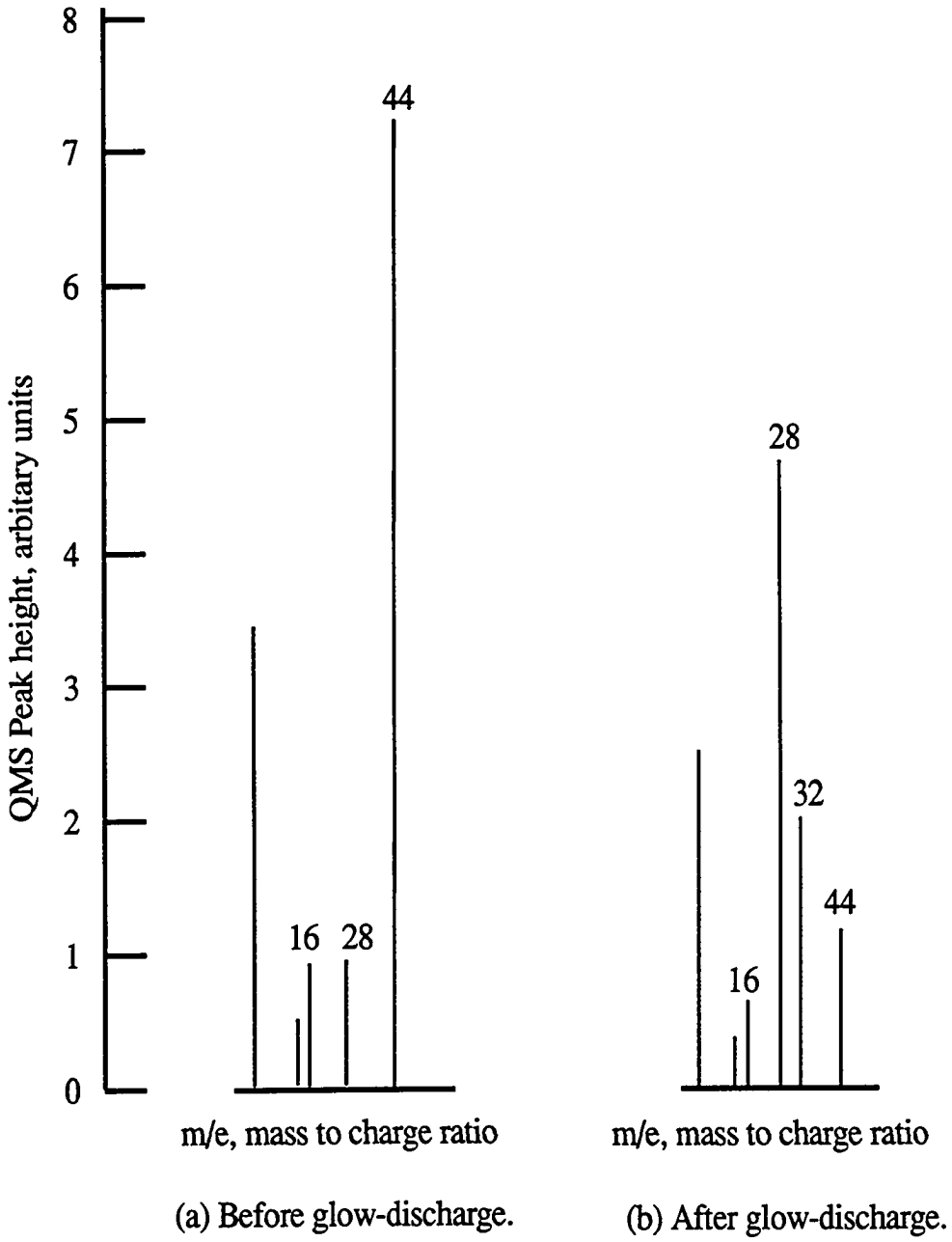

Fig. 5.15 QMS spectrums before and after the glow-discharge in CO_2.

shown in Fig. 5.16. It can be seen that the glow-discharge dissociation of CO_2 was very efficient, about 75% of the CO_2 was dissociated at a 5 mA discharge current. But most of the O atoms dissociated from CO_2 recombined to form O_2 before they reached the membrane. In the vicinity of the membrane surface, 50% of the gas is CO, 24% of the gas is O_2, and only about 0.65% of the gas is atomic oxygen. This number is very close to the dissociation rate (about 0.8%) obtained by Sabadil[24] under the same pressure and discharge current conditions. Accurate measurement of changes for the atomic oxygen component as a function of discharge current and the membrane-probe distance is difficult because the large contribution on the 16 peak from 44, 32 and 28 peaks masked the small component due to the atomic oxygen. The trend of the O_2 and CO partial pressure as a function of discharge current and membrane-probe distance was as expected (the partial pressure for 10 mA is larger than 10 mA discharge current and for 2.5 mm is larger than 5.0 mm membrane-probe distance). Volchenok[23] also used the mass spectrometer to measure the atomic oxygen generated by a glow-discharge but he used O_2-He (1:10) under 2 torr conditions to reduce the recombination rate and increase the sensitivity of mass spectrometer. This restriction is not applicable to our experiment. Although this experiment did not give a very accurate measurement of the atomic oxygen as expected, it did give an approximation of how much atomic oxygen arrived at the membrane and the contribution of this small amount of atomic oxygen to the overall oxygen adsorption on the membrane surface.

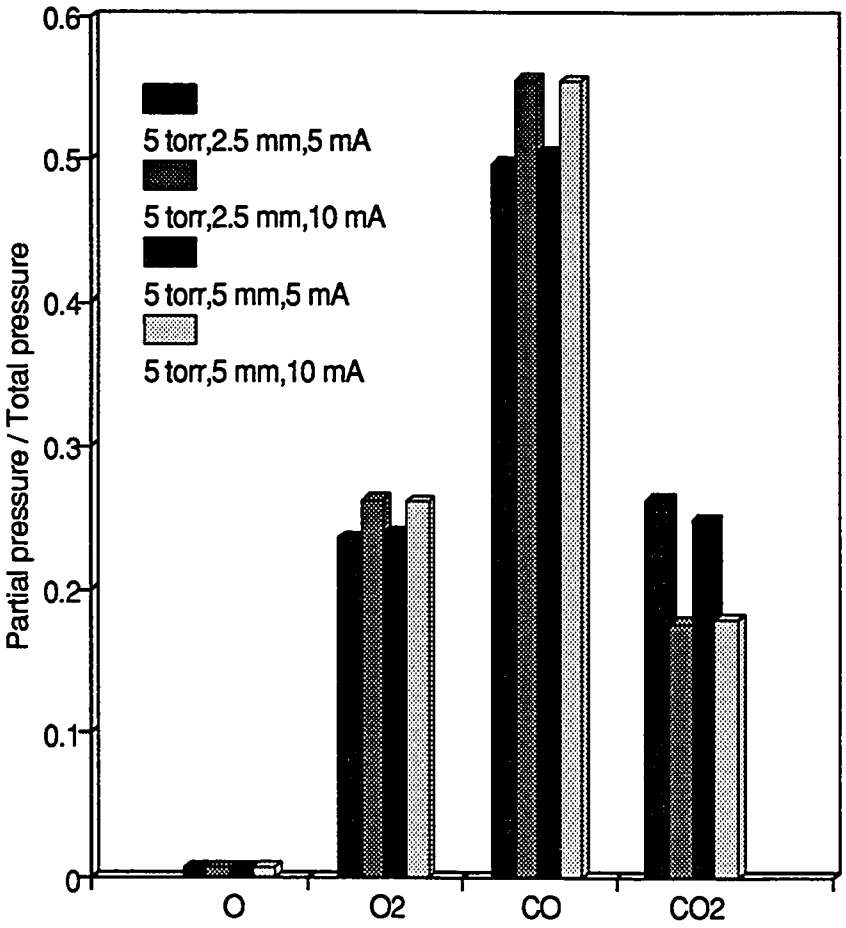

Fig. 5.16 QMS analysis of gas composition inside a dc glow-discharge near cathode

5.4 Sticking Coefficient of Atomic Oxygen on Silver

It is generally accepted that the characteristic shape of the sticking probability is a consequence of the formation of a weakly adsorbed precursor to chemisorption. Kisliuk[63,64] considered the probabilities of the various steps available to the precursor state molecules and calculated the sticking probability curves theoretically for single-site adsorption and two-site adsorption and the results turned out to be quite different. Instead of discussing the various surface processes in terms of probabilities, Tamm and Schmidt[65] suggested an analogous method and gave the sticking probability, S, curve as:

$$S=\frac{S^*}{1+k_d^*/k_a h(\theta)} \qquad (5.1)$$

where S^* is the condensation coefficient, k_d^* is the rate constant for desorption and k_a is the rate constant for the adsorption. The function, $h(\theta)$, is the coverage dependence function, representing the probability that gas atoms find a vacant site and the θ is the fractional coverage which is defined as number of adsorbed atoms over the number of adsorbed atoms at saturation conditions, σ/σ_0. For single-site adsorption, as for atomic oxygen, $h(\theta)$ is taken to be $1-\theta$ and for two-site adsorption, as for molecular oxygen, $h(\theta)$ is $(1-\theta)^2$. For atomic oxygen, the adsorption rate constant could be significantly larger than for molecular oxygen since it doesn't require extra energy for the dissociation. Equation (5.1) suggests that the sticking coefficient for atomic oxygen is likely to be significantly larger than for molecular oxygen.

Under equilibrium conditions, assuming a Langmuir-like isotherm, the rate of adsorption must be equal to the rate of desorption plus the rate of dissolution:

$$\nu f_1(\theta)s=\eta f_2(\theta)+\mu f_3(\theta) \tag{5.2}$$

Here, ν is the collision frequency on the surface, which at steady state is equal to $p/(2\pi mkT)^{1/2}$; s is the sticking coefficient; η and μ are the specific constants for desorption and dissolution respectively (at the specific membrane temperature), and $f_1(\theta)$, $f_2(\theta)$ and $f_3(\theta)$ are the functions representing the fractional coverage probabilities. For dissociative adsorption (for molecular oxygen):

$$f_1(\theta)=(1-\theta_m)^2,\ f_2(\theta)=\theta_m^2,\ \textit{and}\ f_3(\theta)=\theta_m, \tag{5.3a}$$

and for non-dissociative adsorption (for atomic oxygen):

$$f_1(\theta)=(1-\theta_a),\ f_2(\theta)=\theta_a^2,\ \textit{and}\ f_3(\theta)=\theta_a. \tag{5.3b}$$

Hence, the ratio of sticking coefficient for atomic to molecular oxygen will be:

$$\frac{s_a}{s_m}=\frac{P_m}{\sqrt{2}P_a}\frac{\theta_a}{\theta_m}\frac{(1-\theta_m)^2}{(1-\theta_a)}\frac{(\eta\theta_a+\mu)}{(\eta\theta_m+\mu)} \tag{5.4}$$

where P_a and P_m are the upstream partial pressures of the oxygen atoms and molecules, respectively. Since the atomic oxygen chemisorbed on the surface is found to recombine and desorb at 314°C[30], it is likely that most of the atoms will desorb instead of dissolve into the bulk. So, $\mu\theta \ll \eta\theta^2$ and we can simplify the ratio of the sticking coefficient to:

$$\frac{s_a}{s_m}=\frac{P_m}{\sqrt{2}P_a}\frac{\theta_a^2}{\theta_m^2}\frac{(1-\theta_m)^2}{1-\theta_a} \tag{5.5}$$

Assuming the total flux is due to the partial pressure of molecular oxygen and the atomic oxygen in the upstream gas phase and ignoring the impact of excited states, we can separate the flux due to atomic oxygen from the flux due to molecular oxygen:

$$J_{gd}=J_a+J_m=\frac{DC_a}{d}+\frac{DC_m}{d} \tag{5.6}$$

where C_a and C_m are the surface concentrations from atoms and molecules, respectively. The coverage θ of each component can then be calculated by

$$\theta_a=\frac{\sigma}{\sigma_0}=\frac{C_a\delta}{\sigma_0},\quad \theta_m=\frac{\sigma}{\sigma_0}=\frac{C_m\delta}{\sigma_0} \tag{5.7}$$

Here, δ is the thickness of surface layer which is about 2×10^{-8} cm and assuming σ_0 is about 1×10^{15}. The results for the sticking coefficient ratio of atomic oxygen to molecular oxygen on silver can been obtained from Eqs. (5.5) and (5.7) and are shown in Fig. 5.17. The ratio sticking coefficients appears to be a constant (4×10^{-5}) at low temperatures (below 400°C) and decreases exponentially with increasing temperatures. Since the sticking coefficient normally decreases with increasing temperatures, the result of this calculation shows that the sticking coefficient for atomic oxygen decreases at about the same rate as for molecular oxygen at low temperatures, but much more rapidly at higher temperatures. Because few grains of a polycrystalline surface are perfectly oriented crystals, it is reasonable to approximate the mean sticking coefficient of O_2 on a polycrystalline surface by assuming the lowest sticking coefficient experimentally observed for molecular oxygen on silver. Campbell[34] observed the sticking coefficient of oxygen on Ag(111) at 217°C as 10^{-6} and Banndorf[66] observed the sticking coefficient of oxygen on both Ag(111) and Ag(100) at 27°C as on the order of 10^{-5}. By extending our data points to 217°C, we can obtain the sticking coefficient of atomic oxygen on silver as 0.4 at 217°C and can very roughly estimate that it is close to 1 at room temperature. Gregory el al. have made orbital measurements of 5 eV hyperthermal

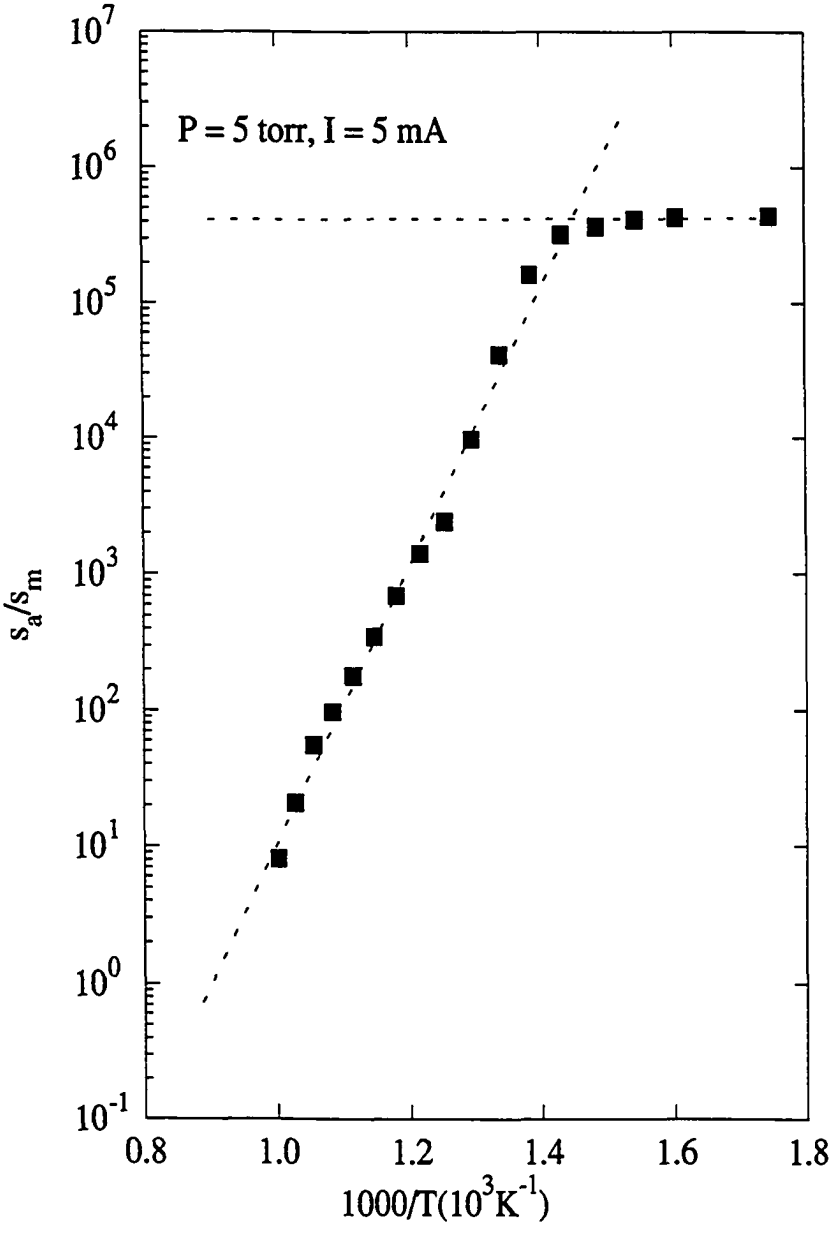

Fig. 5.17 The sticking coefficient of atomic oxygen on silver as a function of reciprocal temperatures.

atomic oxygen on Ag films at room temperature and have estimated that the sticking coefficient is near unity. Although this is a very rough estimate, it is important to see that the sticking coefficient for atomic oxygen on silver can be significantly larger than molecular oxygen on silver at low temperatures. It is also important to see the trend that it decreases exponentially with temperature at higher temperatures.

5.5 Confirmation of Thickness Dependence

The overall oxygen flux through the Ag membrane should be proportional to 1/d (where d is the thickness of the membrane) for diffusion controlled kinetics described by Fick's laws and shown experimentally in Eq. (3.32):

$$K=\frac{P_{eq}fd}{P_0^{1/2}Akt} \tag{3.32}$$

The oxygen flux through a 0.1 mm thick Ag membrane, which is about 1/4 the thickness of the previously studied membranes, is shown in Fig. 5.18. The Arrhenius plot shows a permeation flux which is approximately 4 times larger than the levels observed previously, thus confirming the diffusion controlled kinetics. Therefore, one method of increasing the oxygen flux is to reduce the thickness of the membrane to technologically achievable limits. A thin Ag film membrane with a thickness on the order of one micron is being developed. Such membranes require physical support since they are so thin that the films would rupture under ordinary differential pressures. Silver mesh and porous ceramic plates are presently being studied for this purpose. At this time, a 12 μm pin hole free, free standing film has been achieved as shown in Fig. 5.19 and also shown schematically in Fig. 5.20. This was accomplished by rolling/annealing process. Successful experiments with physical vapor deposition on a Geltech porous ceramic (average pore size of 2.5 nm) have also been conducted. Experiments in physical vapor deposition of Ag in 1 μm steps using Ar ion to assist in closing pin holes combined with burnishing have recently been successful. Pin hole free Ag films of 1 μm thickness supported on Geltech substrates are being developed. It is estimated that a two to three

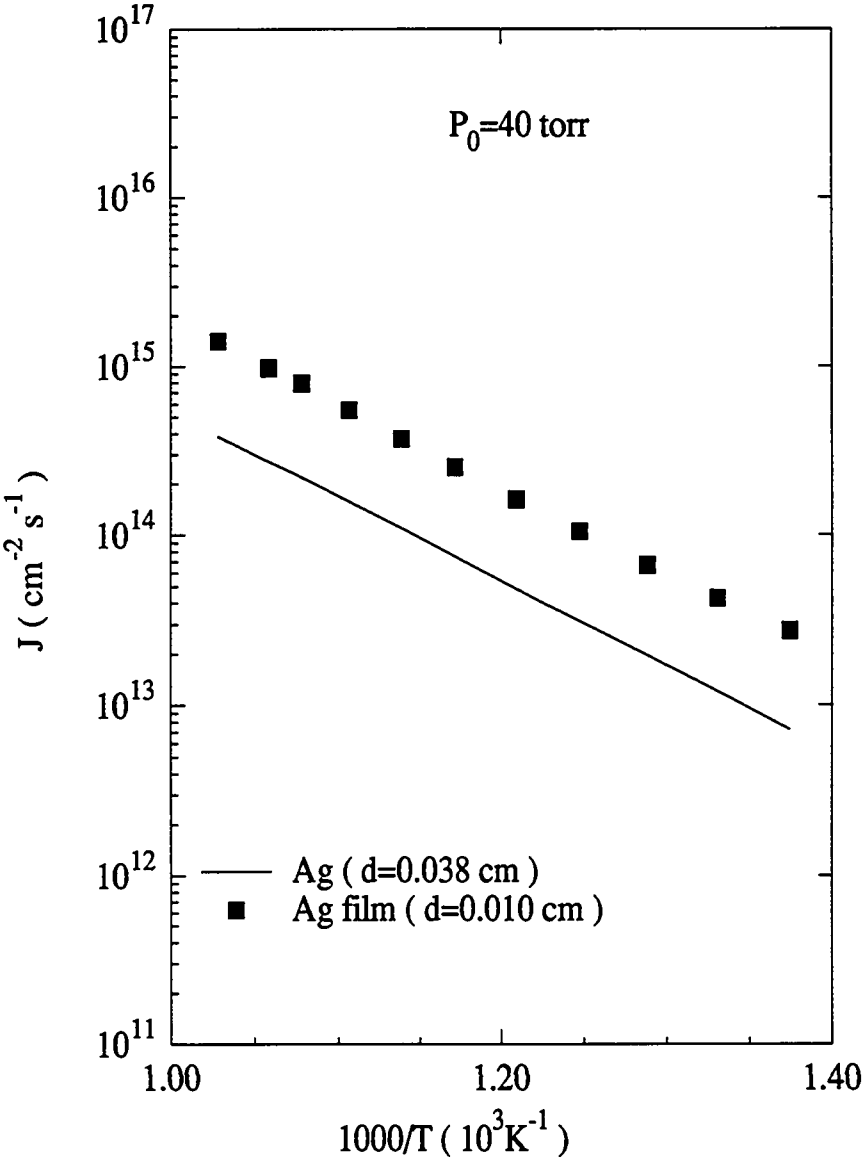

Fig. 5.18. Variation of permeation rate with reciprocal temperature for two different membrane thicknesses.

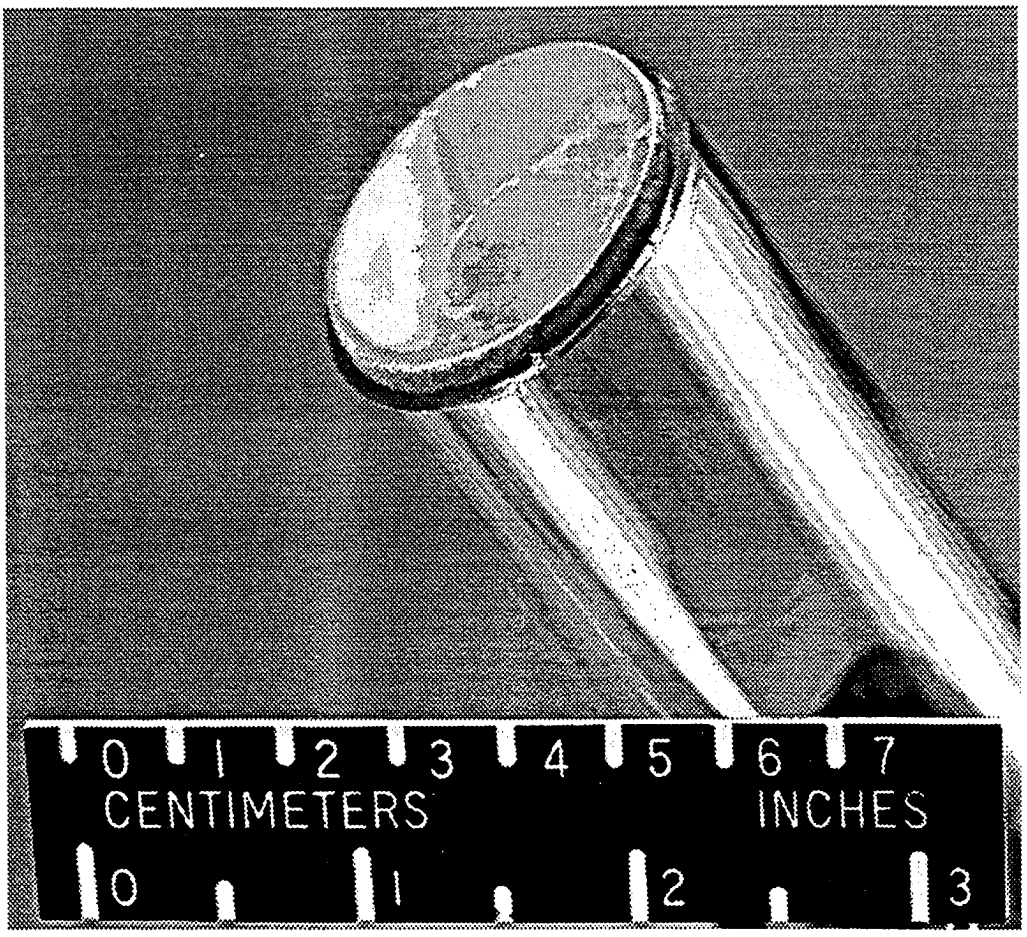

Fig. 5.19 12 μm pin hole free, free standing Ag film supported by a porous ceramic plates.

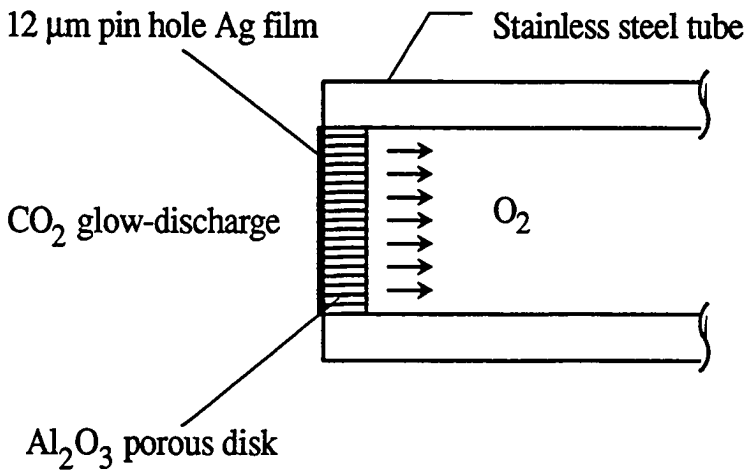

Fig. 5.20 Schematic of 12 μm Ag film supported by a ceramic porous disk.

decade improvement in the oxygen flux level can be achieved ultimately with this method. With a maximum oxygen flux of 1.07×10^{14} at 450°C obtained previously and assuming two decade improvement with thin film technique, only 1.5 m^2 membrane surface area is needed to support an astronaut on Mars surface on a continuous bases. This is not a difficult task for engineer up-scaling. Further, these thin silver films could possibly be supported on a stabilized zirconia substrate, operated as an electrochemical pump, thus augmenting the oxygen production systems developed previously.

Chapter 6

CONCLUSIONS

A glow discharge can be sustained in ambient Mars atmosphere (about 5 torr and composed of 95% carbon dioxide) resulting in the dissociation of carbon dioxide molecules into carbon monoxide and oxygen. If the glow-discharge zone is maintained adjacent to a silver membrane, atomic and molecular oxygen, produced by the discharge, can be separated from other species by diffusing through the membrane and then be collected. Experiments have been conducted that characterize the behavior of the glow discharge in molecular oxygen and carbon dioxide environments, and the permeation of oxygen through a silver membrane. The interactions of atomic and molecular oxygen with silver were also studied. It was found that for the geometry studied the dissociation of CO_2 in a dc glow discharge is very efficient. More than 70% of CO_2 was dissociated with only 5 mA discharge current. The dissociation was found to be most efficient in the negative glow region inside the glow discharge. The atomic oxygen generated by the glow discharge will quickly recombine to form O_2 as it migrates toward the membrane. In the vicinity of the membrane(anode) with 2.54 mm separation distance from discharge probe(cathode) and with 5 mA discharge current, 50% of the gas was CO, 24% of the gas was O_2 presumably from recombined atomic oxygen, and only about 0.65% of the gas was atomic oxygen.

The sticking coefficient of the atomic oxygen on silver, which has never been measured before, was approximated and found to be much higher than molecular oxygen on silver at low temperatures because it bypasses the normal thermal dissociative adsorption step for molecular oxygen and can adsorbed onto the surface more efficiently. It was estimated to be close to 1 at room temperature, which is five orders of magnitude higher than molecular oxygen on silver. The ratio of the sticking coefficient for atomic oxygen to molecular oxygen on silver appears to be a constant of about $4x10^5$ at low temperatures, which suggests that the decrease in s with increasing temperatures is similar for atoms and molecules at low temperatures. This ratio also appears to decrease exponentially at higher temperatures.

It was also found that silver membranes are far from oxygen saturation at low temperatures. Combined with its high sticking coefficient, s_a, the small amount of atomic oxygen, generated by the glow discharge, still increases the surface concentration significantly and increases the oxygen flux through the membrane as well. Because the atomic oxygen will quickly recombine to form O_2 as it migrates toward the silver membrane, the negative glow region inside the glow discharge should be maintained in close proximity to the membrane surface in order to take full advantage of the high adsorption rate of the atomic oxygen on silver.

For normal operations, in which the glow discharge was concentrated on the tip portion of the discharge probe, the oxygen flux through the membrane increased linearly with the discharge current, which indicated a proportional increase of atomic oxygen in the gas phase. The oxygen flux also increased slightly with increasing CO_2 pressure.

At temperatures below 425°C, the oxygen flux through the membrane with glow discharge was much higher than that for oxygen without glow discharge because the concentration gradient was substantially higher due to the higher sticking coefficient for atomic oxygen. The activation energy for the permeation with glow discharge, 19.5 kcal/mol, is about the same as the permeation of molecular oxygen without glow discharge (22.2 kcal/mol). This increase of the flux reached a limit of 1.07×10^{14} atoms/cm^{2}s at 450°C and then, gradually approached the flux level of oxygen permeation without glow discharge because of the significant decreases in the sticking coefficient for atomic oxygen on silver at higher temperatures.

The permeation was also found to be diffusion controlled which means the oxygen flux through the membrane is limited by bulk diffusion and is proportional to the reciprocal of the membrane thickness. An one micron thick thin film silver membrane is being developed which will improve the oxygen flux level two to three order of magnitude which will give 10^{16} to 10^{17} atoms/cm^{2}s with full optimization. With two decades improvement, less than 1.5 m^2 membrane surface area, which is not difficult for engineering scale up, would be required to support a person continuously on Mars surface (assuming 0.84 kg/person-day). This approach of producing oxygen from the Martian atmosphere can serve as a possible low-temperature alternative to eliminate mechanical filtration, compression and heating of the Mars atmosphere as was proposed previously by the electrochemical methods.

REFERENCES

1. Zubrin, R.M., Baker, R.M., and Gwynne, O., "Mars Direct: A Simple, Robust, and Cost Effective Architecture for the Space Exploration Initiative," AIAA Paper No. 91-0326, Jan. 1991.

2. Zubrin, R.M. and Weaver, D.B., "Practical Methods for Near-Term Piloted Mars Missions," AIAA Paper No. 93-2089, Jun. 1993.

3. Gonzales, A., Harper, L., Dunsky, E., and Roberts, B., "Mars Surface Mission Life Support Summary," Presented to Mars Exploration Workshop II, NASA Ames Research Center, May 24, 1993.

4. Carr, M.H., The Surface of Mars, Yale U. P., New Haven and London, 1982.

5. Wood, S.E. and Paige, D.A., "Modeling the Martian Seasonal CO_2 Cycle," ICARUS 99, 1992, pp. 1-27.

6. Ash, R.L., Dowler, W.L., and Varsi, G., "Feasibility of Rocket Propellant Production on Mars," Acta Astronautica, Vol. 5, Pergamon Press Ltd., 1978, pp. 705-724.

7. Stancati, M.L., Niehoff, J.C., Wells, W.C., Feingold, H., and Ash, R.L., "In Situ Propellant Production for Improved Sample Return Mission Performance," AAS Paper No. 79-177, 1979.

8. Richter, R., "Basic Investigation into the Production of Oxygen in a Solid Electrolyte Process," AIAA Paper No. 81-1175, Jun. 1981.

9. Romaholli, K.N.R., and Sridhar, K.R., "Extraterrestrial Materials Processing and Related Transport Phenomena," AIAA Paper No. 91-0309, Jan. 1991.

10. Outlaw, R.A., "O_2 and CO_2 Glow-Discharge-Assisted Oxygen Transport Through Ag," Journal of Applied Physics, Vol. 68, 1990, pp. 1002-1004.

11. Loeb, L.B., Basic Processes of Gaseous Electronics, University of California Press, Berkeley CA, 1960.

12. Von Engel, A., Ionized Gases, Clarendon, Oxford, 1965.

13. Brown, S.C., Basic Data of Plasma Physics, MIT Press, Cambridge MA, 1959.

14. Francis, G., Ionization Phenomena in Gases, Butterworths, London, 1960.

15. Granovsky, V.L., Electric Current in Gas (Steady Current), Nauka, Moscow, 1971.

16. Raizer, Y.P., Fundamentals of Modern Physics of Gas Discharge Processes, Nauka, Moscow, 1980.

17. Howatson, A.M., An Introduction to Gas Discharges, Pergamon, Oxford, 1976.

18. Cherrington, B.E., Gaseous Electronics and Gas Lasers, Pergamon, Oxford, 1982.

19. Vossen, J.L., and Kern, W., Thin Film Processes, Academic, Orlando, 1978.

20. Rossnagel, S.M., Cuomo, J.J., and Westwood, W.D., Handbook of Plasma Processing Technology, Noyes Publications, 1990.

21. Raizer, Y.P., Gas Discharge Physics, Springer-Verlag, 1991.

22. Corvin, K.K., and Corrigan, S.J.B., "Dissociation of Carbon Dioxide in the Column of a Glow Discharge," Journal of Chemical Physics, Vol. 50, No. 6, Mar. 1969, pp. 2570-2574.

23. Volchenok, V.I., Komarov, V.N., and Kupriyanov, S.E., "Mass-spectrometer Determination of the Concentration of Atomic Oxygen in Glow Discharge in O_2, CO, and CO_2," Soviet Journal of Plasma Physics, Vol 4, No. 4, Jul./Aug. 1978, pp. 483-486.

24. Sabadil, H., and Pfau, S., "Measurements of the Degree of Dissociation in Oxygen DC Discharges," Plasma Chemistry and Plasma Processing, Vol. 5, No. 1, 1985, pp. 67-79.

25. Penkin, N.P., Smirnov, V.V., and Tsygir, O.D., "Investigation of the Electrokinetic Properties and of the Dissociation of O_2 Molecules in an Oxygen Discharge," Soviet Physics, Technical Physics, Vol. 27, No. 8, Aug. 1982, pp. 945-948.

26. Costa, M.D., Zuliani, P.A., and Deckers, J.M., "Chemical Reactions in Glow Discharge. IV. Production and Removal of Oxygen Atoms in the DC Glow Discharge," Canadian Journal of Chemistry, Vol. 57, No. 5, 1979, pp. 568-579.

27. Loureiro, J., "Dissociation Rate and $N(^4S)$ Atom Concentrations in a N_2 Glow-Discharge," Chemical Physics, Vol. 157, 1991, pp. 157-168.

28. Cernogora, G., Hochard, L., Touzeau, M., and Ferreira, C.M., "Population of $N_2(A\ ^3\Sigma^+)$ Metastable States in a Pure Nitrogen Glow Discharge," Journal of Physics B: Atomic and Molecular Physics, Vol 14, 1981, pp. 2977-2987.

29. Sharapov, V.M., and Zakharov, A.P., "Penetration of Hydrogen Through Molybdenum in a Glow Discharge," Soviet Physics, Technical Physics, Vol. 21, No. 3, Mar. 1976, pp. 351-353.

30. Engelhardt, H.A., and Menzel, D., "Adsorption of Oxygen on Silver Single Crystal Surfaces," Surface Science, Vol. 57, No. 2, Jul. 1976, pp. 591-618.

31. Barteau, M.A., and Madix, R.J., "The adsorption of Molecular Oxygen Species on Silver (110)," Surface Science, Vol. 97, No. 1, 1980, pp. 101-110.

32. Backx, C., De Groot, C.P.M., and Biloen, P., "Adsorption of Oxygen on Ag(110) Studied by High Resolution ELS and TPD," Surface Science, Vol. 104, No. 1, Mar. 1981, pp. 300-317.

33. Grant, R.B., and Lambert, R.M., "Basic Studies of the Oxygen Surface Chemistry of Silver: Chemisorbed Atomic and Molecular Species on Pure Ag(111)," Surface Science, Vol. 146, No. 1, Oct. 1981, pp. 256-268.

34. Campbell, C.T., "Atomic and Molecular Oxygen Adsorption on Ag(111)," Surface Science, Vol, 157, No. 1, Jul. 1985, pp. 43-60.

35. Puschmann, A., and Haase, J., "Surface EXAFS of the (2 x 1) Oxygen Allayer on Ag(110)," Surface Science, Vol. 144, No. 2/3, Sept. 1984, pp. 559-566.

36. Eichmans, J., and Otto, A., "The Transition From Physisorbed to Chemisorbed Oxygen on Silver Films Studied by Photoemission," Surface Science, Vol. 149, No. 1, Jan. 1985, pp. 293-312.

37. Peuckert, M., "On the Adsorption of Oxygen and Potassium Hydroxide on Silver," Surface Science, Vol. 146, No. 2/3, Nov. 1984, pp. 329-430.

38. Bange, K., Madey, T.E., and Sass, J.K., "Characterization of OH(ad) Formation by Reaction Between H_2O and O(ad) on Ag(110)," Surface Science, Vol. 152/153, Apr. 1985, pp. 550-557.

39. Prince, K.C., and Bradshaw, A.M., "Valence Level Photoelectron Spectroscopy of the Oxygen and Carbonate Species on Silver (110)," Surface Science, Vol. 126, Nos. 1-3, Mar. 1983, pp. 49-57.

40. Au, C.T., Singh-Boparai, S., Roberts, M.W., and Joyner, R.W., "Chemisorption of Oxygen at Ag(110) Surfaces and Its Role in Adsorbate Activation," Journal of Chemical Society, Faraday Transaction 1, Vol. 79, 1983, pp. 1779-1791.

41. Sporken, R., Thiry, P.A., Pireaux, J.J., Caudano, R., and Adnot, A., "Work Function Measurements with a High Resolution Electron Energy Loss Spectrometer: Application to the Interaction of Oxygen with Ag(110)," Surface Science, Vol. 160, No. 2, Sept. 1985, pp. 443-450.

42. Rovida, G., Pratesi, F., Maglietta, M., and Ferroni, M., "Effects of Oxygen on Silver Surface Structure," Journal of Vacuum Science and Technology, Vol. 9, No. 2, Mar./Apr. 1972, pp. 796-799.

43. Prince, K.C., Paolucci, G., Bradshaw, A.M., Horn, K., and Mariani, C., "Oxygen Adsorption on Ag(110): Observation of a Precursor State," Vacuum, Vol. 33, Nos. 10-12, Oct./Dec. 1983, pp. 867.

44. Kagawa, S., Iwamoto, M., Morita, S., and Seiyama, T., "Isotopic Study of the Temperature Programmed Desorption of Oxygen From Silver," Journal of Chemical Society, Faraday Transaction 1, Vol. 78, 1982, pp.143-146.

45. Rovida, G. and Pratesi, F., "Chemisorption of Oxygen on the Silver (110) Surface," Surface Science, Vol. 52, No. 3, Nov. 1975, pp.542-555.

46. Goddard, P.J. and Lambert, R.M., "Basic Studies of the Oxygen Surface Chemistry of Silver: Oxygen Dioxygen, Oxide and Superoxide on Rubidium dosed Ag(111)," Surface Science, Vol. 107, Nos. 2/3, Jun. 1981, pp. 519-532.

47. Heiland, W., Iberl, F., Taglauer, E., and Menzel, D., "Oxygen Adsorption on (110) Silver," Surface Science, Vol. 53, Dec. 1975, pp. 383-392.

48. Zanazzi, E., Maglietta, M., Bardi, U., Jona, F., and Marcus, P.M., "Test of Structural Models for Ag(110) 1x20 by LEED Intensity Analysis," Journal of Vacuum Science and Technology, Vol. 1, No. 1, Jan./Mar. 1983, pp. 7-11.

49. Joyner, R.W. and Roberts, M.W., "A Study of the Adsorption of Oxygen on Silver at High Pressure by Electron Spectroscopy," Chemical Physics Letters, Vol. 60, No. 3, Jan. 1979, pp. 459-462.

50. Davidson, M.R., Hoflund, G.B., and Outlaw, R.A., "Nondestructive Depth Profile Study of Oxygen-Exposed Large-Grain Silver Using Angle-Resolved Auger Electron Spectroscopy and Ion Scattering Spectroscopy," Journal of Vacuum Science and Technology A, Vol. 9, No. 3, May./Jun. 1991, pp. 1344-1350.

51. Outlaw, R.A., "O_2 and CO_2 Glow-Discharge-Assisted Oxygen Transport Through Ag," Journal of Applied Physics, Vol. 68, 1990, pp. 1002-1004.

52. Sharapov, V.M. and Zakharov, A.P., "Penetration of Hydrogen Through Molybdenum in a Glow Discharge," Soviet Physics, Technical Physics, Vol. 21, No. 3, Mar. 1976, pp. 351-353.

53. Eichenauer, W. and Mueller, G., "Diffusion and Solubility of Oxygen in Silver," Zeitschrift fuer Metallkunde, Bd. 53, 1962, pp. 321-324.

54. Coles, R.E., "The Permeability of Silver to Oxygen," British Journal of Applied Physics, Vol. 14, 1963, pp. 342-344.

55. Beavis, L.C., "Oxygen Permeation Through Silver," The Review of Scientific Instruments, Vol. 43, No. 1, Jan. 1972, pp. 122-127.

56. Ramanarayanan, T.A. and Rapp, R.A., "The Diffusivity and Solubility of Oxygen in Solid Nickel," Metallurgical Transactions, Vol. 3, No. 12, Dec. 1972, pp. 3239-3246.

57. Gryaznov, V.M., Gul'yanova, S.G., and Kanizius, S., "Diffusion of Oxygen Through a Silver Membrane," Russian Journal of Physical Chemistry, Vol. 47, No. 10, 1973, pp. 2694-2696.

58. Outlaw, R.A., Sankaran, S.N., Hoflund, G.B., and Davidson, M.R., "Oxygen Transport Through High-purity, Large-grain Ag," Journal of Material Research, Vol. 3, No. 6, Nov./Dec. 1988, pp. 1378-1384.

59. Mitchell, D.J., Harris, J.M., Patrick, R.C., Boespflug, I.P., and Beavis, L.C., "Deuterium Permeation Through Copper with Trapping Impurities," Journal of Applied Physics, Vol. 53, No. 2, Feb. 1982, pp. 970-978.

60. Outlaw, R.A., Wu, D., Davidson, M.R., and Hoflund, G.B., "Study of the Oxygen Transport Through Ag(110), Ag(poly) and Ag2.0Zr," Journal of Vacuum Science and Technology A, Vol. 10, No. 4, Jul/Aug 1992, pp. 1497-1502.

61. Crank, J., Mathematics of Diffusion, Oxford U.P., Oxford, 1967.

62. Madey, T.E. and Yates, J.T. Jr, "Electron-Stimulated Desorption as a Tool for Studies of Chemisorption: A Review," Journal of Vacuum Science and Technology, Vol. 8, No. 4, Mar. 1971, pp. 525-555.

63. Kisliuk, P., "The Sticking Probabilities of Gases Chemisorbed on the Surfaces of Solids," Journal of Physics and Chemistry of Solids, Vol. 3, 1957, pp. 95-101.

64. Kisliuk, P., "The Sticking Probabilities of Gases Chemisorbed on the Surfaces of Solids - II," Journal of Physics and Chemistry of Solids, Vol. 5, 1958, pp. 78-84.

65. Tamm, P.W. and Schmidt, L.D., "Interaction of H_2 with (100)W. II. Condensation," Journal of Chemical Physics, Vol. 52, 1970, pp. 1150-1160.

66. Benndorf, C., Franck, M., and Thieme, F., "Oxygen Adsorption on Ag(111) in the Temperature Range From 100-500 K: UPS, XPS and EELS Investigations," Surface Science, Vol. 128, 1983, pp. 417-423.

67. Lide, D.R., Handbook of Chemistry and Physics, CRC Press, 1994.

68. Paul, W., Reinhard, H.P., and Von Zahn, U., "Das Elektrische Massenfilter als Massenspektrometer und Isotopentrenner," Zeitschrift fuer Physik, Bd. 152, Heft 2, 1958, pp. 143-182.

APPENDICES

APPENDIX A

THE ION GAUGE

The ion gauge consisted of a nude closed end Bayard-Alpert type ionization gauge (Varian) and a control unit (Varian Ionization Gauge 971-0003). The ionization gauge contains three elements: filament, grid, and collector wire as shown in Fig. A.1. The filament serves as the source of electrons. The grid functions as the electron collector, operating at a positive potential (+130 volts) with respect to the filament, and along the axis of the cylindrical grid structure is a very small diameter ion collector wire which operates at zero potential. Electrons from the filament pass through the grid several times on the average before being collected at the grid. While passing through the interior of the grid structure the electrons ionize gas molecules at a rate which is proportional to the gas density. The positive ions produced on the inside of the grid structure are accelerated toward and neutralized at the collector by electrons from the external circuit. The number of ions produced per electron is proportional to gas density, and the positive ion current to the ion collector is used as an indication of pressure. Thus, for a constant value of accelerating voltage in excess of the ionization potential of the gas, the number of positive ions formed should vary linearly with pressure and the electron current. This is described by the relation:

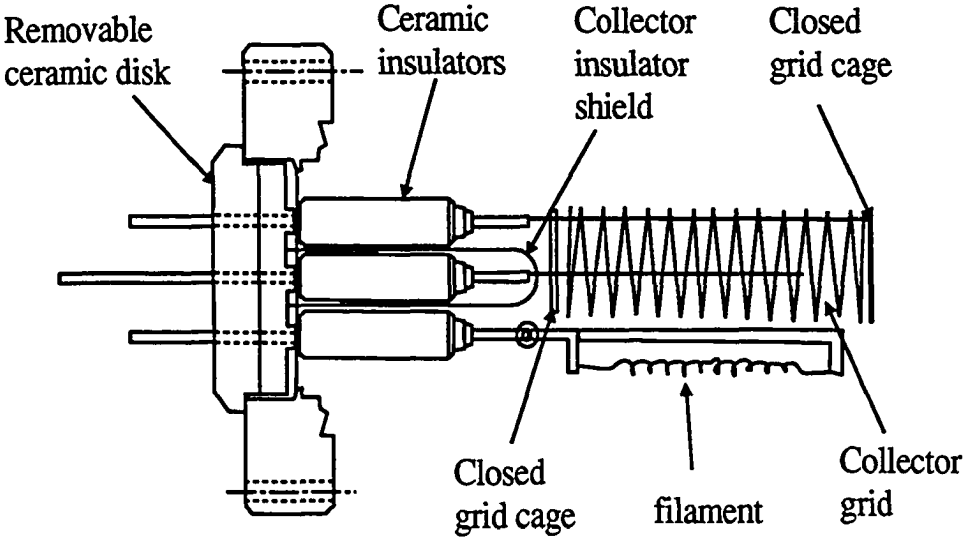

Fig. A.1 Nude Bayard-Alpert ionization gauge with closed grid cage.

$$S=\frac{1}{P}\times\frac{i_c}{i_g} \qquad \text{(A.1)}$$

where i_c is the ion current in amps to the collector, i_g is the electron current in amps to the grid, and P is the pressure in torr. The sensitivity, S, of a given ion gauge is theproportionality constant in the basic ionization gauge equation above. For the given electron current, sensitivity and the measured ion current, P can be calculated. The ion gauge employed in this work has a sensitivity of 30 $torr^{-1}$. This is higher than the 25 $torr^{-1}$ of the sensitivity of the regular gauge because it is enclosed in a high conductance metal envelope. This instrument was the primary downstream pressure measurement, P(t), because its dynamic response was superior to that of the QMS.

APPENDIX B

THE QUADRUPOLE MASS SPECTROMETER

The QMS consisted of three sections: the RF generator, the probe, and the control console. The primary components within the analyzer probe are the ionizer, the quadrupole mass filter and the electron multiplier, as shown schematically in Fig. B.1. The gas molecules within the ionizer are bombarded by electrons from the tungsten filaments and become positively charged ions by electron impact. The ions are then focussed into the mass filter. A combined radio-frequency and electrostatic field is formed by two pairs of metal rods in the filter section. A charged substance with a specific mass-to-charge ratio will have a dynamically stable trajectory within the field formed by the voltages on the rods while all other substances will be filtered out. By continuously varying the applied voltages, a mass range of 1 - 300 AMU can be analyzed. At a particular set of voltages, the ion with a specific m/e value can traverse the length of the filter. These ions arrive at the multiplier and are amplified into an electron current that is 10^6 times the ion current. The output current of the amplifier is referenced against the scan voltage which is in term referenced to a specific m/e of the ions, thereby producing a spectrum of peaks.

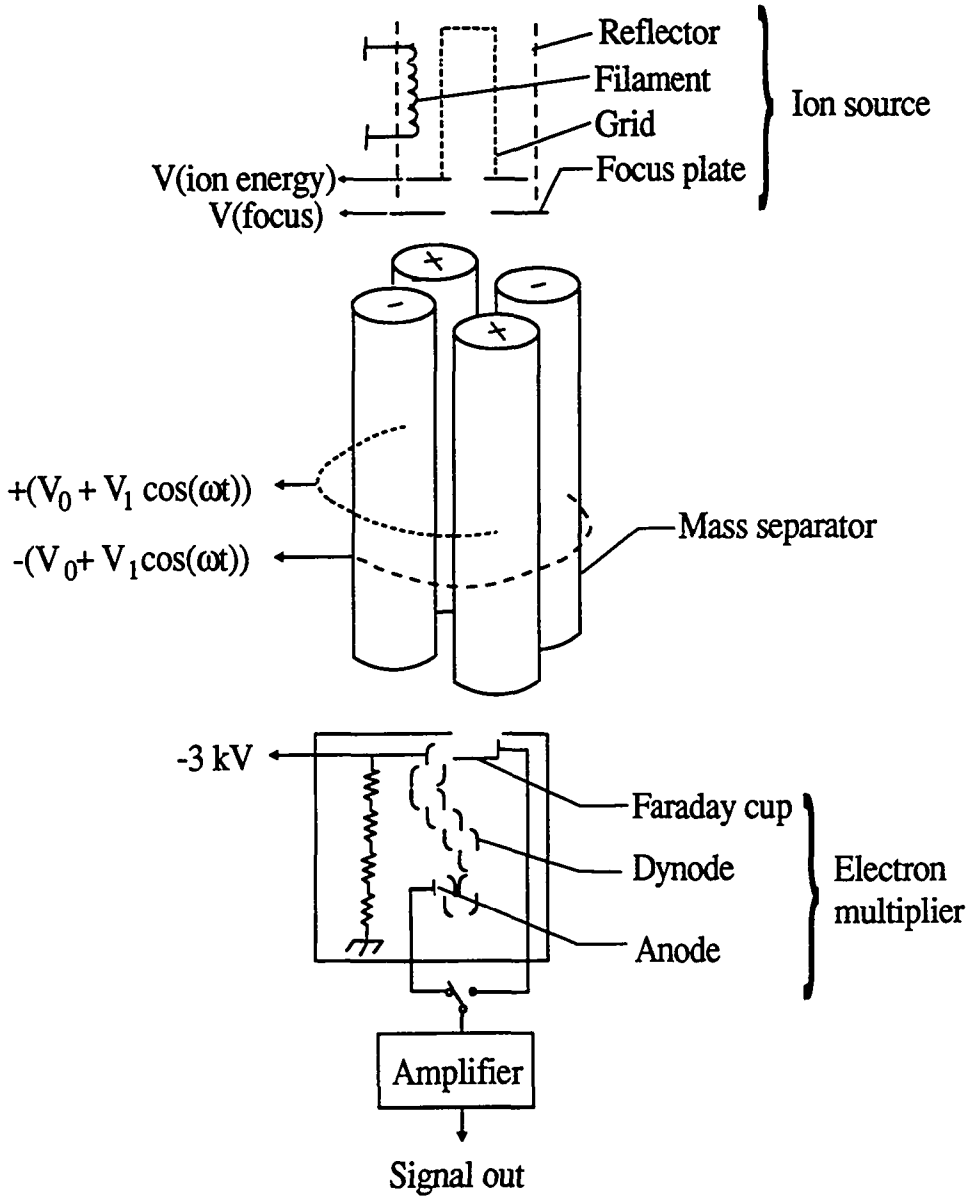

Fig. B.1 Schematic of the analyzer probe.

Ion Source

The ionizer used here is similar to one used in the ion gauge. The primarydifference between an ion gauge and a quadrupole mass spectrometer ionizer is that ion extraction and focusing into the quadrupole mass filter section is required by the QMS. The ultimate resolution is very sensitive to the energy and entrance angles of the incoming ions (to the quadrupole mass filter). Furthermore, the ionizer is designed to minimize the X rays that might transit the filter section to the detector and limit detectability at low pressures.

Quadrupole Mass Filter

Ions are formed in the ionizer and injected into the electrical quadrupole along the Z-axis of the quadrupole. The rods of the quadrupole are energized with a constant dc potential, V_0, and an RF potential $V_1\cos\omega t$[68]. The ions are subjected to a potential of the form

$$\phi=(V_0+V_1\cos\omega t)\frac{x^2-y^2}{r_0^2} \tag{B.1}$$

where V_0 is the dc voltage, V_1 is the RF voltage, R_0 is the radius of the inscribed cross-sectional area of the quadrupole, and x and y are the spatial coordinates of the cross section. The equations of motion for the ions are:

$$m\ddot{x}+2e(V_0+V_1\cos\omega t)\frac{x}{r_0^2}=0 \tag{B.2}$$

$$m\ddot{y}+2e(V_0+V_1\cos\omega t)\frac{y}{r_0^2}=0 \tag{B.3}$$

and

$$m\ddot{z}=0 \tag{B.4}$$

Eqs. (B.2) to (B.4) are Mathieu's differential equations. A transformation of coordinates is introduced as follows:

$$\omega t=2\mu \tag{B.5}$$

$$a=\frac{8eV_0}{mr_0^2\omega^2} \tag{B.6}$$

$$b=\frac{4eV_1}{mr_0^2\omega^2} \tag{B.7}$$

The solutions of the differential equation in z are trivial. The solutions in x and y are infinite series of two types: the stable solution, for which x and y remain finite for all values of μ, and the unstable solution, for which x and y become infinite as $\mu \to \infty$. The stability of the solutions depends on the values of a and b. Figure B.2 shows two regions: (1) ions that fall outside the triangular-shaped area enter unstable oscillations and are collected at the quadrupole electrodes, and (2) ions that fall inside the shaded area oscillate with amplitudes less than r_0 and pass through the analyzer.

The apex of the stability region occurs at b = 0.706, a = 0.23699, and V_0/V_1 = 0.17. At this point, only one mass, given by equations

$$m=\frac{2.85eV_1}{\omega^2r_0^2} \tag{B.8}$$

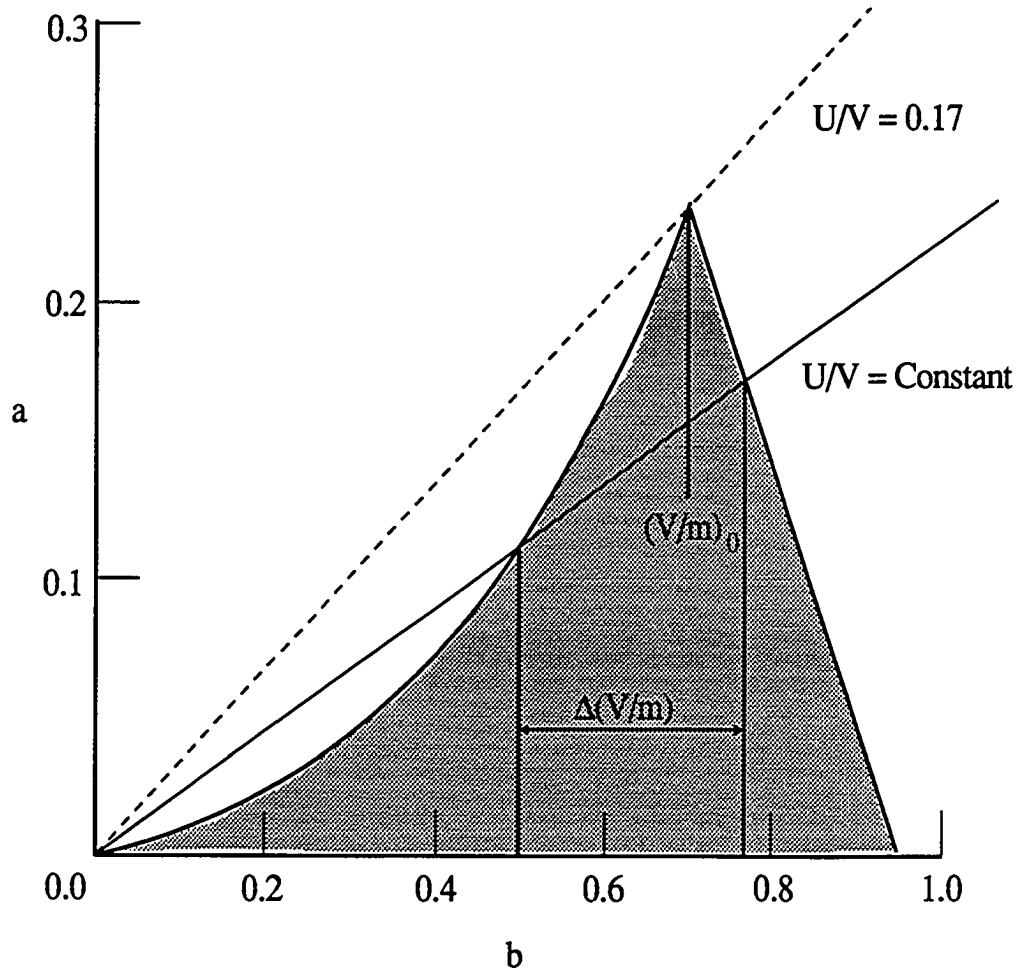

Fig. B.2 Quadrupole operation: Stable path (transmitted) for ions in shaded area.

$$V_0 \approx 0.17 V_1 \tag{B.9}$$

will pass through the analyzer; the resolution is ∞. For practical use, a lower value of V_0/V_1 is selected. The mass range is scanned by varying the RF and dc voltage level and keeping their ratio constant. A constant frequency is used and the resolution varies as 1/m. Certain boundary conditions on the entrance aperture and entrance energy are required for optimum resolution.

Electron Multiplier

The electron multiplier used here is a 16 stage electron multiplier. The discrete-dynodes are a Cu 2 - 4% Be alloy which forms a BeO surface layer. These multipliers can have a gain greater than 10^6 at approximately 100 V per stage. Ions exiting the mass separator are accelerated to the first dynode that is negatively biased 1 to 3 kV. Upon colliding with the dynode, the ions emit, on the average, several electrons per electron. These electrons are attracted to the next dynode with an accelerating potential of 100 to 300 V, where each electron emits, on the average, several more electrons. This process continues through each of the stages until 10^4 to 10^8 electrons from a single ion appear at the collector in a pulse of current. This instrument was used to qualitatively indicate the gas composition (upstream and downstream) and to insure that contamination was minimized before data were taken.

APPENDIX C

THE CAPACITANCE MANOMETER GAUGE

The capacitance manometer gauge consisted of two absolute pressure sensors (MKS Baratron 122A) and a power supply with a digital readout (MKS PDR-C-2C). One of the absolute pressure sensors measured from 10^{-3} torr to 10 torr and the other one measured from 10 torr to 1000 torr. The absolute pressure sensor was simply a diaphragm gauge as shown in Fig. C.1. The pressure inlet tube connected to a small chamber in the sensor body. One wall of this chamber is a thin metal diaphragm which faces a rigidly mounted ceramic disc containing two electrodes in a volume which is permanently evacuated and sealed. When pressure is applied to the diaphragm, its deflection produces a change in distance between the electrodes and diaphragm which produces corresponding changes in the capacitance. The control unit maintains an ac signal to the electrodes. The changes in signal strength produced by the diaphragm are amplified and demodulated in phase, in order to minimize the noise level. The dc output is then used to drive a digital readout. The digital readout can automatically cover the whole pressure range of the two sensors. This instrument has a dynamic range of 5 decades and provided measurement of P_0 from atmosphere to 10^{-3} torr.

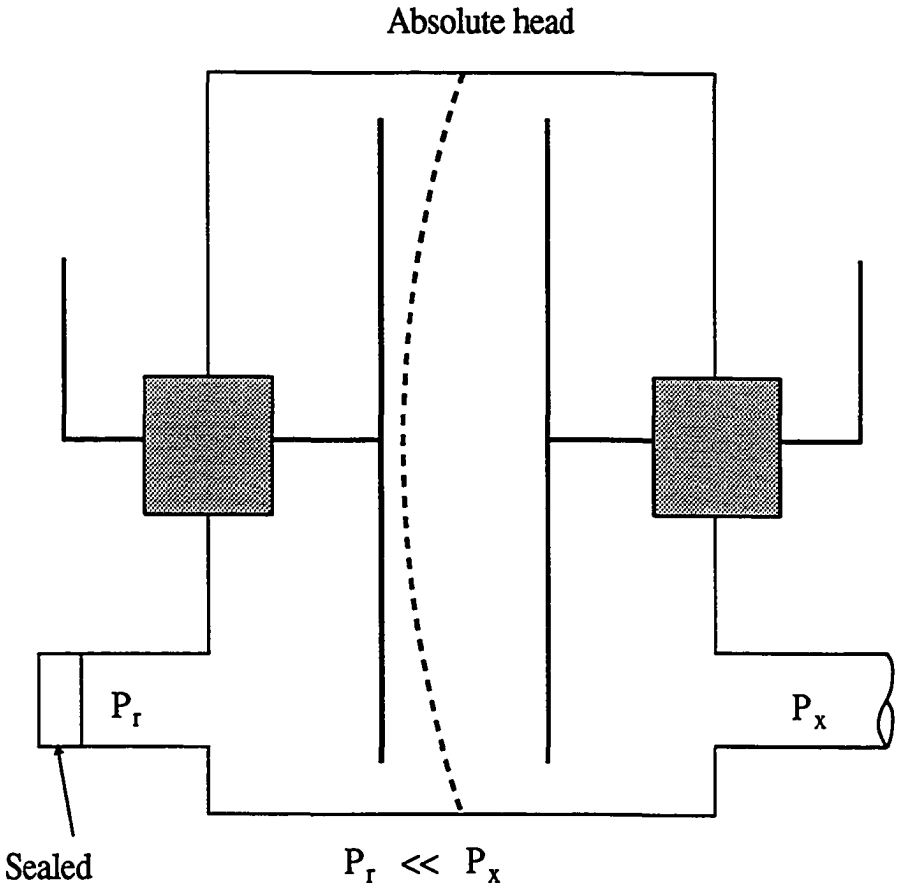

Fig. C.1 Schematic of absolute capacitance manometers
P_r = Reference pressure; P_x = Unknown pressure.

BIBLIOGRAPHY

Dongchuan Wu was born in Shanghai, China on October 12, 1958. He graduated from Chen Du High School in 1976 and worked as a mechanical technician in Shanghai Second Knitting Plant until 1981. He received his Bachelor of Science degree in Mechanical Engineering from Shanghai University of Industry in China in August, 1985. He was awarded the honor of "Best Student of the Year" in his senior year. He worked in Shanghai Second Knitting Plant as an Assistant Engineer for two and half years. He received his Master of Science degree in Physics at Old Dominion University in August 1990. He enrolled in the Ph.D program in Mechanical Engineering at Old Dominion University in August 1990 and received his Ph.D degree in August 1994. He has been working in The Low Pressure Physics Laboratory at the NASA Langley Research Center in Hampton, Virginia as an Research Assistant since August, 1988. He is married to Winnie Fu who is also a graduate of ODU.

Publications:

1. Wu, D., Outlaw, R.A., and Ash, R.L., "Extraction of Oxygen from CO_2 Using Glow-Discharge and Permeation Techniques", to be presented in the 41st National Symposium of American Vacuum Society, October 24-28, 1994, Denver, Colorado.

2. Outlaw, R.A., Wu, D., and Sankaran, S.N., "A Study of the Transport of Oxygen Through Ag-Zr Alloys", submitted to Scripta METALLURGICA et MATERIALIA.

3. Wu, D., Ash, R.L., and Outlaw, R.A., "Glow Discharge Techniques for the Production and Acquisition of Oxygen from the Martian Atmosphere", SAE Paper No. 941254, Jun. 1994.

4. Ash, R.L., Wu, D., and Outlaw, R.A., "A Study of Glow-Discharge and Permeation Techniques for Extraterrestrial Oxygen Beneficiation", Advance Space Research, Vol. 14, No. 6, 1994, pp. 259-263.

5. Wu, D., Outlaw, R.A., and Ash, R.L., "Glow-discharge Enhanced Permeation of Oxygen Through Silver", Journal of Applied Physics, Vol. 74, No. 8, Oct. 1993, pp. 4990-4994.

6. Wu, D., Ash, R.L., and Outlaw, R.A., "Extraction of Oxygen from the Mars Atmosphere Using Glow-Discharge and Permeation Techniques", AIAA Paper No. 93-2243, Jun. 1993.

7. Ash, R.L., Wu, D., and Outlaw, R.A., "A Study of Glow-Discharge and Permeation Techniques to Separate Oxygen from Martian Atmosphere", presented at the World Space Congress, Aug. 28 - Sep. 5, 1992, Washington, D.C.

8. Outlaw, R.A., Wu, D., Davidson, M.R., and Hoflund, G.B., "Study of the Oxygen Transport Through Ag(110), Ag(poly), and Ag2.0Zr, Journal of Vacuum Science and Technology A, Vol. 10, No. 4, Jul/Aug 1992, pp. 1497-1502.

9. Outlaw, R.A., Lee, W.S., Sankaran, S.N., Wu, D., and Clark, R.K., "Titanium Aluminides: Surface Composition Effects as a Function of Temperature," Scripta METALLURGICA et MATERIALIA, Vol. 24, 1990, pp. 171-176.

10. Wu, D., Stephens, R.M., Outlaw, R.A., and Hopson, P., "An Auger Electron Spectroscopy Study of Surface Preparation Contaminants", NASA Technical Paper 2972, Feb. 1990.